Wavelength Tuneable Transmitters for Future Reconfigurable Agile Optical Networks

A thesis submitted in Partial FulFillment of the Requirements
for the Degree of Doctor of Philosophy
(Electronic Engineering)

By
Robert Maher
B.Eng., MIEI, MIEEE

School of Electronic Engineering
Faculty of Engineering and Computing
Dublin City University

Research Supervisor
Prof. Liam P. Barry

2009

DECLARATION

I hereby certify that this material, which I now submit for assessment on the programme of study leading to award of Doctor of Philosophy is entirely my own work, that I have exercised reasonable care to ensure that the work is original, and does not to the best of my knowledge breach any law of copyright, and has not been taken from the work of others save and to the extent that such work has been cited and acknowledged within the text of my work.

Signed: _____

ID no.: _____

Date: _____

ACKNOWLEDGMENTS

First and foremost I would like to thank my supervisor Prof. Liam Barry for providing me with the motivation and the continual support that was required for the completion of this work. I would also like to thank Dr. Prince Anandarajah for his guidance and advice throughout my time in Dublin City University. My gratitude must also be extended to those whom I collaborated with in the University of Limerick and the Tyndall National Institute.

I would also like to thank all of the past and present members of the Radio and Optical Communications Group for their friendship, constructive advice and support. Without the light hearted atmosphere created within the lab over the past few years, this work would not have been so enjoyable.

Finally I would like to thank my family and Sarah who provided me with their un-wavering commitment, financial support and encouragement throughout my 'eternal' education. It is to you guys that this thesis is dedicated.

Robert Maher,

February 2009

ABSTRACT

Wavelength tuneable transmission is a requirement for future reconfigurable agile optical networks as it enables cost efficient bandwidth distribution and a greater degree of transparency. This thesis focuses on the development and characterisation of wavelength tuneable transmitters for the core, metro and access based WDM networks.

The wavelength tuneable RZ transmitter is a fundamental component for the core network as the RZ coding scheme is favoured over the conventional NRZ format as the line rate increases. The combination of a widely tuneable SG DBR laser and an EAM is a propitious technique employed to generate wavelength tuneable pulses at high repetition rates (40 GHz). As the EAM is inherently wavelength dependant an accurate characterisation of the generated pulses is carried out using the linear spectrogram measurement technique. Performance issues associated with the transmitter are investigated by employing the generated pulses in a 1500 km 42.7 Gb/s circulating loop system. It is demonstrated that non-optimisation of the EAM drive conditions at each operating wavelength can lead to a 33 % degradation in system performance. To achieve consistent operation over a wide waveband the drive conditions of the EAM must be altered at each operating wavelength.

The metro network spans relatively small distances in comparison to the core and therefore must utilise more cost efficient solutions to transmit data, while also maintaining high reconfigurable functionality. Due to the shorter transmission distances, directly modulated sources can be utilised, as less precise wavelength and chirp control can be tolerated. Therefore a gain-switched FP laser provides an ideal source for wavelength tuneable pulse generation at high data rates (10 Gb/s). A self-seeding scheme that generates single mode pulses with high SMSR (> 30 dB) and small pulse duration is demonstrated. A FBG with a very large group delay disperses the generated pulses and subsequently uses this CW like signal to re-inject the laser diode negating the need to tune the repetition rate for optimum gain-switching operation.

The access network provides the last communication link between the customer's premises and the first switching node in the network. FTTH systems should take advantage of directly modulated sources; therefore the direct modulation of a SG DBR tuneable laser is investigated. Although a directly modulated TL is ideal for reconfigurable access based networks, the modulation itself leads to a drift in operating frequency which may result in cross channel interference in a WDM network. This effect is investigated and also a possible solution to compensate the frequency drift through simultaneous modulation of the lasers phase section is examined.

TABLE OF CONTENTS

LIST OF FIGURES

LIST OF TABLES

LIST OF ACRONYMS

ACA	Amplifier Coupler Absorber
APol RZ-DQPSK	Alternate Polarization RZ-DQPSK
ASE	Amplified Spontaneous Emission
AWG	Arrayed Waveguide Grating
BER	Bit Error Rate
CapEx	Capital Expenditure
C-band	Conventional wavelength band
CRZ	Chirp Return-to-Zero
CSRZ	Carrier Suppressed Return-to-Zero
CW	Continuous Wave
DBR	Distributed Bragg Reflector
DCA	Digital Communications Analyser
DCF	Dispersion Compensating Fibre
DCM	Dispersion Compensation Module
DFB	Distributed Feedback
DGD	Differential Group Delay
DI	Delay Interferometer
DPSK	Differential Phase Shift Keying
DQPSK	Differential Quadrature Phase Shift Keying
DS DBR	Digital Supermode Distributed Bragg Reflector
DSF	Dispersion Shifted Fibre
DSL	Digital Subscriber Line
DWDM	Dense Wavelength Division Multiplexing
DXC	Digital Cross-Connects
EAM	Electro-Absorption Modulator
ECL	External Cavity Laser
EDFA	Erbium Doped Fibre Amplifier
ER	Extinction Ratio
ESA	Electrical Spectrum Analyzer
ETDM	Electrical Time Division Multiplexing
FKE	Franz-Keldysh Effect
FP	Fabry-Perot
FROG	Frequency Resolved Optical Gating
FSR	Free Spectral Range
FTTC	Fibre-To-The-Curb
FTTH	Fibre To The Home
FTTN	Fibre-To-The-Node
FWHM	Full Width at Half Maximum
FWM	Four Wave Mixing
GbE	Gigabit Ethernet
GCSR	Grating assisted Co-directional coupler with rear Sampled Reflector
GVD	Group Velocity Dispersion
HDTV	High Definition Television
HFC	Hybrid Fibre Coax
ISI	Inter-Symbol Interference
ITU	International Telecommunication Union
L-band	Long wavelength band
LC FBG	Linearly Chirped FBG
LEF	Linewidth Enhancement Factor
$L_iN_bO_3$	Lithium Niobate

MEMS	Micro Electro-Mechanical System
MG-Y	Modulated Grating Y-branch
MPN	Mode Partition Noise
MQW	Multiple Quantum Well
MZM	Mach-Zehnder Modulator
NOLM	Nonlinear Optical Loop Mirror
NRZ	Non-Return-to-Zero
NZDSF	Non-Zero Dispersion Shifted Fibre
OADM	Optical Add Drop Multiplexer
OBPF	Optical Band Pass Filter
OECD	Organisation for Economic Co-operation and Development
OEO	Optical-to-Electrical-to-Optical
OOK	On-Off Keying
OpEx	Operational Expenditure
OPS	Optical Packet Switched
OSA	Optical Spectrum Analyzer
OSNR	Optical Signal to Noise Ratio
OTDM	Optical Time Division Multiplexing
OXC	Optical Cross Connect
PC	Polarisation Controller
PHASOR	Phased Arrayed
PIC	Photonic Integrated Circuit
PLC	Planar Lightwave Circuits
PLL	Phase Locked Loop
PM	Phase Modulator
PMD	Polarization Mode Dispersion
PON	Passive optical Networks
PPG	Pulse Pattern Generator
PRBS	Pseudorandom Binary Sequence
PSK	Phase Shift Keyed
QCSE	Quantum Confined Stark Effect
RF	Radio Frequency
RMS	Root-Mean-Squared
ROADM	Reconfigurable Optical Add Drop Multiplexer
RZ	Return-to-Zero
SA	Saturable Absorber
SDH	Synchronous Digital Hierarchy
SE	Spectral Efficiency
SG DBR	Sampled Grating Distributed Bragg Reflector
SHG	Second Harmonic Generation
SMF	Single Mode Fibre
SMSR	Side Mode Suppression Ratio
SMSR	Side Mode Suppression Ratio
SOA	Semiconductor Optical Amplifiers
SONET	Synchronous optical Network
SOP	State Of Polarisation
SPM	Self Phase Modulation
SRD	Step Recovery Diode
SSGS	Self-Seeded Gain-Switched
TBP	Time Bandwidth Product
TL	Tuneable Laser
TOJ	Turn On Jitter
TPSR	Temporal Pedestal Suppression Ratio
TTX	Tuneable Transmitter

UDWDM	Ultra Dense Wavelength Division Multiplexing
VCF	Vertical Coupler Filter
VCSEL	Vertical Cavity Surface Emitting Lasers
VDSL	Very high speed Digital Subscriber Line
VMZ	Vertical Mach Zehnder
VoIP	Voice over Internet Protocol
VPI	Virtual Photonics Incorporated
VSB	Vestigial Side-Band
WDM	Wavelength Division Multiplexing
XGM	Cross Gain Modulation
XPM	Cross Phase Modulation

INTRODUCTION

The continued growth in bandwidth hungry services such as VoIP, live video streaming and peer to peer communications has lead to a corresponding increase in consumer demand for high-speed fibre connections, both to the home and to the business. Carriers have employed several multiplexing techniques to accommodate the soaring bandwidth requirements, which are generally offered over optical fibre originally deployed for single or multi-wavelength point-to-point links. Although greater fibre capacities may have alleviated the available bandwidth deficiency, its distribution has become rather cumbersome in today's opaque networks. The need for a more dynamic optical network is therefore becoming more apparent as it is capable of offering greater agility, cost efficiency and transparency. Such networks could enable reduced lead times for the introduction of new services and also allow for the dynamic allocation of stranded or locked bandwidth within the network, thus resulting in fewer lost revenue opportunities and less network management.

A fundamental component for the realisation of such reconfigurable agile optical networks is the wavelength tuneable transmitter. The requirements of high-speed optical transmitters such as data rate, modulation format or transmission distance, varies depending on the application it is intended for. Therefore, various transmitter configurations must be developed for each application and the characterisation of such devices is critical to ensure that acceptable levels of system performance are maintained. This thesis investigates three different transmitters capable of operating in long, medium and short haul reconfigurable optical networks. The development of each transmitter and their respective characterisation requirements is outlined in detail.

Main Contributions

The main contributions of this work are:

- Development and characterisation of a widely tuneable RZ transmitter for long haul applications – The combination of a widely tuneable laser and an electro-absorption modulator provide an ideal source for high-speed stable pulse generation. However, as the characteristics of the carved pulses are dependant on the EAM drive conditions, an extensive pulse analysis is carried out using the linear spectrogram measurement technique. The performance of the EAM based pulse source is demonstrated by implementing the RZ transmitter in a 1500 km transmission system. It is shown that the optimisation of the EAM drive

conditions greatly increases the performance uniformity of the pulse source over a wide wavelength range and also enhances the obtainable transmission reach.

- Development of an all-optical technique to achieve high quality pulse generation for metro based applications – Gain-switching is one of the most simple and cost efficient techniques employed to generate short optical pulses at data rates up to 10 Gb/s. However, inherent impairments associated with this method are SMSR degradation and large timing jitter. Therefore, a novel self-seeding technique is investigated to increase the temporal and spectral purity of such pulses. It is demonstrated that a highly linearly chirped grating can be used to disperse the generate pulses, thus providing a CW like signal for re-injection into the gain-switched laser. This effectively negates the need to tune either the laser cavity length or the pulse repetition rate for optimum gain-switching performance. Pulses with 30 ps durations and side mode suppression ratios of greater that 30 dB over a range of operating frequencies are demonstrated.
- Development of a widely tuneable NRZ transmitter for access based optical networks – A widely tuneable NRZ transmitter, comprising of a directly modulated SG DBR laser is proposed. One inherent problem with this transmitter is that the direct modulation itself causes a time dependant drift in the carrier frequency. Therefore the frequency drift of a commercially available TL module is investigated and the effect it has on DWDM performance is also characterised. A novel compensation technique, which consists of the simultaneous modulation of the lasers gain and phase section is also explored and almost complete compensation of the frequency chirp is demonstrated.

Report Outline

This thesis is structured into six chapters as follows:

Chapter 1 outlines the main motivation for both the implementation and future development of optical communications. An overview of the various multiplexing schemes which will be used to increase the capacity of optical networks such as ETDM, OTDM and WDM are presented. Diverse bandwidth distribution is required to effectively utilise the increased capacity provided by such multiplexing schemes. Therefore, reconfigurable network topologies and the fundamental components required for their realisation are also discussed. Finally the topic of modulation formats is investigated.

Chapter 2 mainly focuses on picosecond pulse generation and a description on the critical pulse parameters that are a requirement for medium to long haul applications. The three main pulse generation techniques, mode locking, gain-switching and pulse carving are reviewed. Some of the most common pulse characterisation techniques, such as fast photodetection are discussed, however emphasis is placed on more advanced pulse measurement techniques such as the linear spectrogram measurement scheme. The main impairments experienced during the transmission of such high-speed RZ pulses are also investigated.

Chapter 3 focuses on the development and characterisation of a widely tuneable RZ transmitter, which consists of a tuneable laser and an electro-absorption modulator. The principle operation of an EAM is explored in detail and a complete characterisation of the generated pulses as a function of EAM drive conditions is performed, using the linear spectrogram measurement technique. Performance issues associated with EAM based pulse carvers are investigated by employing the wavelength tuneable pulse source in a 42.7 Gb/s re-circulating loop transmission system. It is demonstrated that the non-optimisation of the EAM drive conditions at each wavelength can lead to a severe degradation in system performance. Finally a system simulation using the Virtual Photonics Incorporated software package shows excellent agreement when compared to the experimental results.

Chapter 4 explores the operation principles of the gain-switching technique in greater detail, including the important pulse parameters associated with this scheme, such as SMSR, jitter, pulse width and frequency chirp. The two methods commonly employed to increase the temporal and spectral purity of gain-switched pulses, self-seeding and external injection is also presented. Experimental work outlining a novel technique, which provides cost efficient cavity length independent self-seeding of a gain-switched FP laser is performed. Pulse widths and suppression ratios of approximately 30 ps and 30 dB respectively are maintained over a continuous repetition rate tuning range from 2.5 to 10 GHz.

Chapter 5 investigates the direct modulation of a widely tuneable laser for implementation in short haul access based optical networks. The requirements and tuning mechanisms of commercially available TLs are discussed in detail, with focus placed specifically on the SG DBR laser. An inherent problem associated with directly modulated sources is the resulting frequency drift experienced at the output of the laser during modulation. Therefore, the magnitude and settling time of this frequency drift from a commercially available TL module is characterised. The impact of this drift on DWDM performance is analysed through BER measurements in a back-to-back

experimental setup. Finally a novel compensation scheme to reduce the frequency chirp of a SG DBR tuneable laser is explored.

Chapter 6 provides a brief summary and analysis of the main work presented in this thesis,

Chapter 1 - Future Agile Optical Networks

1.1 Introduction

Optical fibre based communications is now the only realistic platform capable of providing the bandwidth requirements necessary for modern day telecom and information technology applications. Therefore, the current progress in optical communications is no longer a matter of mere performance increase, but rather of market development [1]. Statistics released by the Organisation for Economic Co-operation and Development (OECD) showed that broadband penetration increased by 18 % within the OECD member countries in year ending 2007. They also illustrated that high speed, all-optical fibre to the home connections accounted for 8 % of all broadband connections in the OECD. The consumer migration from low speed digital subscriber line (DSL) to high speed fibre connections mirrors the exploding growth of bandwidth hungry services such as high definition television (HDTV), live video streaming, voice over IP (VoIP) and peer-to-peer communications.

To accommodate these bandwidth demands carriers have employed several multiplexing techniques to further exploit the bandwidth capabilities of optical fibre. These include wavelength division multiplexing (WDM), optical time division multiplexing (OTDM) and electrical time division multiplexing (ETDM). Although these techniques vastly increase the transmitted data rate, the distribution of this bandwidth has become rather cumbersome in today's static networks. It is therefore perceived that dynamic optical networking could introduce more agile, cost effective systems that offer greater transparency. Such networks could dynamically provision locked or stranded bandwidth to areas in greater need, thereby improving efficiency, scalability and flexibility [2].

This chapter will further discuss the multiplexing techniques employed to increase system capacity, some of the key enabling components for re-configurable agile optical networks and the modulation formats such all-optical networks utilize.

1.2 Multiplexing Techniques for High Speed Networks

Once a single wavelength fibre optic link reaches its upper limit for serial bit transmission, whether that is 10 or 40 Gb/s, the only solution to increase the system capacity is to install a second fibre cable or to use a data multiplexing scheme [3].This can be achieved optically through wavelength division multiplexing and optical time division multiplexing. The most commonly installed technique used to exploit the terahertz bandwidth capacity of optical fibre is WDM and this scheme will become the

primary network layer for future service providers. In order to increase the data rate per WDM channel, it is envisaged that ETDM may replace OTDM at a bit rate of 100 Gb/s (for 100 GbE) or even 160 Gb/s in the future, once high bandwidth (BW) and high gain electrical amplifiers are realised at these data rates. Until such technology is sufficiently developed OTDM will remain an important technique that may be incorporated in hybrid multiplexing schemes combined with WDM. It enables the efficient generation of 160 Gb/s data signals and has the capability to generate terabit per second signals on a single channel with currently available technology [4].

1.2.1 Electrical Time Division Multiplexing

For high capacity optical systems, the cost per transmitted bit per second can be reduced by employing electrical time division multiplexing. This cost reduction could be attributed to smaller power consumption, smaller footprint, reduced management and system complexity [5]. An example of a basic ETDM system is illustrated in Fig. 1.1. Several lower bit rate electrical data signals are aggregated together by temporally multiplexing them into one single line. This combined signal is then electrically amplified before being applied to an optical carrier with the aid of a high speed modulator. The optical signal then travels through the dispersion compensated transmission line before being detected by a high speed photodiode. Electrical clock recovery is performed before the signal is de-multiplexed back into its constituent data tributaries.

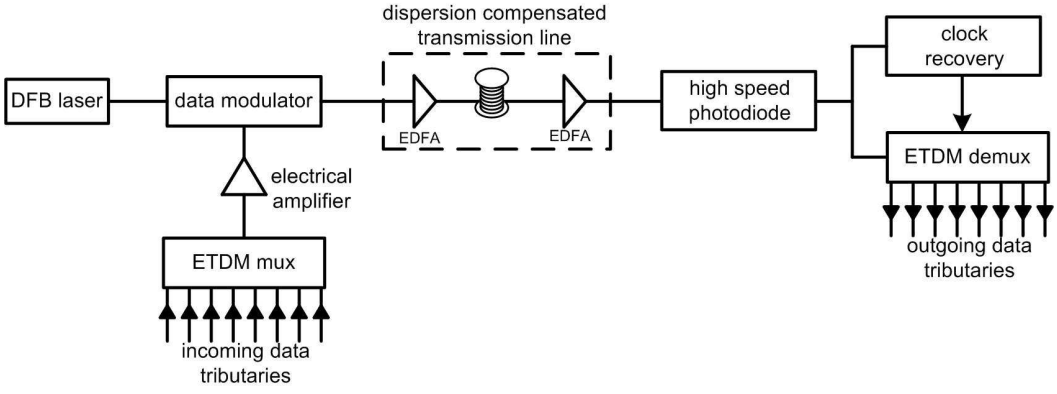

Fig. 1.1. Basic ETDM system.

As 40 Gb/s optical systems are currently being rolled out, the next step in the data rate hierarchy, if SONET/SDH prevails, will be 160 Gb/s. For ETDM applications, this data rate is currently out of reach, due to a number of fundamental issues, namely the current speed of electronics and the availability of high speed electro-optic or electro-absorption modulators. Therefore, 80 Gb/s (twice the current standard data rate) or 100 GbE (100 Gb/s Ethernet), seems likely to be the most interesting applications for future ETDM

systems, although even for these bit rates to be realised numerous problems will have to be resolved [6]. Firstly, for the transmitter, the combined electrical data signal will have to be amplified before being applied to an optical modulator, which typically requires a large modulation voltage swing (3-6 V). The realisation of high-gain amplifiers at data rates above 40 Gb/s has proved to be quite difficult, although there have been demonstrations using amplifiers with 3-dB bandwidths of approximately 60 GHz operating at data rates of 80 and 85 Gb/s [7, 8]. These low driving voltage amplifiers could thus be used in conjunction with an optical modulator that requires a low modulation voltage, for example an electro-absorption modulator (EAM) [9] or a low drive mach-zehnder modulator (MZM) [10].

The receiver side of a high speed ETDM system also suffers from speed limitations. High speed photodiodes capable of detecting 100 Gb/s data signals are only in the research stage [11] and generally require large input powers due to low responsivity, although there have been successful demonstrations of 100 Gb/s receivers [12]. Therefore, binary ETDM is still a number of years away from entering the 100 GbE market as a viable contender. In order to meet the cost points, commercially available optical modulators, electrical amplifiers and photodiodes operating at this data rate need to be introduced and at a reasonable price. Alternatively, a multi-level modulation format could be implemented, such as differential quadrature phase shift keying (DQPSK) where a symbol rate of 50 Gbaud is used to generate a 100 Gb/s data signal [13]. The advantage of this technique is that the electronics will only need to operate at 50 Gb/s to achieve the 100 Gb/s data signal.

1.2.2 Optical Time Division Multiplexing

The principle behind OTDM involves modulating a number of lower bit rate electrical NRZ data signals onto an optical pulse source to generate a corresponding number of RZ data channels, which are all on the same carrier wavelength. These RZ signals are then passively interleaved in the temporal domain providing a combined higher bit rate signal on the one wavelength channel. Fig. 1.2 illustrates the basic setup diagram of a 160 Gb/s OTDM transmission system. The pulse stream is split into four copies which are then individually modulated using four separate modulators driven at a repetition rate of 40 Gb/s [14]. The four modulated signals are temporally delayed relative to each other and are therefore bit interleaved generating a 160 Gb/s signal. The key component in an OTDM transmitter is the short optical pulse source. The optical pulses must exhibit low temporal jitter, high extinction ratio, low amplitude noise and a pulse width that is significantly shorter than the bit period of the multiplexed signal [4]. Gain-switching of a laser diode, pulse carving using an EAM and mode-locking are all excellent candidates

to perform as the short optical pulse source in such an OTDM transmitter as they have the potential to generate short pulses with low timing jitter and low frequency chirp.

The receiver side of the system incorporates a clock recovery unit and an optical demultiplexer. There are various demultiplexing solutions employed to perform this task, for example using either electro-optic modulators or all-optical techniques [14, 15]. When using an optical modulator the gate width must be large enough to demultiplex the entire tributary but must not overlap into an adjacent bit slot, which would inevitably cause degradation in BER performance due to cross channel interference. At data rates beyond 160 Gb/s however, the more sophisticated all-optical demux techniques are required, like a nonlinear optical loop mirror (NOLM) for example [16]. Once the signal is demultiplexed back into its constituent data signals, they are received using individual 40 Gb/s optical receivers.

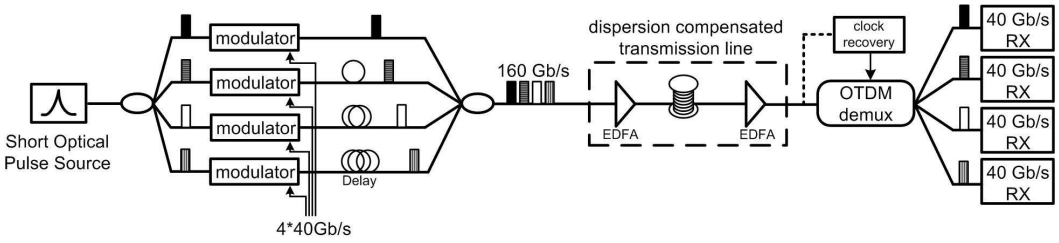

Fig. 1.2. 160 Gb/s OTDM system.

As research currently continues on 100 Gb/s ETDM, such high speed OTDM systems have been demonstrated over a decade ago [17]. Therefore the future for OTDM is to investigate the feasibility of ultra-high speed data transmission and to determine the ultimate capacity for fibre transmission on a single wavelength channel, as demonstrated in [18]. The advantages of such high speed OTDM systems will eventually be eroded however by the substantial increase in system impairments, such as dispersion tolerance and fibre non-linearity. It is therefore envisaged that future OTDM systems may be incorporated in a hybrid scheme combined with another multiplexing technique such as WDM.

1.2.3 Wavelength Division Multiplexing

Wavelength division multiplexing is an alterative technique employed to increase the capacity of a transmission system. The transmission spectrum is sliced up into several different channels, each with a different wavelength carrying a convenient bit rate, similar to that of frequency division multiplexing in radio technology [19, 20]. The spectral efficiency (SE) (measured in bits per second per hertz) with which this bandwidth can be accessed is becoming important as it defines the upper limit on the number of available operational wavelength channels. WDM takes advantage of the fact

that optical sources have very narrow spectral linewidth and can therefore be tightly packed together without causing any cross channel interference when transmitted down a single fibre [21].

The channel spacing (the range between two consecutive peak wavelength emissions) in current WDM systems is as low as 50 GHz as defined by the International Telecommunication Union (ITU) standardised grid. Such systems are known as dense WDM (DWDM) and recent research has demonstrated a much smaller spacing of 25 and 12.5 GHz for ultra DWDM (UDWDM) [22, 23]. The channel spacing in a WDM system has to be chosen carefully in order to avoid crosstalk, therefore maintaining the signals integrity for subsequent retrieval at the receiver side of the network. Fig. 1.3 illustrates a schematic of a simple WDM system. Many different wavelength channels are generated using an array of transponders which simultaneously modulate the light-wave signal with an electrical NRZ data signal. Conventional transponders have incorporated fixed wavelength distributed feedback (DFB) lasers to generate the WDM channels [24], however as optical networks have become more flexible, these fixed wavelength devices have been replaced with more agile transmitters that utilize tuneable lasers.

For efficient multiplexing and demultiplexing of the WDM channels, more advanced technologies have also been used in place of optical couplers and filters. One such component is the arrayed waveguide grating (AWG) [25, 26], which will be discussed in more detail in section 1.5.2. Gain-flattening optical amplifiers which incorporate gain-equalisation filters to reduce the intrinsic wavelength dependant gain curve of an erbium doped fibre amplifier (EDFA) are also required to amplify the WDM signal, overcoming the accumulated attenuation of the fibre link. At the receiver the combined signal is demultiplexed into the constituent wavelengths using a second AWG before they are optically received and processed.

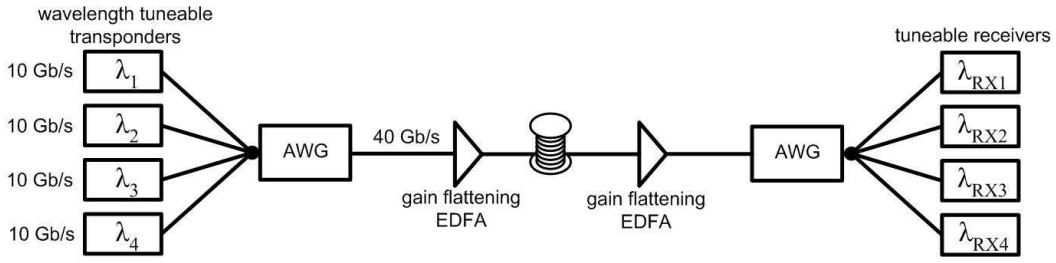

Fig. 1.3. Simple WDM system.

Driven by the desire to augment the capacity demands and increasing cost of scaling SONET/SDH connectivity, WDM has emerged as the primary transport network layer for current and future service providers [27]. In the first quarter of 2008, sales of WDM optical systems overtook sales of SONET/SDH multiplexing equipment for the first

time, due to the continual upstart in IP transformation projects by service providers [28]. The main areas driving this growth in WDM systems are corporate networks, storage networking, consumer broadband (including IPTV and IP video) and service provider mobile backhaul. The per channel bit rate in a WDM system used to accommodate these services is currently limited by the speed of commercially available electronics (40 Gb/s), therefore in order to increase the overall capacity of a DWDM system another multiplexing scheme must be incorporated, like OTDM for example.

1.2.4 Hybrid OTDM/WDM Systems

As previously discussed, one way to currently increase the overall capacity of a WDM system is to increase the per channel data rate. OTDM is an ideal candidate for this hybrid approach as it can offer enhanced bandwidth by placing time multiplexed coding on top of each WDM channel. This technique offers greater transmission capacity without increasing the number of WDM channels and thus further reduces the cost per bit ratio. This technique was first demonstrated in [29] where four wavelength channels each carrying a 100 Gb/s OTDM signal was transmitted over 100 km of dispersion shifted fibre. Such hybrid schemes have advanced substantially in the last decade with multi-terabit systems demonstrated [30, 31]. A common key requirement of such hybrid schemes is the multi-wavelength short optical pulse source. This source must be wavelength tuneable if reconfigurable functionality is required.

1.3 Network Topology

While the optical layer of current transport networks is generally static, the emergence of on demand services has lead to fluctuating traffic patterns that are difficult to predict. The need for more agile, flexible and reconfigurable optical networks is therefore becoming more apparent. As bandwidth requirements continue to soar, this evolution towards next generation optical networks is prevalent to not only the metro and access network, but also the core network infrastructure. Such reconfigurability however, relies on the continual development of various optical components such as tuneable lasers, optical add/drop multiplexers, optical cross connects and wavelength converters.

1.3.1 Network Agility and Scalability

As carrier networks scale to accommodate the significant increases in bandwidth requirements and the fluctuating traffic patterns in today's diverse environment, there exists a new focus for the WDM networks to become truly agile and reconfigurable. These networks must support quick provisioning and frequent reconfiguration in order to meet customer needs [32]. This diverse environment is proving difficult to be served by

current opaque WDM networks that are based on frequent optical-to-electrical-to-optical (OEO) conversions. Such OEO conversions take place for each wavelength and require significant power consumption, therefore rendering them very expensive. In the quest to reduce this cost the optical add drop multiplexer (OADM) was developed [33] to extract the individual channels from a WDM signal for local add/drop or through-pass functionality. However, most OADM systems fixed which wavelengths were to be dropped and added at each specific node in the network, thereby restricting the reconfigurability in response to new service demands [34].

To overcome this problem and to increase the agility and dynamic nature of the optical network, the reconfigurable OADM (ROADM) was developed [35]. ROADMs provide carriers with the ability to provision resources remotely, thereby ensuring that there is sufficient optical capacity in the right areas of the network, where changing traffic patterns and up-take in next generation services are experienced. They also offer the advantage of simpler planning and engineering, thus future proofing the network for any un-forecasted bandwidth requirements. ROADMS have been implemented in all-optical schemes [36] and also in new digital configurations where cheap OEO conversions are implemented using highly dense photonic integrated circuits (PIC) [32].

There are significant cost advantages to both capital expenditure (CapEx) and operational expenditure (OpEx) for carriers that implement such optical cross connect (OXC) based agile optical networks, by negating the need for expensive OEO regeneration for each WDM channel. For a truly transparent reconfigurable optical network however, the following functions should also be supported:

- various advanced modulation formats
- bit-rate specific services
- scalability
- optical performance monitoring

To achieve these goals variable bit rate transmitters and receivers that are capable of tuning to a number of modulation formats are desired to cope with services that may require a number of different bit rates and coding schemes. Network scalability, in terms of bit rate and modulation format is also a key factor for reducing CapEx when new services are required. The reconfigurable optical network will therefore become a key transport platform for future WDM core, metro and access networks [37].

1.3.2 Core Networks and Long Haul Transmission

The core network is the backbone of any optical fibre communication system and is required to have terabit per second transmission capacity that is capable of travelling

several thousand kilometre distances between transmitter and receiver. Legacy backbone long haul networks typically operated with OEO regenerators which converted every wavelength back into the electrical domain, regardless if the traffic was destined for that node or not. The line rate was typically 2.5 Gb/s or in some instances 10 Gb/s providing a total fibre capacity of approximately 50-200 Gb/s, carried on WDM channels over the entire C-band wavelength range [38]. With the continued deployment of fibre to the home (FTTH), access speeds of up to 100 Mb/s per user are envisaged in the near future putting a strain on the core network.

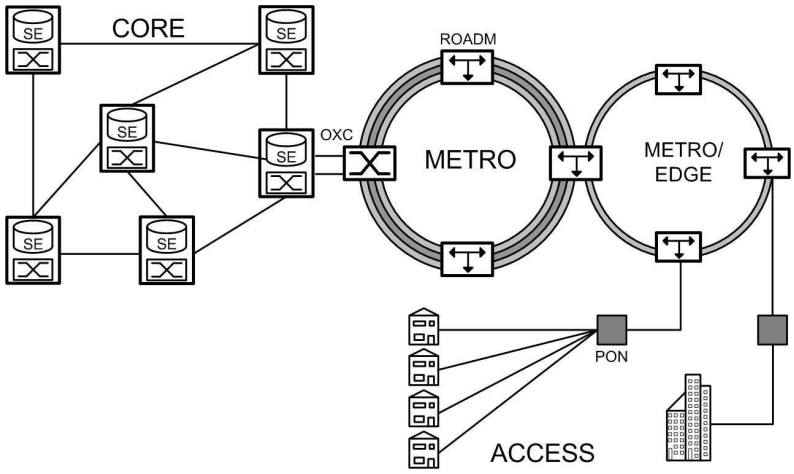

Fig. 1.4. Schematic of telecommunication network.

To accommodate such system requirements the capacity of current backbone networks have been increased dramatically over the past five-to-ten years. The most significant development is the optical by-pass in the head nodes, where traffic can remain in the optical domain if it is not intended for that location, therefore reducing the cost and size of the digital cross-connects (DXC) significantly [2]. The nodes can also be remotely reconfigured providing optimum distribution of services. The number of operating wavelength channels has increased to approximately eighty, covering both the C and L-bands, with 40 Gb/s data rates per channel. This has increased the fibre capacity to over 3 Tb/s, which is a vast improvement on legacy networks [39]. Fig. 1.4 illustrates the basic concept of a telecommunication network displaying the core, metro and access networks. The core network represents an amplified DWDM link interconnected by a number of nodes that combine either all optical switching or digital OEO conversions and some service element, in a mesh configuration. The distance between core nodes can be very large and it is important from a CapEx and OpEx perspective that these distances can be traversed using only optical amplification, thereby avoiding expensive regeneration modules [40].

Long haul high capacity transmission systems are mainly limited (assuming optimum per channel dispersion compensation and gain equalisation is carried out) by accumulated amplified spontaneous emission (ASE) EDFA noise and fibre non-linearity [41]. ASE noise degrades the optical signal to noise ratio (OSNR) of the WDM channels; therefore a larger optical launch power is needed to ensure an adequate OSNR at the receiver [42]. This increase in power combined with long transmission distance results in severe signal distortions due to fibre non-linear effects. To overcome these effects advanced modulation formats have been employed on long haul transmission systems. The initial legacy networks started with the non-return-to-zero (NRZ) format but this was later replaced by the RZ and chirped RZ (CRZ) formats due to their greater robustness to non-linearity's [43, 44]. More recently the RZ differential phase shift keying (DPSK) format has been employed in long haul systems due to its enhanced non-linear tolerance and the 3 dB improvement on receiver sensitivity it offers over other formats. The various advantages and disadvantages of each modulation scheme will be discussed in greater detail in section 1.4. It is important to note however that optical pulses are required for all RZ coding schemes making the wavelength tuneable optical pulse source a fundamental component in long haul core networks, where reconfigurability is employed. A widely tuneable laser combined with a sinusoidally driven EAM is one of the most cost efficient and small form factor devices capable of performing this task and this technique is explored in greater detail in chapter three of this thesis.

1.3.3 Metro and Access Networks

The metropolitan area network (metro) usually forms a ring topology (as in Fig. 1.4) and generally spans a maximum distance of approximately 250 km. This feeder ring is used to transparently deliver signals to local nodes or access rings. The metro network is shared among fewer customers than long haul backbone networks and therefore must utilize more cost effective solutions, while also maintaining network reconfigurability and agility. It must also support a large range of traffic types (i.e., IP, ATM, GbE etc.) that may be operating at a number of alternate data rates [45]. The main impairments that limit the size of a metro network are component insertion losses, noise accumulation, fibre and component dispersion, filter concatenation and fibre non-linearity [46]. Due to the lower transmission distances required for metro networks, low cost technologies can be implemented, such as directly modulated lasers, less precise wavelength control and arbitrary fibre types. Gain-switching of a fabry-perot (FP) laser diode is one of the most simple and cost efficient techniques to directly modulate a lightwave signal. It can provide a low cost, small form factor and single mode pulse source ideal for use in metro networks and will be discussed in greater detail in chapter four.

The optical access network or 'the last mile' is the final communications link between the customer's equipment and the first switching node in the network. It is the most expensive part of the network because it is provided on a unique basis to each customer, with this cost intensifying when rural networks are considered due to the geographical spread of the end users [47]. While these high costs have impeded the direct replacement of the copper subscriber network with fibre, the importance of installing the fibre as close as economically possible to the residences has been widely accepted [48]. In the early 1990's cable TV companies began enhancing their cable TV infrastructure with hybrid fibre coax (HFC) systems which brought fibre to within approximately one kilometre of the end user [49]. This access penetration has now been extended to use fibre-to-the-curb (FTTC) systems, which places a cabinet close to a home at the curb, bringing the fibre to within 150m of the end user. This is also a hybrid technique and is used in conjunction with DSL or very high speed DSL (VDSL) over the existing twisted copper pair infrastructure. There are many variants to this technology such as fibre-to-the-node (FTTN) which bring the fibre to within 1.5 km of the user. For all these hybrid approaches however, as the distance between the fibre plant termination and the end user increases, the bandwidth capacity of the copper based systems decreases.

To ensure the maximum available data rate can be supplied directly to the user, the final part of the access network can be achieved all-optically by employing FTTH. This technology differs from FTTC and HFC in the fact that no active devices and powering are required outside the plant. Passive optical networks (PON) distribute FTTH using point to multi-point passive components, negating the need for any active devices and ultimately reducing cost [50]. FTTH systems must also take advantage of low cost directly modulated NRZ transmitters that are capable of operating over short transmission distances. This application could be realised by employing a directly modulated tuneable laser which would allow for reconfigurable functionality to be achieved. This will become an important aspect in future WDM PON based architectures as it will allow for the dynamic distribution of bandwidth to accommodate the fluctuating and unpredictable traffic patterns in modern optical networks. Today FTTH is becoming a reality with 1.4 million FTTH connections in Europe, 3.4 million in the United States and 27.4 million in the Asian Pacific (APAC) region [51].

1.4 Modulation Formats

In high capacity long haul or even metro WDM systems, it is of great interest to increase the optical launch power prior to transmission to allow for greater distances between optical amplifiers or repeaters, thus reducing the overall cost and complexity of the optical system. The upper limit of the signal power is determined by the fibre non-

linearities, such as cross phase modulation (XPM) and four wave mixing (FWM) due to inter-channel effects and self phase modulation (SPM) due to intra-channel effects [43]. Therefore as optical systems continue to upgrade to base rates of 40 Gb/s, modulation formats and line coding techniques have become an integral topic of research in the attempt to mitigate the linear and non-linear impairments experienced in transmission systems. In the last decade the conventional non-return-to-zero format has been replaced with the RZ and CRZ formats in long haul submarine systems due to their enhanced non-linear performance. However for current and future transoceanic and terrestrial systems operating at even higher bit rates (100 Gb/s or above) more advanced formats are being investigated, namely RZ differential phase shift keying [52].

1.4.1 Standard Formats: NRZ or RZ?

The non-return-to-zero on-off keying (OOK) modulation format is the simplest to generate and detect, making it the most widely deployed format in fibre optic communications today. The NRZ format is generated by modulating the amplitude of an optical carrier in the time domain and can be achieved by applying an electrical NRZ signal directly to a laser diode or by externally modulating a continuous wave (CW) source with an optical modulator. As indicated by the name itself, the optical power does not return to zero between two consecutive “1” bits [53]. An example of a 10 Gb/s optical spectrum and intensity eye diagram is illustrated in Fig. 1.5(a) and (b) respectively. Due to the inherent simplicity of NRZ and hence the subsequent low cost, this format has been extremely popular for high speed systems. However, at 40 Gb/s the NRZ modulation format is generally out-performed by almost all other coding schemes due to its limited robustness to fibre non-linear effects at this data rate, thus restricting the maximum channel launch power.

The RZ modulation format out performs the NRZ coding scheme at higher data rates over longer transmission spans [54] and generally requires 1-3 dB lower optical signal to noise ratio (OSNR) for a given BER due to the reduced impact of inter-symbol interference (ISI) [55]. The broader spectrum of the short optical pulses also generally favours non-linear transmission especially at high data rates of 10 Gb/s and above. The RZ format is generated by employing a second optical modulator (either EAM or MZM) and driving it with a sinusoidal signal at the same repetition rate of the NRZ data. This technique essentially carves the optical pulses out of the NRZ signal. Pulse shaping using an MZM can typically generate three distinctive RZ formats that exhibit different duty cycles (bit slot duration for a given modulation rate):

- Sinusoidally driving a MZM at half the data rate between the minima transmission peaks produces a pulse whenever the drive voltage passes the transmission maximum, producing 33 % duty cycle pulses, Fig. 1.5 (c, d).
- Sinusoidally driving the MZM at the data rate between the minimum and maximum transmission points results in optical pulses with a full width half maximum (FWHM) of 50 % of the bit duration, Fig. 1.5 (e, f).
- Sinusoidally driving the MZM at half the data rate between the maxima transmission peaks produces pulses with 67 % duty cycle and an alternating phase. This format is known as carrier suppressed RZ (CSRZ), Fig. 1.5 (g, h).

CSRZ is characterized by reversing the sign of the optical field at each bit transition and is completely independent of the information carrying part of the signal. Due to the phase inversion between adjacent bits, half the optical '1' bits have positive sign and the other half have a negative sign, resulting in a zero mean optical field envelope. Therefore the optical carrier at the centre frequency disappears. CSRZ generally provides an increased resistance to self phase modulation and has a larger dispersion tolerance than NRZ and RZ systems. Therefore higher input powers per WDM channel can be used providing a greater transmission reach and a larger OSNR [43, 56].

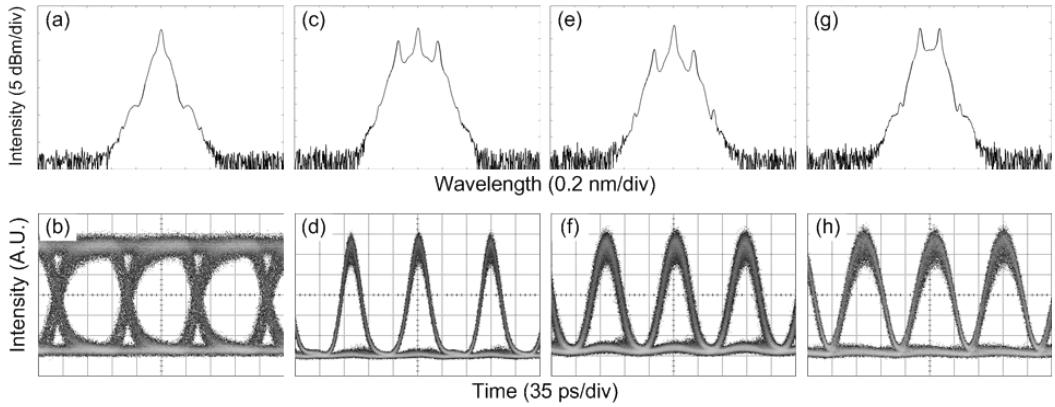

Fig. 1.5. Optical spectra and optical intensity eye diagrams of standard NRZ and RZ modulation formats. (a, b) NRZ-OOK, (c, d) 33 % RZ-OOK, (e, f) 50 % RZ-OOK and (g, h) 67 % CSRZ

Another variant of the RZ modulation format is chirped RZ. This technique utilizes a third optical modulator, which is generally a lithium niobate ($L_iN_bO_3$) phase modulator (PM) which is sinusoidally driven to impart a varying chirp on the optical RZ pulses. Although this technique spectrally broadens the signal bandwidth, which reduces its spectral efficiency, it generally increases its robustness to fibre non-linearity. It has been used predominantly for ultra-long haul transoceanic transmission systems where full periodic dispersion compensation is carried out. As some uncompensated dispersion slope remains across the wavelength band, the ability to generate a tuneable chirp across

the transmitted pulses becomes very important to counteract the varying residual dispersion at each wavelength [57]. Therefore, past submarine transmission systems with capacities of a few hundred gigabits per second and SE's of approximately 0.1 b/s/Hz, utilized the CRZ modulation format. However as today's systems capacities have grown to several terabits per second, advanced modulation formats such as DPSK have been proposed for next generation high speed optical networks [58].

1.4.2 Advanced Modulation Formats

On-off keying modulation formats carry information by modulating the amplitude of the optical carrier, but can also modulate the phase in a non-information bearing way such as CRZ and CSRZ as previously discussed. Conversely phase shift keyed (PSK) formats carry the information in the optical phase itself. Due to the phase insensitivity of direct-detection receivers, the phase of the preceding bit is used as a relative phase reference for demodulation, resulting in the differential phase shift keying modulation format. In the DPSK format, optical power appears in each bit slot (either NRZ or RZ) and is encoded with either a 0 or π phase shift between adjacent bits, by using a continuously oscillating straight line PM or MZM [59]. A PM modulates the phase of the optical signal and a second modulator is used to carve the optical pulses as seen in Fig. 1.6 (a).

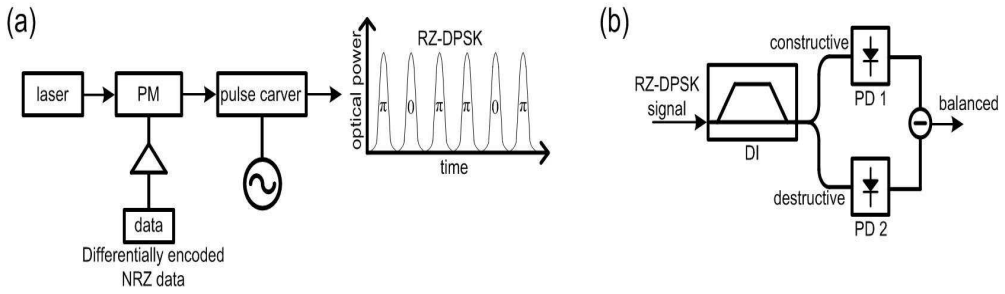

Fig. 1.6. (a) Typical RZ DPSK transmitter and (b) balanced DPSK receiver

Fig. 1.6 (b) illustrates a balanced receiver which is required to detect the phase modulated signal. The RZ DPSK signal initially passes through a delay demodulation stage known as a MZM delay interferometer (DI) which acts as a phase-to-intensity convertor [60]. The signal is essentially split into two paths with one arm delayed by one bit period and reinserted back into the signal path. There is constructive interference if the phase difference between the two interfering portions of the signals is zero and destructive interference if it is π. Hence the signal acts as a phase reference to itself. Both the destructive and constructive signals are detected using two photodiodes and then subtracted giving a balanced electrical output. The advantage of such a complex modulation format and balanced detection scheme is the requirement of a lower OSNR of 3 dB for a given BER over OOK modulation formats. This OSNR advantage can

directly translate into double the obtainable transmission reach and as DPSK has shown to be quite robust to fibre non-linearity [61], it has been employed to demonstrate many transmission records at 10 and 40 Gb/s over the past few years [62, 63].

Even greater transmission distances and higher spectral efficiencies have been obtained by using variants of the DPSK modulation format. Differential quadrature PSK is the only true multilevel modulation format as it transmits two bits per symbol by using four separate phase levels. Therefore, for a 40 Gb/s signal, the symbol rate is only 20 Gsymbol/s, reducing the spectral content by a factor of two making this technique ideal for 50 GHz spaced DWDM systems. This technique has also been advanced to include alternate polarization on every other bit and is known as APol RZ-DQPSK. It offers a greater non-linear threshold over standard DQPSK formats [64, 52].

1.5 Key Components in Reconfigurable Optical Networks

The ability to realise a truly transparent reconfigurable optical network depends on the continual development of dynamic, agile components capable of operating over a large wavelength range, varying bit rates and numerous modulation formats. Tuneable lasers are becoming critical for the future development of agile networks as they can switch between any channels on the ITU grid in the nanosecond time frame. They can also be employed with remotely controlled reconfigurable optical add drop multiplexers or optical cross connects to enable the dynamic provisioning of services, thus increasing the flexibility and efficiency of the DWDM network. A complimentary component for these aforementioned devices is the all-optical wavelength converter which is capable of performing conversions at extremely high bit rates, which cannot be performed in the electrical domain due to the current speed limitation of electronics. Future networks will incorporate all of these components to harness the full capacity of the optical transport layer in a more flexible, efficient and scalable configuration.

1.5.1 Tuneable Laser

Traditional DWDM systems use fixed frequency DFB lasers to generate the broad range of wavelength channels needed for transmission. Therefore dozens of different wavelength specific line cards must be manufactured and inventoried in case a replacement is needed in the future. As the DWDM industry has seen enormous growth, it has been difficult to forecast and supply the line cards with the correct wavelength. As a result, widely tuneable lasers (TL) capable of accessing any channel on the ITU grid were considered as a cost effective solution to fixed frequency devices. Albeit a slightly unglamorous application, tuneable lasers are currently employed to reduce sparing costs and inventory, thus alleviating the difficult forecasting of line card requirements [65].

For future dynamic and reconfigurable networks the tuneable laser is set to play a more critical role. As discussed earlier in this chapter ROADMs are a key component for future agile optical networks. Tuneable lasers are a complimentary component in such ROADM based systems, as they can switch between any channel on the ITU grid to provide a new channel for re-modulation and transmission. Other switching mechanisms which require TLs are photonic cross-connects and fast packet switching for optical packet switched (OPS) networks [66]. The ability for some tuneable lasers to be implemented on photonic integrated circuits with a range of other optical components such as modulators also represents an important trend in optical communications as it reduces the power consumption, size and cost, while also greatly increasing the functionality of the device [67].

There are several key tuneable laser technologies that are vying for supremacy in the telecom industry. Some examples of these include external cavity lasers (ECL), vertical cavity surface emitting lasers (VCSEL), grating assisted co-directional coupler with rear sampled reflector (GCSR) laser and the sampled grating distributed Bragg reflector (SG DBR) laser. Almost all can generate wavelength channels over a large tuning range (> 40 nm) with a high side mode suppression ratio (SMSR) of greater that 40 dB and high output powers.

1.5.2 Arrayed Waveguide Grating

The arrayed waveguide grating, or phased arrayed (PHASOR) grating, is a simple yet ingenious technique to demultiplex several wavelength channels from a single fibre input [68]. It has proved to be of significant importance for several reconfigurable DWDM applications such as optical cross connects, ROADMs and wavelength convertors. AWGs are typically implemented on passive planar lightwave circuits (PLC) using silica on silicon or InP technology, providing a small form factor low loss device [69]. The layout of a typical AWG demultiplexer is illustrated in Fig. 1.7.

The AWG consists of input/output waveguides, two focussing slab regions and a phased array of multiple channel waveguides with a constant path length difference of ΔL between them. The fibre input to the first propagation region carries a number of wavelength channels ($\lambda 1$, $\lambda 2$, $\lambda 3$,..λn) and is split equally into N parts, with each part coupled into one of the waveguides in the phased array. As the optical signals traverse the arrayed waveguides they acquire a different phase delay due to the different path lengths, which is also dependent on the channel wavelength. According to the phase relationship between the same wavelengths from the N waveguides, each wavelength interferes constructively in a specified location after the second free space propagation

region and interferes destructively elsewhere. Therefore by placing a fibre at the position where each wavelength experiences a maximum in constructive interference, the different wavelength channels can be demultiplexed into separate fibres [70].

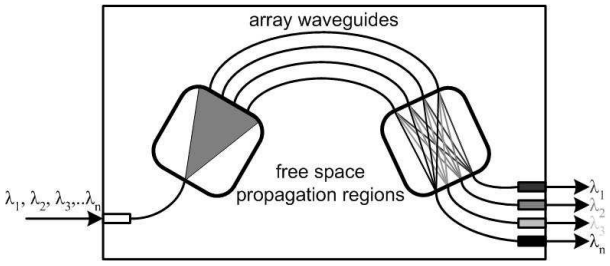

Fig. 1.7. Schematic configuration of an arrayed waveguide grating demultiplexer

1.5.3 Reconfigurable Optical Add/Drop Multiplexer

An optical add/drop multiplexer is a device that allows simultaneous access to all wavelength channels in a WDM system and can be located at any point in the network to provide dynamic provisioning of services [33]. Any incoming channel to the OADM can be removed (dropped), for its content to be transmitted onto another optical fibre. A replacement WDM channel can then be inserted (added) before being multiplexed with the combined signal to resume transmission. A typical OADM usually consists of an input and output port combined with a demultiplexer and multiplexer with some sort of wavelength selective filtration device in between. Fixed OADMs are static switching devices where the channels or band of channels to be dropped or added is usually chosen during the system design phase and reconfigurability is realised through manual intervention at each OADM node, resulting in high OpEx costs.

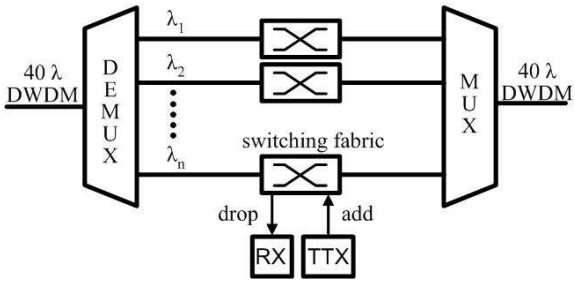

Fig. 1.8. Architecture of a reconfigurable optical add/drop multiplexer

For this reason ROADMs were developed which allow the remote configuration of the add/drop multiplexer providing a more cost efficient method to dynamically provision services. Fig. 1.8 illustrates the basic configuration of a single degree reconfigurable OADM. Each wavelength can perform a through-pass function or can be dropped using a switching fabric device. Channels are added using a tuneable transmitter (TTX) which

incorporates a TL [71]. The implementation of remotely configurable OADMs provides many advantages for network providers including:

- Simple and flexible delivery of any service/wavelength to any node
- Maximum service capacity, thus minimizing the need for costly line overbuilds
- Maximum wavelength capacity to avoid stranded or locked bandwidth
- Remote hands free provisioning, thus reducing OpEx

1.5.4 Optical Cross Connect

Unlike ROADMs, which are generally used to add or drop data from a single WDM path, optical cross connects are required where two or more WDM paths cross, for example at the interconnecting nodes in the core network (as seen in Fig. 1.4). In Fig. 1.9(a) any incoming wavelength channels from the west can be dynamically switched to any output port on the north, east or south nodes. In practical OXC, channels could arrive from any direction and require add/drop functionality, therefore a multi-degree ROADM with cross wavelength selectable switches would be required.

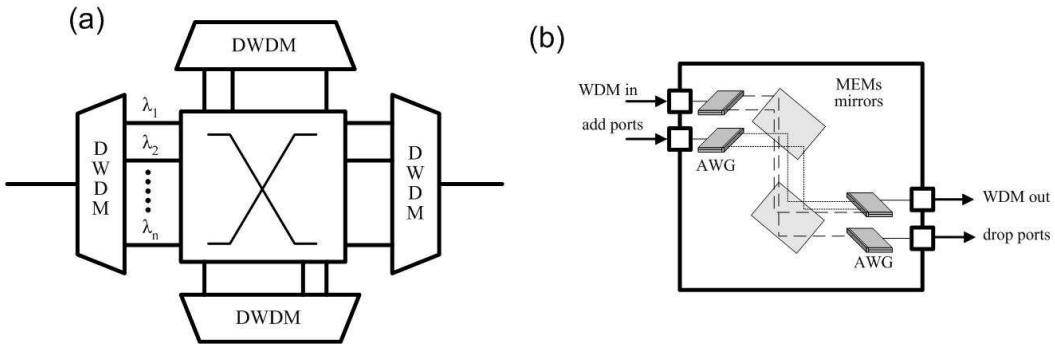

Fig. 1.9. (a) Typical optical cross connect and (b) MEMs based OXC switch

There are two types of optical cross connects that require switching at different granularities. The first is on the fibre level, where all the combined optical WDM channels are rerouted from one fibre to another. This enables the OXC to provide a function of restoration in the optical layer (such as a cable or fibre cut) and for future maintenance of the transmission line [72]. Alternatively the OXC can switch at the wavelength level, where the input signal is demultiplexed before the WDM channels are individually switched to any number of output multiplexers before transmission is resumed. This technique enables individual wavelength paths to be groomed. Many optical cross connect switching fabrics have been proposed such as liquid crystal, lithium niobate, thermo-optic and micro electromechanical system (MEMS) switches [73]. Fig. 1.9 (b) illustrates a typical MEMS switch where the input optical signal is demultiplexed

using an AWG before the individual wavelengths are switched using the 3-D MEMS mirror matrix and multiplexed again using a second AWG prior to transmission.

1.5.5 Wavelength Converter

Wavelength converters are seen as an important component for future reconfigurable optical networks to combat wavelength contention between nodes or network edges. The conversion process allows WDM channels to be spectrally relocated adding to the network flexibility and efficiency. A simple scheme involves using an optoelectronic regenerator in which the signal is received at λ_1 and converted to the electrical domain. The transmitter then modulates the electrical data signal back onto an optical carrier at a different wavelength, λ_2. Such a technique is easy to implement using currently available electrical components but comes at the cost of limited transparency to bit rate and modulation format and is also limited by the speed of electronics [74].

To overcome the limitation of the current speed of electronics and the inherently expensive OEO conversions, all-optical wavelength convertors have been proposed. There are many approaches capable of performing all-optical wavelength conversion including FWM in fibre, XPM or cross gain modulation (XGM) in semiconductor optical amplifiers (SOA) and $L_iN_bO_3$ waveguides [75]. Recently, demonstrations have illustrated operation of a XPM SOA based wavelength converter capable of performing an error free conversion of a 640 Gb/s OTDM signal, thus illustrating the prevalence of an all-optical wavelength converter for future high speed systems [76].

1.6 Summary

Advances in the core backbone network technology over the past decade have shifted the bandwidth and operational bottlenecks into the metro and access networks. However, in order to combat the continual growth of bandwidth hungry applications such as video streaming and HDTV, service providers have began to install FTTH based access networks capable of providing up to 100 Mb/s per customer. Such high speed on demand applications has led to fluctuating and unpredictable traffic patterns, thus placing a strain on current opaque metro and core networks. It is therefore envisaged that next generation core and metro networks will require significant improvements in capacity, reconfigurability and resiliency. Capacity demands will almost certainly be met by DWDM combined with some sort of time multiplexing technique. The choice of which TDM technique will depend on the required transmission speed, cost per bit, performance, power consumption and complexity. The ideology of an all-optical transparent network will also continue to depend on the growth and development of key optical components and advanced modulation formats. In this thesis, novel all optical

components/subsystems are presented for high speed wavelength tuneable pulse generation and processing to meet the demands of future core, metro and access networks.

REFERENCES

[1] E. Desurvire, “Optical communications in 2025,” in Proc. of European Conference on Optical Communication (ECOC), paper Mo2.1.3, Sep. 2005.

[2] M.J. O’Mahony et al., “Future optical networks,” IEEE/OSA J. Lightwave Technol., vol. 24, no. 12, pp. 4684-4696, Dec. 2006.

[3] W. Goralski, “WDM and DWDM,” in Optical networking and WDM, Osborne/McGraw-Hill, 2001.

[4] H-G. Weber et al., “Ultrahigh-speed OTDM-transmission technology,” IEEE/OSA J. Lightwave Technol., vol. 24, no. 12, pp. 4616-4627, Dec. 2006.

[5] E. Lach and K. Schuh, “Recent advances in ultrahigh bit rate ETDM transmission systems,” IEEE/OSA J. Lightwave Technol., vol. 24, no. 12, pp. 4455-4467, Dec. 2006.

[6] E. Lach et al., “Challenges for 100 Gbit/s ETDM transmission and implementation,” in Proc. of Optical Fiber Communications (OFC), paper OWE1, Mar. 2007.

[7] W.S. Lee et al., “Implementation of an 80 Gbit/s full ETDM multi-format ASK optical transmitter,” in Proc. of European Conference on Optical Communication (ECOC), paper We2.2.4, Sep. 2005.

[8] K. Schuh et al., “85.4 Gbit/s ETDM transmission over 401 km SSMF applying UFEC,” in Proc. of European Conference on Optical Communication (ECOC), paper Th4.1.4, Sep. 2005.

[9] H. Fukano et al., “Very low driving-voltage InGaAlAs/InAlAs electroabsorption modulators operating at 40 Gbit/s,” IEE Electron. Lett., vol. 41, no. 4, pp. 211-212, Feb. 2005.

[10] K. Tsuzuki et al., “A 40 Gb/s InGaAlAs-InAlAs MQW n-i-n mach-zehnder modulator with a drive voltage of 2.3 V,” IEEE Photon. Technol. Lett., vol. 17, no. 1, pp. 46-48, Jan. 2005.

[11] A. Beling et al., “Miniaturized waveguide-integrated p-i-n photodetector with 120-GHz bandwidth and high responsivity,” IEEE Photon. Technol. Lett., vol. 17, no. 10, pp. 2152-2154, Jan. 2005.

[12] R. Ludwig et al., “100 Gb/s ETDM receivers,” in Proc. of Lasers and Electro-Optics Society (LEOS), paper TuEE2, Oct. 2007.

[13] M. Daikoku et al., “100 Gbit/s DQPSK transmission experiment without OTDM for 100G Ethernet transport,” in Proc. of Optical Fiber Communications (OFC), paper PDP36, Mar. 2006.

[14] T. Ohara et al., “160 Gb/s OTDM transmission using integrated all-optical MUX/DEMUX with all-channel modulation and demultiplexing,” IEEE Photon. Technol. Lett., vol. 16, no. 2, pp. 650-652, Feb. 2004.

15 T. Morioka et al., “Multiple output, 100 Gbit/s all-optical demultiplexer based on multichannel four-wave mixing pumped by a linearly chirped square wave,” IEE Electron. Lett., vol. 30, no. 23, pp. 1959-1960, Nov. 1994.

[16] N.J. Doran and D. Wood, “Nonlinear optical loop mirror,” OSA Optics Lett., vol. 13, no. 1, pp. 56-58, Jan. 1988.

[17] S. Kawanishi et al., “Fully time-division-multiplexed 100 Gbit/s optical transmission experiment,” IEE Electron. Lett., vol. 29, no. 25, pp. 2211-2212, Dec. 1993.

[18] H.G. Weber et al., “Single channel 1.28 Tbit/s and 2.56 Tbit/s DQPSK transmission,” IEE Electron. Lett., vol. 42, no. 3, pp. 178-179, Feb. 2006.

[19] W. Tomilson, “Wavelength multiplexing in multimode optical fibers,” OSA Appl. Opt., vol. 18, no. 7, pp. 2180-2194, Aug. 1977.

[20] H. Ishio et al., “Review and status of wavelength-division-multiplexing technology and its applications,” IEEE/OSA J. Lightwave Technol., vol. LT-2, no. 4, pp. 448-463, Aug. 1984.

[21] P. Bayvel, “Future high-capacity optical telecommunication networks,” Phil. Trans., Royal Society Lond. A., vol. 358, no. 1765, pp. 303-329, Jan. 2000.

[22] G. Varaille and J.F. Marcerou, “1.8 Tbit/s 6500 km transoceanic NRZ system assessment with industrial margins using 25 GHz channel spacing,” in Proc. of European Conference on Optical Communication (ECOC), paper Th4.1.4, Sep. 2005.

[23] H. Susuki et al., “Application of super-DWDM technologies to terrestrial terabit transmission systems,” IEEE/OSA J. Lightwave Technol., vol. 24, no. 5, pp. 1998-2005, May 2006.

[24] N. Kaida et al., “A series of small form laser modules with driver IC for 10 Gb/s transmission over from 600 m up to 40 km,” in Proc. of Optical Fiber Communications (OFC), paper ThGG72, Mar. 2002.

[25] M.K. Smit, “New focussing and dispersive planar component based on an optical phased array,” IEE Electron. Lett., vol. 24, no. 7, pp. 385-386, Mar. 1988.

[26] H. Takahashi et al., “Arrayed-waveguide grating for wavelength division multi/demultiplexer with nanometre resolution,” IEE Electron. Lett., vol. 26, no. 2, pp. 87-88, Jan. 1990.

[27] J. Berthold et al., “Optical networking: past, present, and future,” IEEE/OSA J. Lightwave Technol., vol. 26, no. 9, pp. 1104-1118, May 2008.

[28] FibreSystems Europe Magazine, pp. 9, Jul./Aug. 2008.

[29] T. Morioka et al., “100 Gbit/s x 4ch, 100 km repeaterless TDM-WDM transmission using a single supercontinuum source,” IEE Electron. Lett., vol. 32, no. 5, pp. 468-470, Feb. 1996.

[30] A. Suzuki et al., “8x160 Gb/s (1.28 Tb/s) DWDM/OTDM unrepeatered transmission over 140 km standard fiber by semiconductor based devices,” in Proc. of European Conference on Optical Communication (ECOC), paper Mo.3.6.1, Sep. 2003.

[31] S. Kawanishi et al., “3 Tbit/s (160 Gbit/s x 19ch) optical TDM and WDM transmission experiment,” IEE Electron. Lett., vol. 35, no. 10, pp. 826-827, May 1999.

[32] S. Melle, “Building Agile Optical Networks,” in Proc. of Optical Fiber Communications (OFC), paper NME2, Feb. 2008.

[33] K. Okamoto et al., “16-channel optical add/drop using silica-based arrayed-waveguide-gratings,” IEE Electron. Lett., vol. 31, no. 9, pp. 723-724, Apr. 1995.

[34] M. Allen et al., “Digital optical networks using photonic integrated circuits (PICs) address the challengers of reconfigurable optical networks,” IEEE Communications Magazine, vol. 46, no. 1, pp. 35-43, Jan. 2008.

[35] C.G.M. Vreeburg et al., “First InP-based reconfigurable integrated add/drop multiplexer,” IEEE Photon. Technol. Lett., vol. 9, no. 2, pp. 188-190, Feb. 1997.

[36] L. Eldada et al., “40-channel ultra-low-power compact PLC-based ROADM,” in Proc. of Optical Fiber Communications (OFC), paper NThC4, Mar. 2006.

[37] A.E. Willner, “Stable and reconfigurable optical networks,” in Proc. of Lasers and Electro-Optics Society (LEOS), paper WFF1, Oct. 2007.

[38] A.A.M. Saleh and J.M. Simmons, “Evolution towards the next-generation core optical network,” IEEE/OSA J. Lightwave Technol., vol. 24, no. 9, pp. 3303-3321, Sep. 2006.

[39] D.G. Foursa et al., “2.56 Tb/s (256 x 10 Gb/s) transmission over 11,000 km using hybrid Raman/EDFAs with 80 nm of continuous bandwidth,” in Proc. of Optical Fiber Communications (OFC), paper FC3-1, Mar. 2002.

[40] D.Z. Chen et al., “New field trial distance record of 3040 km on wide reach WDM with 10 and 40 Gb/s transmission including OC-748 traffic without regeneration,” IEEE/OSA J. Lightwave Technol., vol. 25, no. 1, pp. 28-37, Jan. 2007.

[41] A.N. Pilipetskii, “High-capacity undersea long-haul systems,” IEEE J. Sel. Topics in Quant. Electron., vol. 12, no. 4, pp. 484-496, Jul./Aug. 2006.

[42] T. Li, “The impact of optical amplifiers on long-distance lightwave telecommunications,” in Proc. of the IEEE, vol. 81, no. 11, Nov. 1993.

[43] B. Bakhshi et al., “Comparison of CRZ, RZ and NRZ modulation formats in a 64 x 12.3 Gb/s WDM transmission experiment over 9000 km,” in Proc. of Optical Fiber Communications (OFC), paper WF4-1, Mar. 2001.

[44] C.R. Davidson et al., “1800 Gb/s transmission of one hundred and eighty 10 Gb/s WDM channels over 7000 km using the full EDFA C-band,” in Proc. of Optical Fiber Communications (OFC), paper PD25-1, Mar. 2000.

[45] A.A.M. Saleh and J.M. Simmons, “Architectural principles of optical regional and metropolitan access networks,” IEEE/OSA J. Lightwave Technol., vol. 17, no. 12, pp. 2431-2448, Dec. 1999.

[46] N. Madamopoulos et al., “Study of the performance of a transparent and reconfigurable metropolitan area network,” IEEE/OSA J. Lightwave Technol., vol. 20, no. 6, pp. 937-945, Jun. 2002.

[47] M.G. Foxton and M.W. Trussler, “Optical access networks in rural telecommunications,” in Proc. of International Conference on Rural Telecommunications, pp. 101-106, May 1988.

[48] P.W. Shumate, “Fiber-to-the-home: 1977-2007,” IEEE/OSA J. Lightwave Technol., vol. 26, no. 9, pp. 1093-1103, May 2008.

[49] A. Paff, “Hybrid fiber/coax in the public telecommunications infrastructure,” IEEE Communications Magazine, vol. 33, no. 4, pp. 40-45, Apr. 1995.

[50] R.E. Wagner et al., “Fiber-based broadband-access deployment in the united States,” IEEE/OSA J. Lightwave Technol., vol. 24, no. 12, pp. 4526-4550, Dec. 2006.

[51] The 2008 half year FTTH council global rankings, Jul. 2008 [Online]. Available: http://www.ftthcouncil.eu.

[52] G. Charlet, “Progress in optical modulation formats for high-bit rate WDM transmissions,” IEEE J. Sel. Topics in Quant. Electron., vol. 12, no. 4, pp. 469-483, Jul./Aug. 2006.

[53] P.J. Winzer and R.J. Essiambre, “Advanced optical modulation formats,” in Optical fiber telecommunications V, B: Systems and networks, Academic Press, Elsevier, 2008.

[54] R. Ludwig et al., “Experimental comparison of 40 Gb/s RZ and NRZ transmission over standard singlemode fibre,” IEE Electron. Lett., vol. 35, no. 25, pp. 2216-2218, Dec. 1999.

[55] P.J. Winzer and A. Kalmar, “Sensitivities enhancement of optical receivers by impulsive coding,” IEEE/OSA J. Lightwave Technol., vol. 17, no. 2, pp. 171-177, Feb. 1999.

[56] A. Hdzic et al., “Alternative modulation formats in N x 40 Gb/s WDM standard fiber RZ-transmission systesms,” IEEE/OSA J. Lightwave Technol., vol. 20, no. 4, pp. 598-607, Apr. 2002.

[57] R.-M. Mu et al., “Dynamics of the chirped return-to-zero modulation format,” IEEE/OSA J. Lightwave Technol., vol. 20, no. 1, pp. 47-57, Jan. 2002.

[58] A.H. Gnauck et al., “High-capacity optical transmission systems,” IEEE/OSA J. Lightwave Technol., vol. 26, no. 9, pp. 1032-1045, May 2008.

[59] A.H. Gnauck et al., “Optical phase-shift-keyed transmission” IEEE/OSA J. Lightwave Technol., vol. 23, no. 1, pp. 115-130, Jan. 2005.

[60] E.A. Swanson et al., “High sensitivity optically preamplified direct detection DPSK receiver with active delay-line stabilization,” IEEE Photon. Technol. Lett., vol. 6, no. 2, pp. 263-265, Feb. 1994.

[61] A.H. Gnauck et al., “Comparison of modulation formats for 42.7 Gb/s single-channel transmission through 1980 km of SSMF,” IEEE Photon. Technol. Lett., vol. 16, no. 3, pp. 909-911, Mar. 2004.

[62] J.-X. Cai et al., “A DWDM demonstration of 3.73 Tb/s over 11000 km using 373 RZ-DPSK channels at 10 Gb/s,” in Proc. of Optical Fiber Communications (OFC), paper PD22-1, Mar. 2003.

[63] A.H. Gnauck et al., “2.5 Tb/s (64 x 42.7 Gb/s) transmission over 40 x 100 km NZDSF using RZ-DPSK format and all-Raman-amplified spans,” in Proc. of Optical Fiber Communications (OFC), paper FC2-1, Mar. 2002.

[64] P.J. Winzer et al., “Advanced modulation formats for high-capacity optical transport networks,” IEEE/OSA J. Lightwave Technol., vol. 24, no. 12, pp. 4711-4728, Dec. 2006.

[65] L.A. Coldren et al., “Tunable semiconductor lasers: A tutorial,” IEEE/OSA J. Lightwave Technol., vol. 22, no. 1, pp.193-202, Jan. 2004.

[66] G. Fish, “Tunable lasers and their impact on optical networks,” [Online], CommsDesign: An EE Times Community, Sep. 2001. Available: http://www.commsdesign.com.

[67] D.A. Ackerman et al., “Telecommunication Lasers,” in Optical fiber telecommunications IV, A: Components, Academic Press, Elsevier, 2002.

[68] M.K. Smit, “New focusing and dispersive planar component based on an optical phased array,” IEE Electron. Lett., vol. 24, no. 7, pp. 385-386, Mar. 1988.

[69] M.K. Smit, “Progress in AWG design and technology,” in Proc. of IEEE/LEOS workshop on fibres and optical passive components, pp. 26-31, Jun. 2005.

[70] S.V. Kartalopoulos, “Optical components,” in DWDM: Networks, devices and technology, IEEE Press, Wiley-Interscience, 2003.

[71] J. Homa and K. Bala, “ROADM architectures and their enabling WSS technology,” IEEE Aplications & Practice: Optical Communications and Networks, pp. 150-154, Jul. 2008.

[72] H. Tsushima et al., “Optical cross-connect system for survivable optical layer networks,” Hitachi Review, vol. 47, no. 2, pp. 85-90, 1998.

[73] V. Aksyuk et al., “Low insertion loss packaged and fibre connectorised MEMS reflective optical switch,” IEE Electron. Lett., vol. 34, no. 14, pp. 1413-1414, Jul. 1998.

[74] G.P. Agrewal, “Multichannel lightwave systems,” in Fiber-Optic Communication Systems: Second Edition, Wiley-Interscience, 1997.

[75] D.A. Reid et al., “Characterisation of a turbo-switch SOA wavelength converter using spectrographic pulse measurement,” IEEE J. Sel. Topics in Quant. Electron., vol. 14, no. 3, pp. 841-848, May/Jun. 2008.

[76] M. Galili et al., “640 Gbit/s wavelength conversion,” in Proc. of Optical Fiber Communications (OFC), paper OTuD4, Feb. 2008.

Chapter 2 - High Speed Optical RZ Transmitters

2.1 Introduction

Wavelength tuneable picosecond pulse generation is of paramount importance for the development of future dynamically reconfigurable high speed communication systems. As network carriers begin to deploy systems operating at speeds up to 40 Gb/s, more advanced modulation formats that exhibit a greater tolerance to transmission line impairments are required. It has been demonstrated that almost any variant of the RZ coding scheme offers enhanced transmission performance over the NRZ format [1]. Therefore, stable picosecond pulses that exhibit a high degree of spectral and temporal purity will become a pre-requisite for future high speed core or even metro based networks. There are many pulse generation techniques that are capable of producing wavelength tuneable picosecond pulses such as, mode-locking of a semiconductor laser, pulse carving and gain-switching. However, before they can be implemented in a high speed system, a number of critical pulse parameters must be met. These requirements include high SMSR, high temporal pedestal suppression, low timing jitter and low frequency chirp.

While most of the critical pulse parameters can be assessed using conventional photodetection monitoring schemes, the phase of the optical pulses cannot. The full electric field characterisation of a short optical pulse is vital prior to transmission in order to verify the effects of impairments such as chromatic dispersion and fibre non-linearity. Therefore more sophisticated pulse characterisation techniques such as frequency resolved optical gating and the linear spectrographic technique are required. This chapter therefore presents an overview of the most common pulse generation techniques and the vital parameters the pulses must adhere to before being implemented in a high speed system. Several pulse characterisation methods are considered and the prevalent effects that limit the transmission performance of such pulses are also explored.

2.2 Important Picosecond Pulse Parameters

Picosecond optical pulses are a fundamental requirement for long haul optical systems that utilise any variant of the return-to-zero modulation format. They are also a key component for high speed OTDM systems which require extremely narrow pulses suitable for temporal interleaving. Before any optical pulse can be considered for such systems they must first adhere to a number of critical parameters, such as pulse width, spectral width, timing jitter, frequency chirp, side mode suppression ratio (SMSR),

extinction ratio and temporal pedestal suppression ratio (TPSR) [2]. The importance of each pulse parameter will be discussed in greater detail in this section.

2.2.1 Pulse Width and Spectral Width

The duration of an optical pulse is defined as the full width at half the maximum (FWHM) power and determines the upper limit on transmission capacity for a high speed OTDM system. It has been demonstrated that a duty cycle of less than 40 % is required to reduce penalties due to the incoherent crosstalk between neighbouring OTDM channels. This duty cycle is also generally accepted for serial per channel transmission in a high speed WDM system. Therefore, pulse widths of approximately 9 and 2 ps would be required for optimum transmission in 40 and 160 Gb/s systems respectively. For an OTDM system, as the pulse width decreases the obtainable overall transmission capacity increases because more pulse trains can be physically interleaved generating a higher bit rate signal [3]. As a result there has been extensive research over the past two decades into ultra-short optical pulse generation for communications applications in the pico and femtosecond range, leading to demonstrations of terabit per second systems utilizing pulses with durations less than 500 fs [4, 5].

The optical spectrum illustrates the corresponding frequency components of an optical pulse and is an extremely important parameter when considering WDM or OTDM transmission. The spectral width determines the upper limit on transmission distance due to the influence of fibre dispersion, which is measured in ps/nm.km and is intrinsically dependant on the spectral width itself. Therefore if the spectral width of an optical pulse is greater than its minimum value, the effect of fibre dispersion will be increased, leading to crosstalk between adjacent time slots ultimately manifesting as degradation in system performance. For WDM systems it is also important to have narrow spectral widths to decrease channel spacing, thus increasing system capacity and to reduce the effects of cross channel interference. As a result pulses that exhibit a minimum spectral width, known as transform limited, are generally required for high speed transmission. The time bandwidth product (TBP) is a measurement which illustrates how transform limited the pulses are and is calculated by multiplying the FWHM of the pulse (s) by the spectral width (Hz) which is also measured at the FWHM. As this product is a function of pulse shape, the TBP for a Gaussian and a sech^2 pulse are 0.441 and 0.315 respectively [6].

2.2.2 Timing Jitter

Timing jitter is defined as a short term variation of the position of an optical pulse from its ideal position in time. Fig. 2.1 displays a short optical pulse which exhibits a large temporal jitter and a pulse with a small value of jitter. Large temporal jitter can result

from a number of different processes such as large carrier phase noise, direct modulation (gain-switching), walk off between the data and control signals in an optical receiver, the Gordon-Haus effect (soliton transmission) or through intersymbol interference[7,8,9,10]. Jitter can cause bit errors by preventing the clock recovery circuit in the receiver from sampling the signal at the optimum instant in time and can also prove prohibitive when demultiplexing in high speed systems. Although its effect may be approximately negligible at low dates (i.e. 2.5 Gb/s), it becomes extremely important at data rates greater than 40 Gb/s where pulse-to-pulse timing jitter becomes the dominant process. Experiments and theory have illustrated that the tolerable timing jitter should be less than one twelfth of the switching window width to achieve a bit error rate (BER) of 10^{-9}, when using a 20 % duty cycle pulse [11]. Thus, for a 40 Gb/s system the root-mean-squared (RMS) jitter must remain below 2 ps for a 25 ps switching window to achieve error free performance. This requirement is more stringent at 160 Gb/s where the RMS jitter must remain below 500 fs for a 6.25 ps switching window.

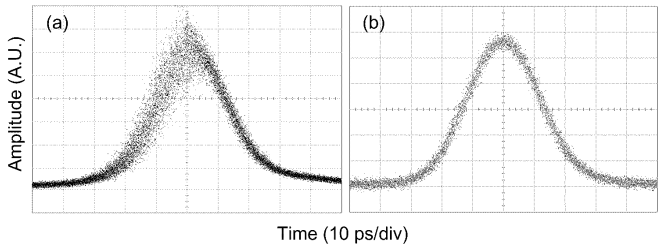

Fig. 2.1. Optical pulse illustrating (a) large temporal jitter and (b) low temporal jitter

2.2.3 Frequency Chirp

Frequency chirp is a variation of the instantaneous frequency of an optical pulse and can be acquired when a pulse propagates in optical fibre because the different frequency components of the pulse travel at slightly different speeds due to the group velocity dispersion (GVD) of fibre. In standard single mode fibre (SMF) the red components travel faster than the blue components, thus a time delay between the different spectral components is experienced leading to frequency chirp. This chirp, due to the fibre transmission is linear and the accumulated pulse broadening will eventually cause ISI resulting in a closed optical eye and poor BER performance. Conversely, in the anomalous dispersion regime however, the blue components of the pulse travel faster than the red [12].

Frequency chirping also occurs in directly modulated lasers and in some external modulators. Chirp due to directly modulated sources arises from refractive index changes in the active layer caused by carrier density modulation, while for an EAM for example, an alternate chirp profile is exhibited at each bias point due to the Kramer-Kronig relation

[13]. This chirp is deemed deleterious for optical communications systems as it limits the transmission distance by enhancing the broadening of the data bits. However if the sign and magnitude of the frequency chirp can be tuned, it can have an opposing effect to GVD, thereby achieving greater transmission reach. This in essence is similar to the CRZ modulation format discussed in section 1.4.1 and can be achieved by tuning the bias and radio frequency (RF) drive applied to an EAM [14]. Fig. 2.2 illustrates a short optical pulse with both negative and positive chirp profiles obtained from a sinusoidally driven EAM by slight adjustment of the bias voltage.

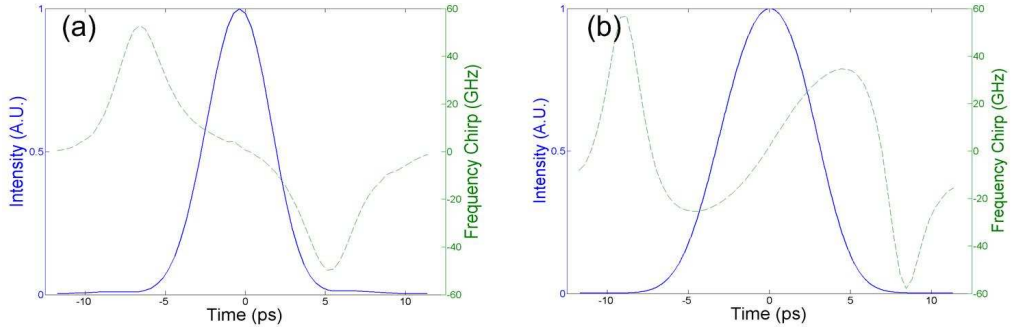

Fig. 2.2. Optical pulse exhibiting, (a) negative frequency chirp and (b) positive chirp

2.2.4 SMSR and TPSR (Extinction Ratio)

Side mode suppression ratio is defined as the ratio of the intensity of the main spectral lasing mode to the intensity of the next largest mode and is a critical parameter associated with optical pulse propagation in communication systems. In WDM networks, signal lasers that exhibit a poor SMSR contain modulated side modes that propagate throughout the network and destructively interfere with adjacent WDM channels leading to cross talk. This interference generates a beat noise which can seriously degrade the BER performance of the optical system by manifesting as temporal jitter, thus decreasing the opening of the received optical eye. This potential impairment from poor SMSR is suppressed by using sources with a suppression ratio greater than 30 dB [15, 16].

Mode partition noise (MPN) is also a limiting factor when considering CW or pulsed sources for optical communications systems. It is caused by random fluctuations between the longitudinal modes in multimode or nearly single mode lasers, combined with optical filtration and/or dispersion [17]. For a gain-switched pulse source for example, as the multi-mode pulse propagates through optical fibre the spectral components travel at different speeds and hence spread out in the temporal domain. The random fluctuations between these modes will manifest as intensity noise, thus reducing system performance. To overcome the prohibitive effect of MPN the SMSR must be increased to greater than 30 dB, as seen in Fig. 2.3 (a) [18].

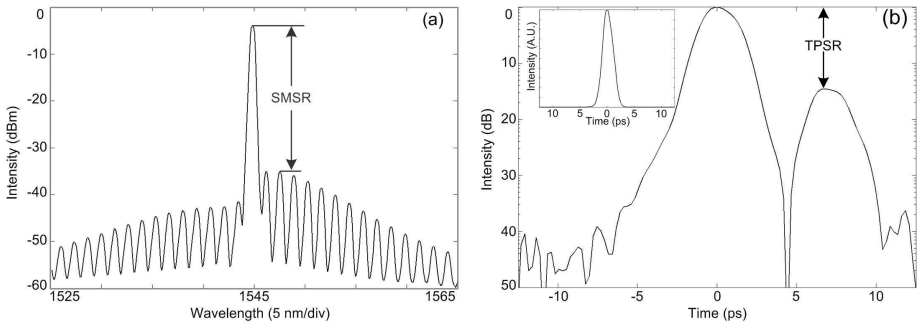

Fig. 2.3. (a) SMSR of an externally injected FP laser and (b) TPSR of a mode-locked source

The optical pulse extinction ratio (ER) is defined as is the ratio of the pulses on-state power to the off-state power. As most pulse generation techniques create a 'satellite' pulse or pedestal, the ER can be referred to as the temporal pedestal suppression ratio. If an optical pulse is employed in a high speed OTDM system the TPSR becomes extremely important to maintain an optimum level of system performance. If the TPSR is two small, the pedestal may interact with the adjacent OTDM channel thus causing interference. As a result, this interaction between the pulses pedestal and the next OTDM channel generates coherent interference noise, thus degrading BER performance [19]. In order to suppress this effect a TPSR of greater than 30 dB is required [20]. Inset of Fig. 2.3 (b) illustrates the pulse intensity profile of a mode-locked laser source. The pulse is represented on a linear scale and appears to have a good ER. However, if presented in a logarithmic scale (Fig. 2.3), the TPSR is approximately 16 dB. This poor level of extinction would cause severe performance degradation in an OTDM system. It is therefore of paramount importance to accurately characterise the generated pulses for both TPSR and SMSR.

2.2.5 Wavelength Tunability

Widely wavelength tuneable pulse sources are becoming a key component for future dynamically reconfigurable long haul and regional optical networks. There are several techniques available to generate short tuneable pulses. For example, the emission wavelength of a directly or externally modulated DFB laser can be thermally tuned over approximately three to four nanometres, therefore an array of 8-10 DFB lasers with central wavelength spaced approximately 4 nm apart can access most wavelengths on the C-band ITU grid. Alternatively a number of FP modes can be seeded in a gain-switched source providing tunability over approximately 30 nm. As with the DFB laser, more than one FP laser mode spectrum can be placed side by side offering an even greater tuning range [21]. Mode locking of a semiconductor laser with an integrated wavelength selective device can also provide widely tuneable short optical pulses, however the most common technique and the simplest is to combine a tuneable laser with a sinusioally

driven modulator [22]. The ability to generate stable wavelength tuneable pulses with high TPSR, tuneable chirp, small PW and large SMSR will be examined throughout the remainder of this thesis.

2.3 Pulse Generation Techniques

One of the key requirements of a dynamically reconfigurable OTDM or long haul WDM network is the wavelength tuneable optical pulse source, since they provide several of the important functions necessary for high speed systems, such as sources for optical modulation, demultiplexing, optical clocks and optical logic [23]. As previously discussed, a pre-requisite for a short optical pulse source is its ability to generate pulses that are both temporally and spectrally pure, but also provide the greatest resilience to transmission impairments such as, chromatic dispersion and fibre non-linearity. There are several established pulse generation techniques that are capable of performing this task with the most common being, mode-locking, pulse carving and gain-switching.

2.3.1 Mode-Locking of a semiconductor laser

When a conventional semiconductor laser is operating in its normal regime, it will resonate over all the frequencies in the cavity where the gain of the medium can overcome the losses. These modes are known as longitudinal modes and are separated by a finite frequency which is a function of the round trip time of the cavity, given by: $\Delta f = (c/2nL)$, where c is the speed of light and L is the cavity length. These modes are continuously competing for gain by stimulated emission and therefore experience large fluctuations in relative amplitude and phase. As a result of this, the output of the laser diode will fluctuate with time in an uncontrolled manner. If the phase relationship between the modes is fixed and the frequency spacing remains constant, a constructive beating occurs at a specific instant in time between the phase locked modes. At the same instant destructive beating occurs everywhere else in the cavity except at a short distance from the point of constructive interference. The greater the number of modes the shorter this distance becomes and hence the shorter the optical pulses become. When the laser is in this regime it is said to be mode-locked [24, 25]. The mode-locking condition of a semiconductor laser can be induced by implementing a passive or active approach [26].

Passive mode-locking is performed by inserting a saturable absorber (SA), which inherently has a non-linear transmission function, into the laser gain medium. The SA effectively attenuates light with low incident intensity through absorption and passes light with high incident intensity. Initially, if the unsaturated gain in the cavity is greater than the losses and the oscillating modes have unequal phase, the longitudinal modes will experience a strong fluctuation in their relative amplitudes. As the power increases the

strongest intensity maxima will begin to saturate the SA, thus experiencing the lowest amount of attenuation and therefore will begin to eliminate the lower intensity modes by acquiring all the gain of the medium. This process results in the production of a train of optical pulses which travel back and forth within the cavity and have a duration that is inversely proportional to the spectral width of the mode distribution supporting them [27]. Fig. 2.4 (a) illustrates the combination of the laser gain medium and the non-linear transmission of the SA, which leads to the creation of an optical pulse. Passive mode-locking can generate very short and stable optical pulses, however it can be problematic to initiate the mode-locking regime as it depends on random noise fluctuations [28].

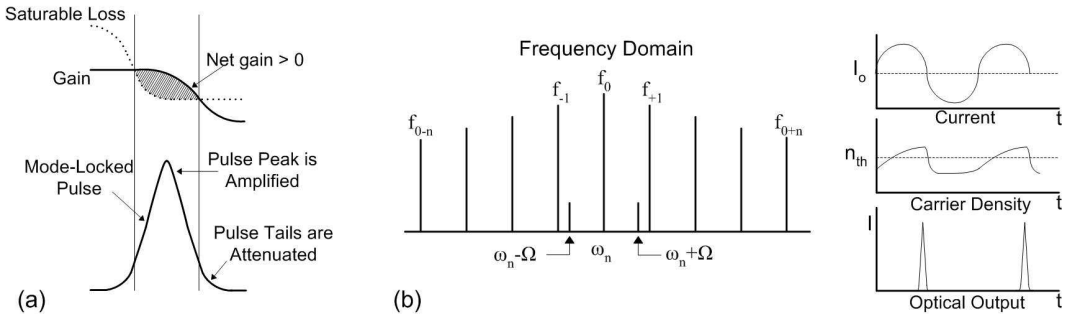

Fig. 2.4. (a) Passive mode-locking with a SA and (b) active-mode locking

Active mode locking is achieved by modulating the loss of the diode laser at a frequency that is equal to or a harmonic of the round trip frequency of the laser cavity. As the modulator is driven by an external power source, the resulting sidebands will lie on top of the existing longitudinal modes or in their near vicinity. As a result the longitudinal modes tend to injection lock with the sidebands causing a global phase locking over the entire spectral distribution, as seen in Fig. 2.4 (b). By correctly adjusting the frequency applied to the loss modulator to approximately one round trip time of the cavity, light that undergoes loss at one instant in time will experience the same loss again after the next round trip. Therefore, all the light will experience a loss; except for the portion that passes through the modulator when its loss is zero. In this way the same portion of light travels back and forth in the cavity thus producing a short optical pulse [25].

Hybrid mode-locking combines a mixture of both passive and active mode-locking. This technique offers the ability to generate short optical pulses similar in width to that achieved through passive locking and can also improve the pulse jitter by bringing it close to that of the applied electrical signal. Wavelength tunability of mode locked pulses can be achieved by placing a tuneable wavelength selective device, such as a diffraction grating, inside the cavity arrangement. Although the mode-locking technique can generate very short pulses that make it ideal for OTDM applications, it suffers from a complex cavity arrangement as just discussed which increases the cost of mode-locked

pulse sources. Another major drawback is the limitation to mode-locking at a harmonic of the cavity frequency due to its fixed cavity length [29].

2.3.2 Pulse Carving using an External Modulator

Pulse carving is an alternative pulse generation technique that requires an external modulator to gate CW light. This pulse generation technique is based on the non-linear transmittance of the modulator as a function of applied voltage and can generate very short pulses at high bit rates (> 40 Gb/s) that can be implemented in high speed long haul networks. The most common intensity modulators are the MZM and the EAM. A MZM is typically constructed using lithium niobate and basically consists of an input straight line waveguide, following by an input Y-branch waveguide that splits the light equally onto an interferometer consisting of two arms. The two waves are then combined from the interferometer arms using an output Y-branch, which is followed by the output straight waveguide. When no voltage (V=0) is applied to one of the interferometer arms, both the input waves propagate with the same amplitude and phase, recombining constructively at the output. Upon an applied voltage (to one arm) the refractive index of the waveguide changes, through a process known as the electro-optic effect, causing a phase difference between the two waves. When the applied voltage equals the value required for a π phase shift (V_π), the waves destructively interfere at the output port and the light amplitude becomes zero. When the applied voltage is between V and V_π, the phase difference and hence the output power varies [30]. An example of the non-linear transmittance of a MZM as a function of applied bias voltage is illustrated in Fig. 2.5 (a).

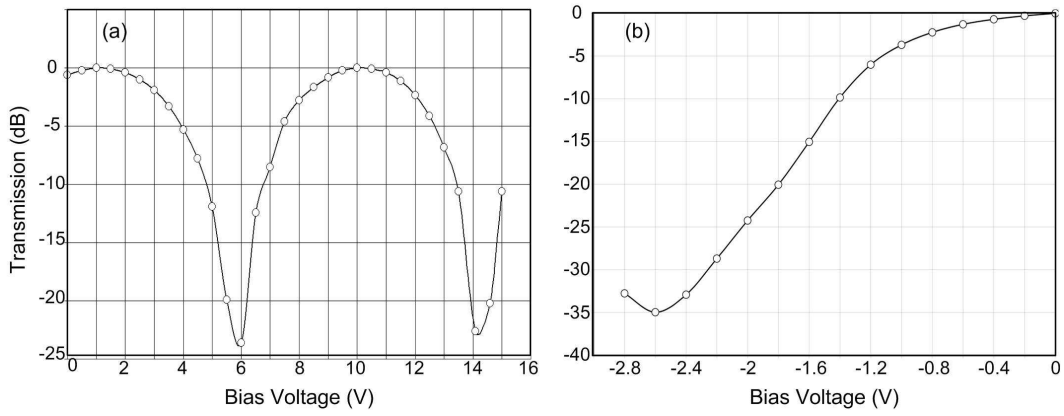

Fig. 2.5. Non-linear transmission profile as a function of applied bias voltage for (a) a MZM and (b) an EAM

Electro-absorption modulators generate short optical pulses by altering the absorption of an optical waveguide to modulate the intensity of the light passing through it. This condition is obtained through an electric field induced wavelength shift and broadening of the semiconductor absorption edge [31]. By applying an electric field to a semiconductor,

a reduction in the effective bandgap can be realised, which in turn shifts the devices absorption edge, thus absorbing photons with energy lower than the bandgap energy. This effect can be achieved through the Franz-Keldysh effect (FKE) in bulk EAMs and the quantum confined stark effect (QCSE) in quantum well EAMs [32]. As the photon energy changes as a function of wavelength, the transmission profile of the EAM changes as a function of wavelength also. Fig. 2.5 (b) illustrates the transmittance of a multiple quantum well EAM as a function of reverse bias at an operating wavelength of 1550 nm.

Although mach-zehnder modulators can generate 33 % duty cycle pulses at data rates up to 40 Gb/s, they are inherently polarisation sensitive and require a large DC bias voltage and modulation voltage to obtain pulses with a satisfactory width and extinction ratio. However as mentioned in section 1.4.2, by modulating the MZM at 2 V_{π}, a pulse train with a repetition rate at twice the value of the modulation frequency can be obtained, although this comes at the cost of even greater power consumption. Alternatively, EAMs require substantially less levels of bias and modulation voltage to obtain much shorter pulses with even greater extinction ratios. The shorter pulses and large ER (> 35 dB) arise from the highly non-linear transmission profile of the device, which can reach 20 dB/V. EAMs can also be fabricated on the same chip as a semiconductor laser, thus reducing its inherently large insertion loss and providing the capacity for an extremely small form factor transmitter. As the ER, PW and most importantly sign and magnitude of the frequency chirp of the generated pulses can be tuned as a function of both bias and modulation voltage at each wavelength, an extended transmission reach in a long haul system may be achieved. Therefore, there is a greater focus placed on this pulse generation technique in chapter three.

2.3.3 Gain-Switching

Gain-switching is one of the simplest and cost effective pulse generation techniques. Unlike mode-locking, gain-switching has the advantage that no external cavity or sophisticated fabrication technologies are required. It is achieved by directly modulating a laser diode with a large amplitude electrical pulse, usually with a sub-gigahertz step recovery diode (SRD) or a large sinusoidal wave. The method originated from observations of relaxation oscillations in the carrier density when turning on a laser diode from below threshold using electrical pulses with a fast leading edge [33, 34]. Therefore if the first spike of the relaxation oscillation was excited and if the electrical pulse was terminated before the onset of the second oscillation, an optical pulse would be emitted, as illustrated in Fig. 2.6.

Gain-switched pulses generally have un-compressed pulse widths varying from 10 to 30 ps depending on the laser parameters and drive conditions. The narrowest obtainable

pulse width achieved through gain-switching is limited due to the difficultly in sustaining a large initial population inversion prior to emission of the optical pulse [35]. The large variation in carrier density also creates a number of detrimental pulse characteristics that are inherent to this technique. These characteristics include SMSR degradation, substantial timing jitter and a large frequency chirp. The pulses exhibit a large chirp because the on-off nature of the applied electrical signal resulting in a continuous variation in carrier density, thus causing a corresponding variation in the refractive index. Although these pulse characteristics would have an adverse effect on performance if employed in a high speed transmission system, there have been numerous simple and cost efficient techniques proposed to mitigate these impairments [36, 37]. Wavelength tunability can also be achieved by externally injecting a gain-switched FP laser [38] or by implementing a number of cascaded directly modulated DFB lasers that can be individually thermally tuned to cover the entire C-band wavelength range.

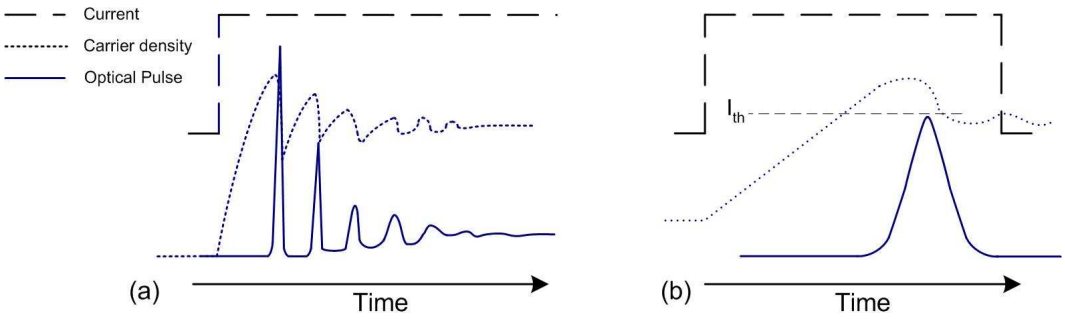

Fig. 2.6. (a) Illustration of relaxation oscillations observed in both the carrier and photon densities of a laser diode when a step current is applied from below threshold and (b) gain-switching process producing a short pulse

As a result gain-switching has become a viable RZ transmitter, especially for metro based optical networks where directly modulated sources are favoured due to their low cost. Therefore a more detailed explanation of the gain-switching process as well as a simple and cheap method to increase the spectral and temporal purity of such pulses is discussed in chapter four.

2.4 Pulse Measurement Techniques

High speed measurement techniques for optical communication systems are extremely importance and enable the continual monitoring of deployed networks and the tracking of impairments within these networks. Before implementing a short optical pulse source in such applications as high speed transmission, all-optical demultiplexing or optical sampling, it is imperative to perform some temporal and spectral diagnostics. The full electric field is required in order to obtain the phase characteristics of an optical pulse, which is crucial when determining long haul transmission performance [39]. However,

sometimes this difficult measurement in not a necessity and there exists many pulse measurement techniques which simplify their operation by only measuring one aspect of the pulse.

2.4.1 Fast Photodetection

The most common component employed to monitor the time dependant intensity of an optical pulse is a high bandwidth photodetector. When used in conjunction with an equally high bandwidth sampling oscilloscope the pulse width, pulse shape, extinction ratio, jitter and optical power can be displayed. This measurement technique is the most widely deployed pulse characterisation method as it is used in communication systems to monitor the optical eye diagram. However this technique requires that the bandwidth of the detector (and oscilloscope) is much higher than that of the pulse to be measured. If the bandwidth of the pulse exceeds that of the detector, information about the pulse intensity is lost and only the impulse response of the photodetector is measured [40].

Fig. 2.7 illustrates the temporal measurement of two different pulse trains, one with a 30 ps pulse width and the other with 2 ps pulse width, both measured using a 50 GHz photodetector in conjunction with a 50 GHz oscilloscope. For the 30 ps pulse, the detection system measures the pulse accurately as the bandwidth of the pulse is inside that of the photodetector. For the 2 ps pulse however, the photodetector is bandwidth limited and no longer provides a good representation of the pulse. The width was over estimated (~ 15 ps) and ringing results in extra artefacts which were not present in the pulse. Although this method for short pulse measurement can obtain many of the important pulse characteristics which are adequate for standard OOK BER analysis, it does not provide phase information, therefore more complex techniques are required.

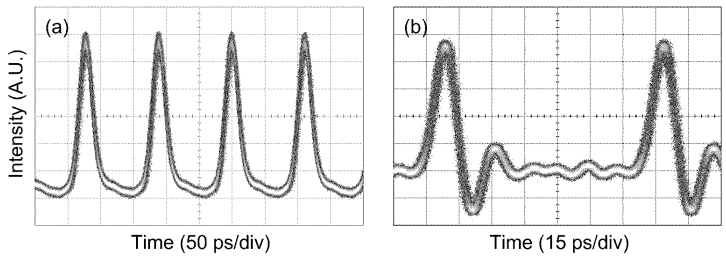

Fig. 2.7. Comparison of pulse measurement using a 50 GHz photodetector in conjunction with a 50 GHz sampling oscilloscope for (a) a 30 ps pulse and (b) a 2 ps pulse

2.4.2 Optical Spectrum Analysis

The spectral analysis of an optical pulse is a very important measurement, especially for DWDM networks as it provides information such as OSNR, channel spacing, transmission wavelength, cross-talk, channel ripple and non-linear induced impairments (such as FWM). The principle technique employed to monitor the pulse spectrum

generally consists of a grating spectrometer or a tuneable filter in conjunction with a slow response optical detector. The precision of the filter determines the spectral resolution of the optical spectrum analyzer (OSA). At low resolution the signal becomes slightly averaged which limits the absolute values, such as spectral width or peak lasing wavelength for example, therefore reducing the accuracy of the device.

2.4.3 Intensity Autocorrelation

One of the most conventional techniques employed to measure the duration of an optical pulse, which is too short for a high speed oscilloscope and detector, is an intensity autocorrelation [41]. Fig. 2.8 illustrates the underlying principle of such an intensity autocorrelator. The input pulse is split into two copies of itself, with one arm experiencing a variable time delay. The two spatially overlapping pulse replicas interact with each other as a function of the delay in a non-linear medium, such as a second harmonic generation (SHG) crystal. As the beams are not co-linear when passing through the crystal, it is possible to individually measure the cross product of the pulse and its copy, while ignoring the single arm signals. SHG produces a light signal that is twice the frequency of the input pulse and is given by:

$$E_{sig}^{SHG}(t-\tau) \propto E(t)E(t-\tau) \tag{2.1}$$

where τ is the delay. This electric field has an intensity that is proportional to the intensities of the two input pulses:

$$I_{sig}^{SHG}(t-\tau) \propto I(t)I(t-\tau) \tag{2.2}$$

As the photodetector is too slow to resolve this intensity, the detected signal produces the time integral, which is the autocorrelation:

$$A(\tau) = \int_{-\infty}^{\infty} I(t)I(t-\tau)dt \tag{2.3}$$

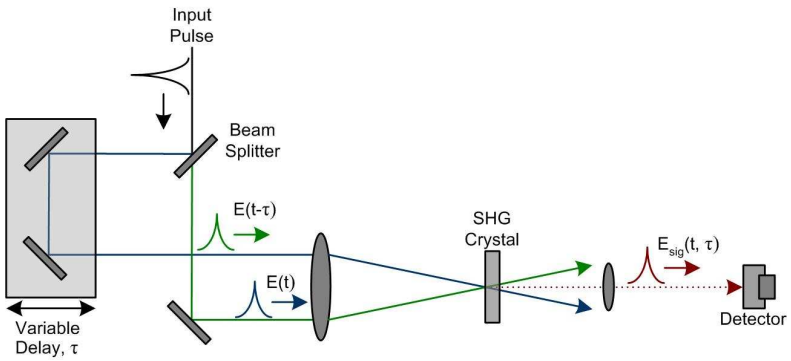

Fig. 2.8. Setup apparatus of a typical SHG intensity autocorrelator

The autocorrelation technique can be implemented in real time and as can be seen from Eq. 2.3, it is defined entirely by the pulse intensity; therefore all the phase information is lost. As a one dimensional sequence is not uniquely defined by the magnitude of its

Fourier transform, there could be an infinite number of pulse shapes that would result in the same autocorrelation. Consequently, to measure an accurate measurement of the pulse duration, it is necessary to know the pulse shape [42].

2.4.4 SHG Frequency Resolved Optical Gating

The need for a complete electric field characterisation, to obtain both intensity and phase information, is highly desirable for any wavelength tuneable RZ transmitter as it enables an accurate optimization of the generated pulses prior to transmission. One such pulse measurement technique capable of retrieving both the intensity and phase is frequency resolved optical gating (FROG) [43]. The second harmonic generation FROG technique is similar to that illustrated in Fig. 2.8 except that the cross product of the two interfering pulses is recorded using a spectrometer. Therefore, unlike autocorrelation, the FROG technique records the spectrum of the gated signal as a function of the delay. This creates a 3-D spectrally resolved representation of the pulse, known as a spectrogram, which can determine the complete electric field E(t). An example of a FROG spectrogram is displayed in Fig. 2.9 (a) and is represented by Eq. 2.4.

$$S(\omega,\tau) = \left| \int E(t)E(t-\tau)\exp(i\omega t)dt \right|^2 \qquad (2.4)$$

As the spectrogram is merely a series of spectral intensity measurements, it does not contain any direct phase information about the pulse or the gate that it consists of. However, if applied to a 2-D phase retrieval algorithm both E(t) and E(t-τ) can be extracted, thus providing the intensity and phase information for both the pulse and the gate. This algorithm is based on an iterative Fourier transform algorithm and is known as the generalised projections algorithm [44]. A conceptual diagram of this phase retrieval technique is illustrated in Fig. 2.9 (b). The algorithm starts with an initial guess for the electric field, E(t) and then generates the signal field $E_{sig}(t, \tau)$ through Eq. 2.1. This field then undergoes a Fourier transform as a function of t, to obtain $E_{sig}(\omega, \tau)$ in the frequency domain. The experimentally measured FROG trace (defined in Eq. 2.4) is applied to this function to obtain an improved signal field, $E'_{sig}(\omega, \tau)$. This signal is then transformed back into the time domain by using an inverse Fourier transform to generate, $E'_{sig}(t, \tau)$. This modified signal is finally used to generate a new, more accurate guess for E(t). This process is repeated and the algorithm generates a better guess after each iteration until the error between the original FROG trace and the generated FROG trace goes below an acceptable value, which is defined as convergence [45].

Although the FROG pulse measurement technique can obtain the intensity and phase information of an extremely short optical pulse in a very quick and efficient manner, it does suffer from some disadvantages [46]:

- It does not measure the absolute phase
- There is no absolute time reference because the pulse is used to measure itself, therefore the pulse arrival time and delay is not measured
- As the pulse and gate are symmetric, there is a timing ambiguity, because if the pulse is reversed temporally it would result in the same spectrogram
- Requires high optical power for good non-linear efficiency

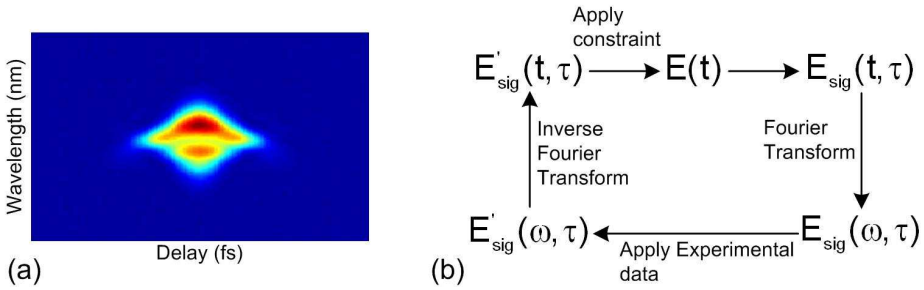

Fig. 2.9. (a) Illustration of FROG spectrogram, where the colour indicates intensity and (b) principle of FROG pulse retrieval algorithm

2.4.5 Linear Spectrographic Pulse Measurement Technique

While FROG is an excellent characterisation technique and still remains one of the most propitious methods to measure ultra-short pulses, it suffers from a few inherent drawbacks which limit its true usefulness for telecommunications applications. Firstly, the sensitivity of the device is proportional to the non-linear efficiency of the SHG crystal. As the duty cycle of the pulses increases, the peak power decreases, resulting in a corresponding decrease in non-linear efficiency. Most telecommunication pulses exhibit duty cycles of approximately 33 %, while also operating at high data rates of up to 40 Gb/s. Therefore, a high saturation power EDFA is required to increase the pulse power before a successful measurement can be made. The SHG technique also requires that the pulse and gate are phase matched, therefore making it highly sensitive to the polarisation of the incoming pulse. This again adds complexity and cost to the measurement scheme. As a result an alternative linear pulse measurement technique has been developed, which uses the gate of an EAM to scan across the incoming pulse to produce a spectrogram [47].

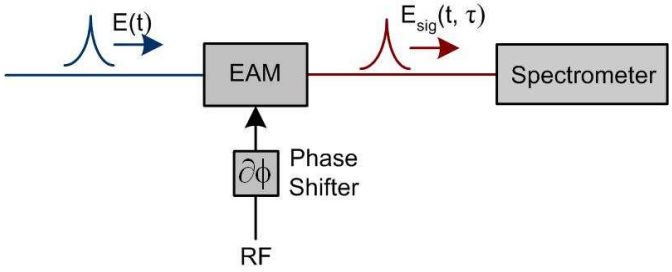

Fig. 2.10. Basic linear spectrographic pulse measurement setup

Fig. 2.10 illustrates the basic setup diagram of the linear spectrogram measurement technique. The incoming pulse to be characterised has an electric field, E(t) and is convolved with EAM gate as a function of the delay between the two. The delay is introduced using an RF phase shifter before the EAM, but can also be achieved with an optical delay line. The spectrogram is created by recording the spectrum of the pulse at each value of delay, τ, using a spectrometer. For fast operation the spectrometer can be a tuneable filter followed by a photodiode or for increased sensitivity, a commercially available grating based OSA. The resultant spectrogram is represented by:

$$S(\omega,\tau) = \left| \int E(t)G(t-\tau)\exp(i\omega t)dt \right|^2 \qquad (2.5)$$

where $G(t-\tau)$ is the EAM gate function.

This technique is equally as powerful as the FROG for retrieving the intensity and phase information of a pulse and uses the same robust phase retrieval algorithm. As it does not rely on non-linear optics it is extremely sensitive and can be implemented completely in fibre with standard commercially available equipment. There is also no restriction on the modulator being used, provided that the gate duration is within a factor of ten of the pulse width. By using an EAM, this technique is virtually polarisation insensitive, further reducing the complexity of the measurement [48].

2.5 Transmission Line Impairments

The main limitation on transmission performance in either a single channel or WDM system is the transmission line impairments. The various phenomena that limit the obtainable transmission reach in an optical communication system are attenuation, chromatic dispersion, polarization mode dispersion (PMD) and fibre non-linearity. It is therefore of critical importance that a detailed analysis of the effects of each impairment is evaluated prior to transmission to ensure an optimum level of performance [49]. This section will describe how these impairments can limit WDM or OTDM systems and briefly discuss some of the solutions that can be implemented to minimise their effects and hence maximise performance.

2.5.1 Attenuation and Chromatic Dispersion

Signal attenuation or optical loss is defined as the ratio of the optical output power from a fibre of given length to the optical input power. Attenuation of the light signal is mainly caused by absorption, scattering and radiative losses of the optical energy due to bending [50]. Attenuation is an important parameter in optical communications as it determines the maximum distance between optical repeaters. Since such repeaters are expensive to install and maintain, the attenuation of an optical transmission line has a large influence

on system cost. Prior to 1990, attenuation was overcome by using electrical repeaters which, as mentioned in chapter one, require expensive per wavelength OEO conversions before the signal can be amplified. With the advent of the EDFA [51], optical gain in excess of 20 dB across the entire C-band wavelength range could be achieved, thereby mitigating the effect of attenuation in a more efficient and cost effective way. Amplifiers aside, there have also been great improvements in the optical fibre itself, with modern commercial fibres exhibiting losses as low as 0.17 dB/km at 1550 nm.

Chromatic dispersion is a more complicated phenomenon associated with optical fibre and arises from the fact that both the refractive index and the propagation constant (β) of the fibre medium are both functions of wavelength [52]. An optical pulse that contains a single moded spectrum is never purely monochromatic, but contains a narrow band of wavelengths. Therefore, as an optical pulse travels through a fibre optic medium, the spectral components travel at different velocities creating a relative delay between them. This causes the pulse to spread out in time and is known as chromatic dispersion. This effect is detrimental in transmission systems as the pulse broadening leads to intersymbol interference which results in a severe degradation in BER performance after detection.

The dispersion of standard single mode fibre is approximately 17 ps.nm/km. Therefore if a conventional 10 Gb/s transform limited pulse with a spectral width of 0.15 nm was transmitted over this fibre, a maximum transmission distance of approximately 50 km would be achieved. When moving to a higher data rate of 40 Gb/s, the constraints due to chromatic dispersion increases by a factor of sixteen [53], thereby further restricting the achievable transmission distance of the communications system. Therefore, in an OTDM transmission system that requires an extremely small bit slot (6.25 ps for 160 Gb/s transmission), chromatic dispersion is critical and can have a severe impact on performance. Fortunately, like fibre attenuation, chromatic dispersion is a linear effect which enables deterministic compensation. This compensation can be achieved through fibres with negative dispersion values such as dispersion compensating fibre (DCF), zero dispersion fibres such as dispersion shifted fibre (DSF) or non-zero dispersion shifted fibre (NZDSF), electronic pre-distortion [54] and dispersion compensating gratings [55].

Current long haul WDM networks employ periodic dispersion compensation schemes where a large local dispersion is maintained to reduce non-linear mixing and a low end-to-end dispersion for high signal fidelity. This regime is accomplished by employing a dispersion managed amplified link, known as a dispersion map. This technique makes use of two fibre types with opposite signs of dispersion, such as standard SMF and DCF [56]. In such a link, the optical signal first incurs positive dispersion (unless pre-compensation is utilised) and then negative until the overall value eventually returns to zero. This

characteristic of returning to zero however is only true for the channels near the mean-zero dispersion wavelengths as seen in Fig. 2.11. Higher wavelength channels accumulate a positive residual dispersion and lower wavelength channels accumulate a negative value. This mismatch in compensation is due to second order dispersion known as dispersion slope and inevitably leads to performance degradation.

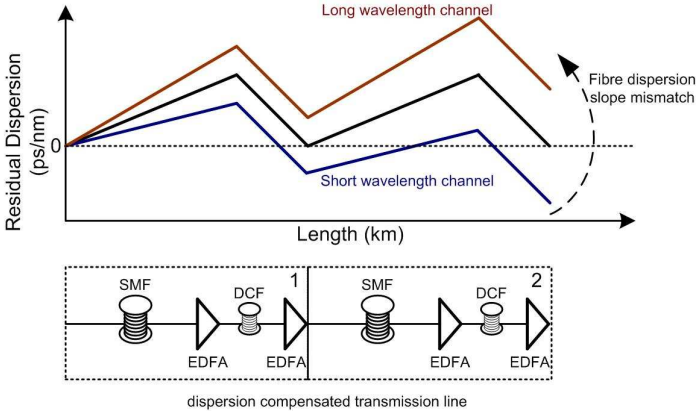

Fig. 2.11. Accumulated residual dispersion as a function of distance for the amplifier chain illustrated at the bottom of the figure

If both fibre types have a positive slope, channels that are located far from the mean-zero wavelengths will experience large residual dispersion resulting in intersymbol interference, once a sufficient amount of compensated links have been passed. It is therefore imperative to overcome this effect and one way of achieving this is to use dispersion matched fibre where the sign of the dispersion slopes are opposite to each other providing large bandwidth compensation [57]. Any further slight mismatch or residual dispersion could be controlled by adjusting the chirp of the transmitted pulses at each wavelength prior to transmission.

2.5.2 Polarization Mode Dispersion

Polarisation mode dispersion is a limiting transmission impairment in optical systems operating at high data rates and over long haul transmission distances. It is caused by random imperfections of the rotational symmetry around the fibre axis known as birefringence. The phenomenon of birefringence is a dependence of the fibre refractive index to the input signals state of polarisation (SOP) [58]. If an optical pulse with an arbitrary SOP traversed an optical link with a high value of PMD, two replicas of the pulse would travel on both the fast and slow axis of the fibre. Due to birefringence, both pulse replicas would travel at different velocities resulting in a relative delay between them, known as differential group delay (DGD). This in effect will result in two time-displaced replicas of the pulse at the receiver, thus limiting the ability of the receivers decision circuitry to distinguish between a one or a zero bit [59].

PMD can be a difficult impairment to monitor as it varies from fibre-to-fibre, from wavelength to wavelength for a given fibre at any instance in time and at each wavelength over time. This is because the fibre permutations that cause PMD are continually changing due to environmental sensitivities and other in-line equipment. Although a serious problem, PMD is mainly a considerable impairment in installed fibre optic routes that were implemented before this problem surfaced and when high data rates (40 Gb/s) were not envisaged [60]. PMD has been dramatically reduced to as low as 0.04 ps/√km with current fibre manufacturing processes. As a result, it does not pose a serious problem at 40 Gb/s with currently available fibre cable. However, when operating over installed fibre of a decade or more ago, some PMD compensation schemes may have to be employed either before, or integrated with the receiver, if long haul transmission at 40 Gb/s is desired [49, 61].

2.5.3 Fibre Non-linearity

Optical fibre non-linearity is another determining factor which underlies the maximum obtainable transmission distance in a single or multi-channel WDM system, governs the maximum optical repeater spacing and causes serious pulse distortions and channel mixing in high speed systems. Non-linearity is a result of very strong confinement of single mode fibres which leads to high optical intensities. If the intensity is large enough the refractive index of the optical fibre can be altered, through a process known as the Kerr effect [62]. This intensity induced change in refractive index alters the phase of the signal, which when combined with chromatic dispersion results in waveform distortion. The Kerr non-linear effects are translated into three major phenomena, SPM which is due to intra-channel effects and XPM and FWM which are due to inter-channel effects [63].

The index of refraction, n, of silica optical fibre is dependant on the power, P, through the following Eq. (2.6):

$$n = n_o + n_2 \frac{P}{A_e} \tag{2.6}$$

$$\varphi(L) = \frac{2\pi n_o L}{\lambda} + \frac{2\pi n_2 IL}{\lambda} \tag{2.7}$$

where n_o is the nominal refractive index at low optical power, n_2 is the non-linear refractive index coefficient of the fibre, which is normally in the region of 2.6×10^{-20} m/W for standard SMF [64] and A_e is the effective area of the fibre. The phase of the light after propagating through the fibre with length L (relative to the phase of the injected light) is given by Eq. 2.7. From this equation it is clear that any change in the optical intensity, I (which is equal to P/ A_e), will result in a corresponding change in the phase due to the non-linear index of refraction of the fibre. As a result of this change in

phase, the peak of the pulse will travel at a different velocity relative to the wings of the pulse. Therefore the leading edge of the pulse acquires a red shift and the trailing edge acquires a blue shift. This effect is known as SPM and results in spectral broadening. The signal is broadened by an amount ΔB as illustrated in Eq. 2.8, where γ is the non-linear coefficient, L_e is the effective non-linear length of the fibre and dP/dt is the time derivative of the pulse power. This broadening can cause performance penalties due to the limited bandwidth requirement of optical filters in a WDM network and can also cause pulse distortion, in the form of amplitude jitter, when combined with the effects of chromatic dispersion [65].

$$\Delta B = \gamma L_e \frac{dP}{dt} \tag{2.8}$$

When the chromatic dispersion is negative the leading edge of the pulse, which is red shifted, travels more quickly and moves away from the centre of the pulse. Conversely, the trailing edge is blue shifted and therefore travels more slowly, thus also moving away from the centre of the pulse. This results in pulse broadening leading to distortion and ISI. In the anomalous dispersion regime where the chromatic dispersion is positive, the opposite effect is experienced and pulse compression is observed. Therefore, SPM can be used to compensate for chromatic dispersion and such pulses are known as solitons [66]. In single channel systems and WDM systems with large channel spacing, SPM is the dominant non-linear impairment. In dispersion compensated transmission links that exhibit large values of local dispersion the pulses broaden rapidly and hence dramatically reduce in peak power, causing a reduction of SPM. A trade-off therefore exists between high optical launch power to provide good OSNR and optical non-linearity, thus illustrating how SPM can have a significant affect on the cost of an optical network.

The effects of cross phase modulation are similar to that of SPM as the intensity fluctuations cause a corresponding phase variation which results in a large timing jitter on the optical pulses and a consequent degradation in BER performance. However, for XPM the responsible intensity fluctuations arise from the modulation of adjacent channels in a WDM system [67]. The resultant spectral broadening due to XPM is given by:

$$\Delta B = 2\gamma L_e \frac{dP}{dt} \tag{2.9}$$

This expression is similar to that of SPM except for the factor of 2. This indicates that the effect of XPM is twice that of SPM, which would lead to the belief that XPM is a more severe limitation on WDM transmission systems. Like SPM, the spectrum of the optical pulses are broadened due to the intensity induced phase variations, however there is no impact of this broadening on the optical pulses unless it is combined with chromatic dispersion, which in turn results in pulse distortion. In a WDM system, each pulse stream

at each different wavelength channel will experience alternate group velocities and will therefore not interfere with each other indefinitely. Therefore large local dispersion helps to suppress the effects of XPM as walk off occurs quickly and the peak power of the pulses is also simultaneously reduced [68]. XPM can also be further reduced if there are differences in polarisation between channels, larger channel spacing and if the optical power is maintained at a sufficiently low level.

Four wave mixing is the second inter-channel non-linear phenomenon experienced in WDM transmission however its effects are considerably different from that of XPM. FWM, in its simplest form, is caused when two co-propagating waves at frequencies f_1 and f_2 mix and beat together. Their difference in frequency modulates the phase of one of the channels at that frequency, generating new tones as sidebands at $2f_1 - f_2$ and $2f_2 - f_1$. These sidebands co-propagate with the initial waves and gain power at their expense [69]. The total number of these ghost wavelengths is given by: number of ghosts = $0.5 \cdot N^2(N-1)$, where N is the number of initial channels. Therefore, if a 32 channel WDM system is considered, through FWM 15872 new spectral components would be created. These new spectral components create shadow pulses in originally empty time slots and add amplitude jitter to the remaining pulses, which both contribute to a reduction in the optical eye opening leading to severe performance degradation [70].

Fortunately, phase matching between the optical frequencies is required for efficient FWM. For this to be realised in single mode fibres, very low amounts of dispersion are required. If the amount of dispersion is low, all the optical frequencies will experience a limited amount of GVD and will therefore travel at the same speed, remaining spatially close to each other. In this regime, the channels can easily influence each other through FWM leading to signal deterioration, which was a problem that was highlighted when carriers considered employing dispersion shifted fibres over SMF [71]. If the chromatic dispersion is large, the interacting waves will have different group velocities, thus destroying the phase matching condition and lowering the efficiency of power generation at new frequencies. Therefore, the use of fibre with larger dispersion such as non-zero DSF and larger or unequal WDM channel spacing will result in a significant suppression of FWM problems [72].

Inter-channel non-linear effects are the dominant cause of serious transmission performance degradation in 10 Gb/s WDM systems, however while operating at data rates of 40 Gb/s or above it is the propagation of each individual channel that dominates performance. Fig. 2.12 illustrates the dominant nonlinear impairments at each bit rate and as a function of fibre chromatic dispersion for the OOK modulation format and was demonstrated by Winzer and Essiambre in [73]. The figure displays the most dominant

non-linearity for a given spectral efficiency and gives the optimum per-channel bit rate that allows for the greatest signal launch power for a fixed penalty due to the non-linearity. It also illustrates how the local fibre dispersion can affect greatly the dominant non-linear transmission impairment. For example it can be observed that the effect of FWM is most dominant when a very low dispersion fibre is used and that intra-channel effects are dominant at data rates greater than 40 Gb/s.

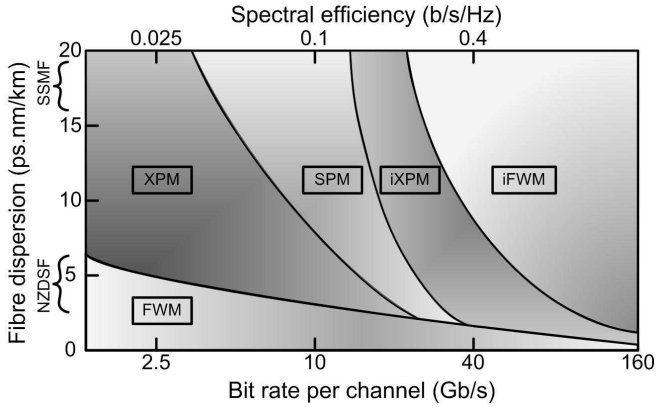

Fig. 2.12. Significance of inter and intra-channel non-linear effects in a WDM system as a function of fibre dispersion and bit rate [73]

2.6 Summary

The need for picosecond pulses for implementation in high speed, long haul RZ transmission systems has been acknowledged for many years now. Numerous pulse generation techniques have been developed and almost all are capable of generating pulses with high spectral and temporal purity. Due to the perceived dynamic nature of future communication networks, the ability of such pulse sources to operate over a wide wavelength range is becoming more apparent. Consequently greater research has been attributed to the development of widely tuneable transmitters for a variety of network topologies. Such transmitters should be simple, robust, cost effective, energy efficient and have a small form factor. Therefore, the remainder of this thesis will focus on the development of such wavelength tuneable transmitters for implementation in the core, metro and access networks.

REFERENCES

[1] M. Daikoku et al., “Performance comparison of modulation formats for 40 Gbit/s DWDM transmission systems,” in Proc. of Optical Fiber Communications (OFC), paper OFN2, Mar. 2005.

[2] S. Kawanishi, “Ultrahigh-speed optical time-division-multiplexed transmission technology based on optical signal processing,” IEEE J. Quant. Electron., vol. 34, no. 11, pp. 2064-2079, Nov. 1998.

[3] A.T. Clausen et al., “Pulse source requirements for OTDM systems,” in Proc. of Lasers and Electro-Optics Society (LEOS), paper TuY2, Oct. 2003.

[4] C. Schubert et al., “Single channel transmission beyond 1 Tbit/s,” in Proc. of Lasers and Electro-Optics Society (LEOS), paper ThX12, Oct. 2006.

[5] M. Kroh et al., “Low noise 400 fs pulse generation by monolithic semiconductor mode-locked laser and soliton pulse compression,” in Proc. of Conference on Lasers and Electro-Optics Europe (CLEO), pp. 125, Jun. 2005.

[6] C. Rulliere, “Femtosecond laser pulses: principles and experiments,” Second Edition, Springer 2005.

[7] K. Iwatsuki et al., “Timing jitter due to carrier linewidth of laser-diode pulse sources in ultra-high speed soliton transmission,” IEEE/OSA J. Lightwave Technol., vol. 13, no. 4, pp. 639-648, Apr. 1995.

[8] D. Zibar et al., “The effect of timing jitter on a 160-Gb/s demultiplexer,” IEEE Photon. Technol. Lett., vol. 19, no. 13, pp. 957-959, Jul. 2007.

[9] J.P. Gordon and H.A. Haus, “Random walk of coherently amplified solitons in optical fiber transmission,” OSA Optics Lett., vol. 11, no. 10, pp. 665-667, Oct. 1986.

[10] H.N. Efeifej et al., “Intersymbol interference and timing jitter measurements in a 40-Gb/s long haul dispersion-managed soliton system,” IEEE Photon. Technol. Lett., vol. 14, no. 3, pp. 343-345, Mar. 2002.

[11] J. Zhang et al., “Bit error rate analysis of an OTDM systems based on moment generation function,” IEEE/OSA J. Lightwave Technol., vol. 18, no. 11, pp. 1513-1518, Nov. 2000.

[12] G.P. Agrawal, “Group-Velocity Dispersion,” in Nonlinear Fiber Optics: Third edition, Optics and Photonics, Academic Press, 2001.

[13] F. Koyama and K. Iga, “Frequency chirping in external modulators,” IEEE/OSA J. Lightwave Technol., vol. 6, no. 1, pp. 87-92, Jan. 1988.

[14] D.G. Moodie et al., “Electroabsorption modulators for ultra high speed OTDM systems,” IEE Colloquium of Towards Terabit Transmission, pp. 3/1-3/5, May 1995.

[15] B.R. Hemenway et al., “Transmission modes, cross talk requirements, and performance of the circuit-switched A-service in the all optical network,” in Proc. of Optical Fiber Communications (OFC) Technical Digest, paper TuE2, Mar. 1996.

[16] J. Buus et al., “Fundamental laser diode characteristics,” in Tunable Laser Diodes and Related Sources: Second edition, Wiley-interscience, 2005.

[17] N.H. Jensen et al., “Partition noise in semiconductor lasers under CW and pulses operation,” IEEE J. Quant. Electron., vol. 23, no. 1, pp. 71-80, Jan. 1987.

[18] L.P. Barry and P.M. Anandarajah, “Effect of side-mode suppression ratio on the performance of self-seeded gain-switched optical pulses in lightwave communications systems,” IEEE Photon. Technol. Lett., vol. 11, no. 11, pp. 1360-1362, Nov. 1999.

[19] A.M. Clarke et al., “80-Gb/s OTDM system analysis of a vertical microcavity-based saturable absorber for the enhancement of pulse pedestal suppression,” IEEE Photon. Technol. Lett., vol. 19, no. 5, pp. 321-323, Mar. 2007.

[20] P.L. Mason et al., “The effects of pedestal suppression on gain-switched laser sources for 40 Gb/s OTDM transmission,” in Proc. of Lasers and Electro-Optics Society (LEOS), paper TuS2, Nov. 1997.

[21] P.M. Anandarajah et al., “Self-seeding of a gain-switched integrated dual-laser source for the generation of highly wavelength-tunable picosecond optical pulses,” IEEE Photon. Technol. Lett., vol. 16, no. 2, pp. 629-631, Feb. 2004.

[22] Y.A. Akulove et al., “Widely tunable electroabsorption-modulated sampled-grating DBR laser transmitter,” IEEE J. Sel. Topics in Quant. Electron., vol. 8, no. 6, pp. 1349-1357, Nov./Dec. 2002.

[23] M. Saruwatari, “All-optical signal processing for terabit/second optical transmission,” IEEE J. Sel. Topics in Quant. Electron., vol. 6, no. 6, pp. 1363-1374, Nov./Dec. 2000.

[24] L.E. Hargrove et al., “Locking of He-Ne laser modes induced by synchronous intracavity modulation,” Appl. Phys. Lett., vol. 5, no. 1, pp. 4-5, Jul. 1964.

[25] P.W. Smith, “Mode-locking of lasers,” in proc. of the IEEE, vol. 58, no. 9, pp. 1342-1357, Sep. 1970.

[26] E.A. Avrutin et al., “Monolithic and multi-gigahertz mode-locked semiconductor lasers: constructions, experiments, models and applications,” in proc. of the IEE Optioelctron., vol. 147, no. 4, pp. 251-278, Aug. 2000.

[27] A. Ducasse et al., “Methods for the generation of ultrashort laser pulses: mode-locking,” in Femtosecond Laser Pulses: Principles and Experiments, second edition, Springer Science and Business Media, 2005.

[28] A.E. Siegman, “Lasers,” University Science Books, 1986.

[29] J.E. Bowers et al., “Actively mode-locked semiconductor lasers,” IEEE J. Quant. Electron., vol. 25, no. 6, pp. 1426-1439, Jun. 1989.

[30] R. Madabhushi et al., “Lithium niobate optical modulators,” in WDM Technologies: Active Optical Components, Academic Press, Elsevier Science, 2002.

[31] P. Bhattacharya, “Optical Processes in semiconductors,” in Semiconductor Optoelectronic Devices: Second Edition, Prentice Hall, 1997.

[32] B. Mason, “Electroabsorption modulators,” in WDM Technologies: Active Optical Components, Academic Press, Elsevier Science, 2002.

[33] H. Ito et al., “Picosecond optical pulse generation from an RF modulated AlGaAs DH laser diode,” IEE Electron. Lett., vol. 15, no. 23, pp. 738-740, Nov. 1979.

[34] H.F. Liu et al., “Gain-switched picosecond pulse (< 10 ps) generation from 1.3 µm InGaAsP laser diodes,” IEEE J. Quant. Electron., vol. 25, no. 6, pp. 1417-1425, Jun. 1989.

[35] K.Y. Lau et al., “Gain-switching of semiconductor injection lasers,” Appl. Phys. Lett., vol. 52, no. 4, pp. 257-259, Jan. 1998.

[36] L.P. Barry et al., “Simple technique to improve the spectral quality of gain-switched pulses from a DFB laser,” IEE Electron. Lett., vol. 30, no. 25, pp. 2143-2145, Dec. 1994.

[37] P.M. Anandarajah et al., “Optimised pulse source employing an externally injected gain-switched laser diode in conjunction with a non-linearly chirped grating,” IEEE J. Sel. Topics in Quant. Electron., vol. 12, no. 2, pp. 255-264, Mar./Apr. 2006.

[38] A.M. Clarke et al., “Generation of widely tunable picosecond pulses with large SMSR by externally injecting a gain switched dual laser source,” IEEE Photon. Technol. Lett., vol. 16, no. 10, pp. 2344-2346, Oct. 2004.

[39] C. Dorrer, “High-speed measurements for optical telecommunication systems,” IEEE J. Sel. Topics in Quant. Electron., vol. 12, no. 4, pp. 843-858, Jul./Aug. 2006.

[40] M. Westlund et al., “High-performance optical-fiber-nonlinearity-based optical waveform monitoring,” IEEE/OSA J. Lightwave Technol., vol. 23, no. 6, pp. 2012-2022, Jun. 2005.

[41] M. Maier et al., “Intense light bursts in the stimulated Raman effect,” Phy. Rev. Lett., vol. 17, no. 26, pp. 1275-1277, Dec. 1966.

[42] R. Trebino and E. Zeek, “The autocorrelation, the spectrum, and phase retrieval,” in Frequency Resolved Optical Gating: The Measurement of Ultrashort Laser Pulses, Kluwer Academic Publishers, 2000.

[43] K.W. Delong et al., “Frequency-resolved optical gating with the use of second-harmonic generation,” OSA J. Opt. Soc. Am. B, vol. 11, no. 11, pp. 2206-2215, Nov. 1994.

[44] D.J. Kane, “Recent progress toward real-time measurement of ultrashort laser pulses,” IEEE J. Quant. Electron., vol. 35, no. 4, pp. 421-431, Apr. 1999.

[45] R. Trebino, “FROG,” in Frequency Resolved Optical Gating: The Measurement of Ultrashort Laser Pulses, Kluwer Academic Publishers, 2000.

[46] K.W. Delong et al., “Practical issues in ultrashort-laser-pulse measurement using frequency-resolved optical gating,” IEEE J. Quant. Electron., vol. 32, no. 7, pp. 1253-1264, Jul. 1996.

[47] C. Dorrer and I. Kang, “Real-time implantation of linear spectrograms for the characterisation of high bit-rate optical pulse trains,” IEEE Photon. Technol. Lett., vol. 16, no. 3, pp. 858-860, Mar. 2004.

[48] C. Dorrer and I. Kang, “High-sensitivity spectrographic method for characterising picosecond optical pulses and data modulators,” in Proc. of Optical Fiber Communications (OFC), paper FD4-1, Mar. 2002.

[49] P. Mamyshev, “Will it be easy for the telecom carriers to deploy 40 Gb/s transmission systems?,” White Paper, International Engineering Consortium, Annual Review of Communications, 2003.

[50] G. Keiser, “Optical Fiber Communications: Second edition,” McGraw-Hill series in Electrical Engineering, International Edition, 1991.

[51] E. Desurvire et al., “High-gain erbium-doped travelling-wave fiber amplifier,” OSA Optics Lett., vol. 12, no. 11, pp. 888-890, Nov. 1987.

[52] S.V. Kartalopoulos, “Optical components,” in DWDM: Networks, devices and technology, IEEE Press, Wiley-Interscience, 2003.

[53] G. Charlet, “Progress in optical modulation formats for high-bit rate WDM transmissions,” IEEE J. Sel. Topics in Quant. Electron., vol. 12, no. 4, pp. 469-483, Jul./Aug. 2006.

[54] P.J. Winzer and R.J. Essiambre, “Electronic pre-distortion for advanced modulation formats,” in Proc. of Optical Fiber Communications (OFC), paper Tu4.4.2, Mar. 2005.

[55] E. Yamada et al., “10 Gb/s soliton transmission over 2900 km using 1.3 μm singlemode fibers and dispersion compensation using chirped fibre Bragg gratings,” IEE Electron. Lett., vol. 35, no. 9, pp. 728-729, Apr. 1999.

[56] N.S. Bergano, “Wavelength division multiplexing in long-haul transoceanic transmission systems,” IEEE/OSA J. Lightwave Technol., vol. 23, no. 12, pp. 4125-4139, Dec. 2005.

[57] L. Gruner-Nielsen et al., “Design and manufacture of dispersion compensating fiber for simultaneous compensation of dispersion and dispersion slope,” in Proc. of Optical Fiber Communications (OFC), paper WM1-1, Feb. 1999.

[58] C.D. Poole and R.E. Wagner, “Phenomenological approach to polarisation dispersion in long single-mode fibres,” IEE Electron. Lett., vol. 22, no. 19, pp. 1029-1030, Sep. 1986.

[59] C.D. Poole and J. Nagel, “Polarization effects in lightwave systems,” in Optical fiber telecommunications IIIA, Academic Press, 1997.

[60] M. Brodsky et al., “Polarization mode dispersion in installed fibers,” IEEE/OSA J. Lightwave Technol., vol. 24, no. 12, pp. 4584-4599, Dec. 2006.

[61] H. Yaffe, “Overcoming PMD will enable 40 Gbit/s optical networks,” EE Times, Mar. 2002. [Online]. Available: http://www.eetimes.com.

[62] R.H. Stolen and A. Ashkin, “Optical Kerr effect in glass waveguide,” Appl. Phys. Lett., vol. 22, no. 6, pp. 294-296, Mar. 1973.

[63] G.P. Agrawal, “Nonlinear Fiber Optics: Third edition,” Optics and Photonics, Academic Press, 2001.

[64] K.S. Kim et al., “Measurement of the nonlinear index of silica-core and dispersion-shifted fibers,” OSA Optics Lett., vol. 19, no. 4, pp. 257-259, Feb. 1994.

[65] F. Forghieri et al., “Fiber nonlinearities and their impact on transmission systems,” in Optical fiber telecommunications IIIA, Academic Press, 1997.

[66] L.F. Molleneuer et al., “Experimental observation of picosecond pulse narrowing and solitons in optical fibers,” Phy. Rev. Lett., vol. 45, no. 13, pp. 1095-1098, Sep. 1980.

[67] P.L. Baldeck et al., “Induced-frequency shift of copropagating ultrafast optical pulses,” Appl. Phys. Lett., vol. 52, no. 23, pp. 1939-1941, Jun. 1988.

[68] T.K. Chiang et al., “Cross-phase modulation in fiber links with multiple optical amplifiers and dispersion compensators,” IEEE/OSA J. Lightwave Technol., vol. 14, no. 3, pp. 249-260, Mar. 1996.

[69] K.O. Hill et al., “CW three-wave mixing in single-mode optical fibers,” J. Appl. Phys., vol. 49, no. 10, pp. 5098-5106, Oct. 1978.

[70] P.J. Winzer and R.J. Essiambre, “Advanced optical modulation formats,” in proc. of the IEEE, vol. 94, no. 5, pp. 952-985, May 2006.

[71] S. Bigo, “Technologies for global telecommunications using undersea cables,” in Optical fiber telecommunications V, B: Systems and networks, Academic Press, Elsevier, 2008.

[72] A.R. Chraplyvy, “Limitations on lightwave communications imposed by optical-fiber nonlinearities,” IEEE/OSA J. Lightwave Technol., vol. 8, no. 10, pp. 1548-1557, Oct. 1990.

[73] P.J. Winzer and R.J. Essiambre, “Advanced optical modulation formats,” in Optical fiber telecommunications V, B: Systems and networks, Academic Press, Elsevier, 2008.

Chapter 3 – Wavelength Tuneable Pulse Generation and Transmission using an EAM

3.1 Introduction

The electro-absorption modulator is a very attractive component for high speed transmission and/or processing in a core optical network operating at data rates up to 40 Gb/s. When combined with a widely tuneable laser an EAM can provide stable pulse generation over the entire C-band wavelength range, making it ideal for reconfigurable WDM networks. There are also significant advantages over other modulator types such as size, power efficiency, compatibility with monolithic integration and the ability to generate very short pulses that exhibit zero or negative chirp. Electro-absorption is dominated by two processes, either the Franz-Keldysh effect or the quantum confined stark effect. The QCSE is the dominant process in MWQ modulators and is the most popular modulator configuration as it provides a large on-off ratio and negative chirp with a reasonable insertion loss [1]. In an EAM, intensity modulation is realised by shifting the absorption edge of the semiconductor, therefore such a technique is inherently wavelength dependent. Additionally, as the absorption and hence the change in refractive index is greater for an increased electric field, the generated pulses exhibit varying characteristics as a function of bias and modulation voltage. It is therefore imperative to analyze the generated pulses at each wavelength to ensure optimum transmission performance when operating over a wide wavelength range [2].

This chapter investigates high speed pulse generation and transmission using a 40 GHz MQW EAM. An accurate performance map of the generated pulses, in terms of pulse width, extinction ratio and frequency chirp is constructed using the linear spectrogram measurement technique outlined in section 2.4.5. Each pulse characteristic is recorded as a function of operating wavelength, reverse bias and modulation voltage. Once this characterisation is complete, the EAM is implemented as a 42.7 GHz RZ transmitter in a 1500 km circulating loop transmission setup. It is demonstrated that non-optimisation of the EAM drive conditions, after a WDM switching event has occurred, leads to severe degradation, in terms of both obtainable transmission reach and performance consistency over a wide wavelength range. By constructing an EAM performance map prior to transmission, an optimum bias and drive condition can be selected for each wavelength on the ITU grid, thereby achieving extended transmission reach and a greater level of performance uniformity over the entire C-band wavelength range.

3.2 EAM Device Operation

The electro-absorption effect for optical intensity modulators is based on two dominant mechanisms; the Franz-Keldysh effect for conventional bulk semiconductor modulators and the quantum confined stark effect for multiple quantum well (MQW) modulators, both of which are prominent near the bandgap of semiconductors. As optical absorption is the dominant process by which both EAM structures operate, they are inherently wavelength dependant and also exhibit varying frequency chirp characteristics as a function of absorption [3]. Therefore this section will investigate the differences between the two modulator types and examine how the design process can have a significant affect on the performance of such devices.

3.2.1 Franz-Keldysh Effect in a Bulk EAM

The Franz-Keldysh effect is denoted as the variation in absorption of a semiconductor in the presence of an electric field and results in the absorption of photons with energies less than the bandgap energy of the material [4]. Fig. 3.1 (a) illustrates the band diagram of a transparent bulk semiconductor material when no electric field, E, is applied. Under this condition the valence electron must tunnel through a large barrier from point A to B to absorb an incident photon with energy, $\hbar\omega$, which is less than the bandgap energy, ε_g. Therefore, in the absence of an electric field the absorption of a photon with energy, $\hbar\omega < \varepsilon_g$ is impossible. In the presence of an electric field the band structure tilts and the distance AB decreases, as seen in Fig. 3.1 (b). At this point the electron wavefunctions turn from an oscillatory to a decaying behaviour and begin to overlap. As the overlap of the wavefunctions increase the valance electron can easily tunnel through to the conduction band with the aid of an incident photon. The net result is that a photon with energy $\hbar\omega < \varepsilon_g$ is absorbed and therefore the Franz-Keldysh effect is in essence, photon assisted tunnelling. The probability of this transition and hence the level of absorption of a semiconductor is greater with an increase in the electric field [5].

FKE based electro-absorption modulators provide an excellent source for intensity modulation and exhibit high polarisation insensitivity, in contrast to mach-zehnder modulators which are inherently polarisation sensitive. Bulk EAMs also provide a large spectral bandwidth, making them ideal for integration with widely tuneable lasers [6], however the level of absorption per unit volt of applied bias is much lower than that achieved through the QCSE. Significantly, for FKE based EAMs, the sign of the exhibited chirp profile as a function of operating wavelength is negative and when combined with chromatic dispersion has a detrimental impact on transmission performance. Therefore, in order to obtain optical pulses with positive chirp (to

counteract dispersive effects of fibre) and a large on-off extinction ratio, MQW modulators must be considered [7].

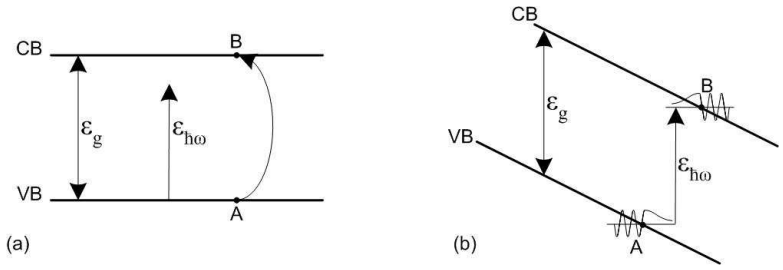

Fig. 3.1. (a) Band diagram of a transparent bulk semiconductor and (b) optical absorption of a photon due to the Franz-Keldysh effect

3.2.2 Quantum Confined Stark Effect in a MQW EAM

A MQW structure consists of a series of thin semiconductors with alternating bandgap energies. In such devices, electrons and holes produced by the absorption of a photon of near bandgap energy pair to form an exciton. Excitons have a dramatic effect on the optical properties of a semiconductor and show strong resonances in the absorption and emission spectra of the material at energies below the band edge. In bulk semiconductor devices the exciton dissociates in a very fast time and is barely detected in the absorption spectra at room temperatures. In MWQ devices however, this situation is vastly altered. By confining the electrons and holes in a small region defined by the well width, the overlap of the wavefunctions is greatly increased, which results is greater oscillatory strength and a greater binding energy, as seen in Fig. 3.2 (a). The binding energy in a MWQ device is approximately four times that of the bulk semiconductor [5].

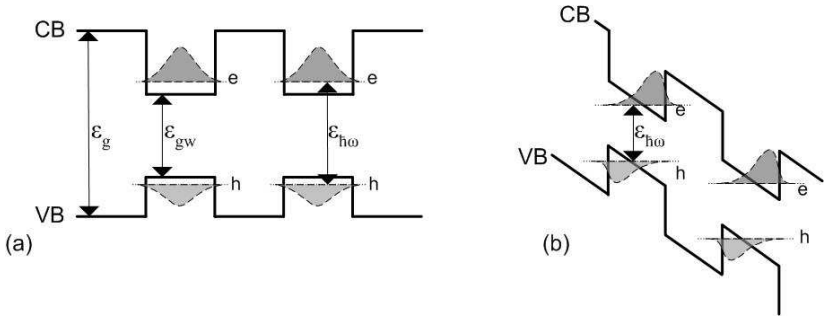

Fig. 3.2. (a) Band structure of MQW EAM under zero field and (b) absorption of a photon due to the QCSE in the presence of an applied electric field

In the presence of a transverse electric field the energy bands tilt and the electron and hole wavefunctions are pushed to opposite sides of the well, making their ground energy states smaller. Consequently, the transition energy required to absorb a photon is reduced and a corresponding change in the exciton binding energy is experienced. This is the dominant process in a MQW EAM and results in a pronounced red shift in the

semiconductor absorption edge, known as the quantum confined stark effect [8]. It is important to note that the binding energy of the exciton is decreased slightly as the electron and hole wavefunctions are pushed to opposite sides of the well; however this effect is about ten times smaller than the shift in the bandgap [1]. This shift is much stronger than that of the Franz-Keldysh effect in bulk semiconductors and therefore demonstrates more efficient absorption characteristics.

The operation of a MQW EAM is therefore quite efficient and works as follows. If the operating wavelength of the CW light source exhibits photon energies 15-20 meV below the exciton resonance at zero applied bias, negligible or no absorption of the incident photons occurs. With the application of a transverse electric field, the excitonic resonance will undergo a red shift and coincide with the photon energy, resulting in strong absorption. If a sinusoidal drive voltage is applied to the device, the absorption characteristics of the EAM can be modulated, producing a short optical pulse [9], therefore very efficient intensity modulation can be realised.

3.2.3 Chirp Characteristics

An important aspect of electro-absorption modulators is the variation in the refractive index of the semiconductor as a function of absorption at a specific operating wavelength. The real and imaginary parts of the refractive index are related to each other through the Kramers-Kronig relations, where the imaginary part is a measure of the loss of a wave propagating through the semiconductor and is therefore directly proportional to the absorption of the material. According to this relation, if the loss that is due to the imaginary part (k) of the refractive index is varied, then the real part (n) will undergo some modulation [10]. The change in the real part of the refractive index is typically associated with the corresponding change in the absorption through the α parameter:

$$\alpha = \frac{\Delta n}{\Delta k} \tag{3.2}$$

The α parameter is sometimes referred to as the chirp parameter as it is directly related to the phase of the optical signal and hence the instantaneous frequency [11]. It is an extremely useful and important measurement of an EAM as it gives an indication of the magnitude and more importantly the sign of chirp the generated pulses will exhibit for a given bias and modulation voltage at each specific wavelength [12]. For long haul communication systems it is desirable to have a negative value for α as this leads to a positive chirp. When combined with the dispersive effects of SMF in the anomalous dispersion regime, the pulses will first experience a small amount of compression due to the positive chirp before eventually broadening, with the net result being an extended transmission reach. However, if the sign of the chirp is negative, it will combine with

fibre dispersion, degrading the optical signal and limiting the obtainable transmission distance. As the absorption characteristics of an EAM vary as a function of wavelength, reverse bias and modulation voltage, the alpha parameter will also exhibit a varying value as a function of the same conditions [13]. Therefore it is important to perform a static characterisation of the alpha parameter profile prior to transmission.

3.2.4 Design Considerations

There are several key parameters that must be considered in the design stage of an EAM for it to be implemented in a high speed transmission system. Such parameters include:

- BW response
- Contrast ratio
- Insertion loss
- Modulation efficiency

Bandwidth response: High bandwidth modulators are a requisite for high speed communication systems operating at serial data rates up to 40 Gb/s. The electrical bandwidth of a device is defined as the frequency range over which its response remains within 3 dB of the peak. This is equivalent to the frequency at which the voltage across the junction capacitor decreases to 50% of the DC value. If the junction capacitance remains low, a greater bandwidth response can be achieved. As the junction capacitance of an EAM scales with the area of the junction and hence the length of the device, it is desirable to limit the overall size of the modulator to maximise the bandwidth capability.

Contrast ratio: The contrast ratio (extinction ratio) of the EAM depends on the number of quantum wells or indeed the length of the active region. Therefore by increasing the number of wells or the length of the device a greater on-off ratio can be achieved. However, one drawback associated with increasing the length of the active region is a corresponding increase in the junction capacitance, ultimately limiting the bandwidth response of the EAM. As a consequence, there will always be a trade off between optical extinction and bit rate. Additionally, increasing the number of quantum wells will provide a greater contrast ratio, but this improvement is impaired by a proportional increase in insertion loss.

Insertion loss: The insertion loss of an EAM is comprised of two main effects, absorption and scattering losses in the waveguide and secondly, coupling losses. Waveguide absorption is caused by residual absorption in the active region while scattering losses result from defects in the material or roughness in the walls of the waveguide. Coupling losses occur when the light exiting the EAM facet is coupled into a fibre core. If the

effective mode guide in the EAM core is too small, the insertion losses will be substantial. The confinement factor can be increased to allow for a larger mode size, although this comes as a trade off to ensure single moded operation within the cavity.

Modulation efficiency: The active layer of an EAM is composed of material with a bandgap energy slightly greater than the photon energy of the wavelength the device is intended to operate at. The difference between the bandgap energy of the device at zero applied bias and the operating wavelength is defined as the detuning energy. By reducing the detuning energy, the modulation efficiency of the device is increases, as it will require a weaker electric field to induce the same level of absorption. However, by reducing the detuning energy the residual absorption at zero bias will increase [1, 14].

3.3 Static Characterisation

From section 3.2 it is evident that the performance evaluation of an EAM is vitally important prior to implementation in a high speed system. Important pulse characteristics such as, extinction ratio, insertion loss and alpha parameter of an EAM can all be easily obtained through various static characterisations. This section will therefore focus on the basic transmission profile of a MQW EAM, which defines the insertion loss and extinction ratio as a function of wavelength and reverse bias. The corresponding alpha parameter profile, which provides an indication of chirp magnitude and sign is also investigated.

3.3.1 Transmission Profile

Fig. 3.3 (a) illustrates the experimental setup used to characterise both the insertion loss and static extinction ratio of a 40 GHz EAM. The EAM used for this characterisation and for the remainder of this thesis was a commercially available fibre pigtailed InP device that operated over the entire C-band wavelength range and had 10 InGaAs wells with InAlAs barriers (specification sheet in Appendix II). A peltier controller, thermistor and heat sink were used to ensure stable temperature performance throughout the measurement. The insertion loss of the modulator was characterised by coupling light from a widely tuneable CW source into the EAM, at the zero bias point. The input power was subsequently subtracted from the output power to give the total loss of the EAM. This process was repeated for several different wavelengths over the operating range of the device. Table 3.1 illustrates the loss of the EAM as a function of operating wavelength. The insertion loss decreases as a function of increasing wavelength because as the spacing between the operating wavelength and the band edge of the device increases, the absorption is reduced, thus limiting the incurred loss. At an operating wavelength of 1525 nm the insertion loss was 18.64 dB which is extremely high and

would render this component unacceptable for implementation in an optical communications system at this wavelength. For wavelengths that have a large detuning energy, the insertion loss is dominated by the coupling losses of the device. This is evident from the minor variation in insertion loss at channels greater that 1565 nm in comparison to the variations demonstrated from 1525 to 1560 nm.

Wavelength (nm)	1525	1530	1535	1540	1545	1550	1555	1560	1565	1570
Insertion loss (dB)	18.64	15.26	13.3	11.83	10.86	10.15	9.356	9.14	7.82	7.26

Table 3.1. EAM insertion loss as a function of wavelength

To measure the static extinction ratio of the device, the CW laser was initially set to operate at 1525 nm. The reverse bias applied to the EAM was altered from 0 to -2.8 V in 0.2 V steps and a power meter recorded the throughput after each adjustment. This technique was repeated for the same wavelength range demonstrated in the table above. Fig. 3.3 (b) illustrates the transmission profile of the EAM as a function of reverse bias and operating wavelength, relative to the throughput at 0 V. It is evident from this graph that the operating wavelengths of 1525 and 1530 nm would not provide optimum pulses if driven with a 40 GHz sinusoidal signal. This is because both wavelength channels are in close proximity to the band edge of the device and therefore exhibit large values of absorption under the application of a relatively weak electric field. The linear response in the low bias voltage range would result in large pulse widths and static maximum on-off extinction of 22 and 26 dB respectively.

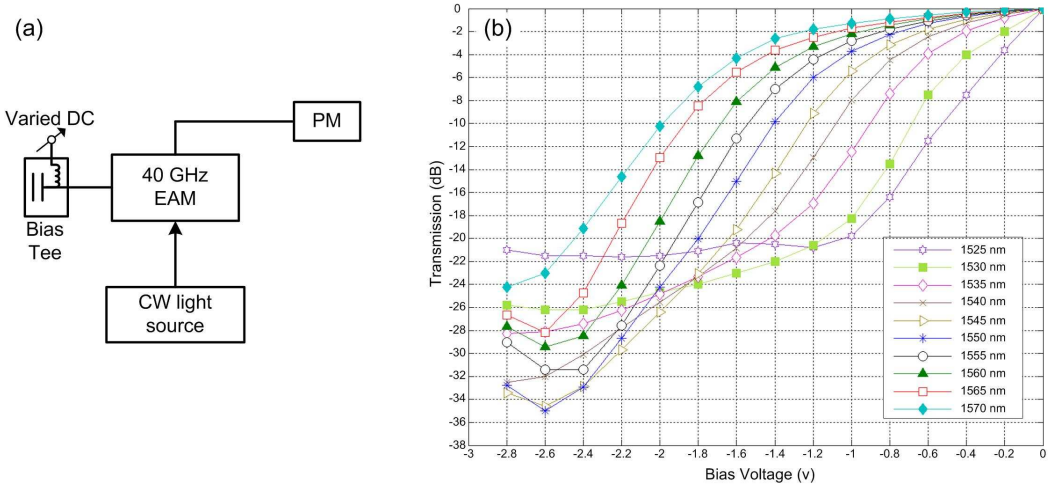

Fig. 3.3. (a) Experimental setup to characterise static transmission profile of commercially available 40 GHz EAM and (b) transmission profile as a function of reverse bias and wavelength

The transmission profile at the remaining wavelength channels exhibit the non-linear characteristic typical of electro-absorption modulators. The absorption curve is initially flat at low bias voltages and then increases rapidly in slope with the application of a larger electric field. Extinction ratios of at least 28 dB are exhibited for all wavelength

channels, with the exception of 1570 nm. Although the insertion loss is lowest while operating at this wavelength, due to its large detuning energy from the bandgap of the device, it undergoes limited absorption as a function of applied electric field and thus exhibits a lower extinction ratio of 24 dB. Therefore to generate pulses with narrow width, high extinction ratio and moderate insertion losses, the optimum operating wavelength range of this device is between 1535 and 1565 nm.

3.3.2 Alpha Parameter

The characterisation of the alpha parameter is important when employing an external modulator as an RZ transmitter. The alpha value determines the magnitude and sign of chirp the generated pulses will possess and hence indicates if the dispersive effects of fibre will enhance or degrade transmission performance. Recalling Eq. 3.2, the alpha parameter is a function of both the refractive index and the absorption of an EAM. The variation in phase (φ) with intensity (I) is also related with the alpha parameter through the equation 3.3 [12]. Therefore, the phase variation of the generated pulses and hence the chirp, is proportional to the alpha parameter.

$$\Delta\varphi = \frac{\alpha \Delta I}{2I} \tag{3.3}$$

A simple and accurate measurement technique for measuring the alpha parameter of an EAM was outlined by Devaux et al. [15]. This technique uses a fibre response method where small signal measurements in the frequency domain are recorded after the light has traversed a length of dispersive fibre. After propagating a specific length of fibre, two simultaneous interferences between the carrier and the two sidebands occurs, resulting in sharp resonance frequencies, appearing as a cancelation in optical power on an electrical spectrum analyzer (ESA). By analyzing the frequencies at which these resonances occur, an accurate value of the alpha parameter can be deduced.

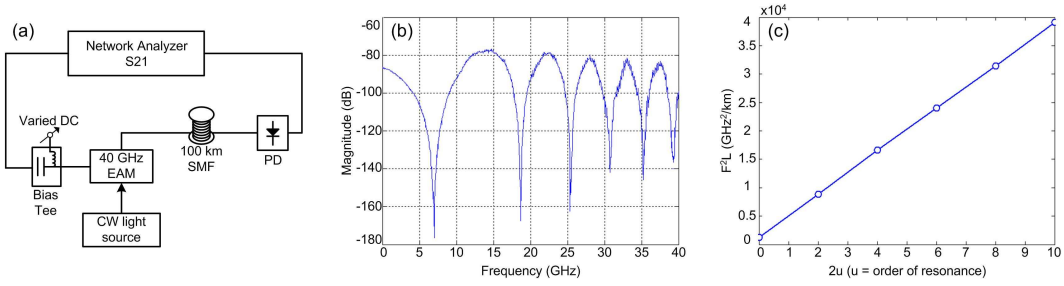

Fig. 3.4. (a) Experimental setup for alpha parameter measurement, (b) small signal frequency response of EAM after transmission through 100 km of SMF and (c) resonance frequencies squared times the fibre length versus twice the resonance order

Fig. 3.4 (a) illustrates the experimental setup used to characterise the alpha parameter of an EAM as a function of both bias voltage and wavelength. An external cavity laser

provided a constant CW light signal to the EAM, which was initially biased at zero volts via a bias tee. Before the small signal analysis of the EAM could be obtained it was important to calibrate the measurement, thus cancelling the frequency response of the modulator, detector and electrical cables. A 50 GHz network analyzer recorded the combined frequency response of these components, which was subtracted from the subsequent bandwidth measurements.

The network analyzer supplied a small signal 1001 point frequency sweep from 0.045 to 40 GHz to the input of the EAM and monitored the detected frequency response of the signal after transmission through the dispersive medium. The frequency response displays a number of resonances which appear as sharp peaks, as seen in Fig. 3.4 (b). By extracting the values of the resonance frequencies (f_u) and plotting them as a function of twice their order (u), a linear relationship should exist, as seen in Fig. 3.4 (c). The intercept of this line can be used to calculate the alpha parameter as both the value of the resonance frequencies and their orders are related to alpha through the equation [15]:

$$f_u^2 L = \frac{c}{2D\lambda^2}\left(1 + 2u - \frac{2}{\pi}\arctan(\alpha)\right) \tag{3.4}$$

From Eq. 3.4, it is evident that the exact value of the fibre dispersion at each operating wavelength is critical in order to obtain a low error in the measurement. Therefore the dispersion of the 100 km reel of SMF was also measured using the same interferometric technique outlined above. However, to overcome the chirp dependence of the EAM, a commercially available chirp-free 40 GHz Mach-Zehnder modulator from Avanex was employed to perform the measurement. The sidebands and the carrier frequency of the intensity modulated signal propagate at different velocities in the fibre due to chromatic dispersion and are detected using a high-speed photodiode. At certain frequencies the chromatic dispersion length product causes the two side bands to be in counter-phase, thereby producing a zero in amplitude [16]. Therefore the frequencies that correspond to a null in amplitude are directly related to the chromatic dispersion times the length, through Eq. 3.5, where D is the dispersion, L is the length of fibre, ΔT is the dispersive delay, Δf is the null frequency and λ is the wavelength.

$$DxL = \Delta T\left(\frac{c}{\lambda^2 \Delta f}\right) \tag{3.5}$$

From this characterisation, the dispersion of the 100 km reel of SMF was measured to be 17.3 ps.nm/km at 1550 nm. The dispersion of the fibre was recorded at operating wavelengths from 1535 to 1565 nm in 5 nm steps. Once an accurate measurement of the dispersion was complete the alpha factor could be calculated at each wavelength using Eq. 3.4. The alpha parameter was recorded at each wavelength as a function of bias

voltage, from 0 to -2.6 V in 0.2 V steps. Fig. 3.5 illustrates the alpha parameter profiles as a function of reverse bias over the desired wavelength range. As the value of alpha is inversely proportional to the absorption through Eq. 3.2, the largest values of chirp should be realised at wavelengths where the least amount of absorption is experienced. Therefore wavelength channels with the greatest detuning energy will have the largest alpha parameter, which is confirmed in our experimental calculation. The alpha parameter decreases with a decrease in both operating wavelength and reverse bias.

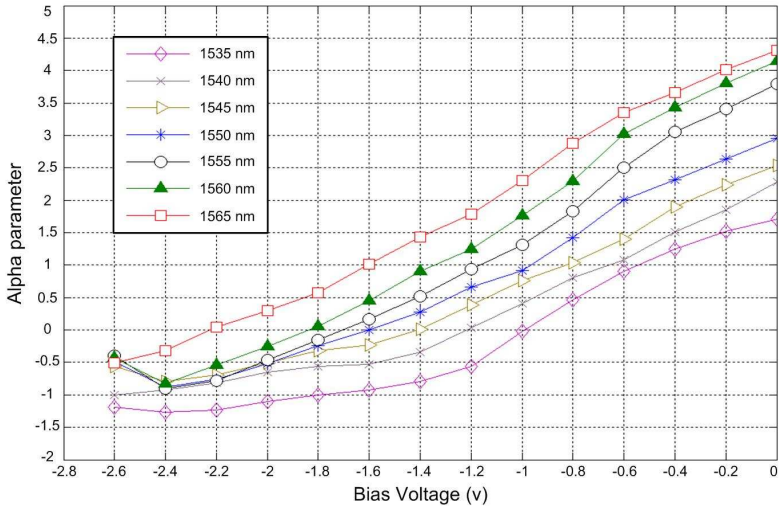

Fig. 3.5. Alpha parameter profile of EAM as a function of bias voltage and operating wavelength

3.4 Dynamic Characterisation

Although the static characterisation of the EAM provides an accurate indication of the insertion loss as a function of wavelength, both the transmission curves and alpha parameter profiles are measured with either simple bias voltage adjustment or small signal analysis. Both of these characteristics will alter under large signal modulation, therefore while the static characterisation offers a good indication of the expected performance of an EAM, it will not provide exact values. Consequently, it is imperative to analyse the carved pulses using either a high speed sampling oscilloscope or a more advanced measurement scheme before employing the pulses in a high speed transmission system. By analysing the pulse extinction, width and chirp as a function of wavelength, bias and modulation voltage, an accurate performance map of the device can be constructed. Such a map could then be used as a quick reference guide to enable the selection of optimum EAM operating conditions at each wavelength, thus providing consistent system performance.

3.4.1 Pulse Characteristics as a Function of EAM Drive Conditions

The experimental setup used to generate short optical pulses from an EAM at a repetition rate of 40 GHz is illustrated in Fig. 3.6. A widely tuneable laser provided a constant CW

light source with an average power of 5 dBm to the EAM. The pulses were then generated by gating the CW light with an amplified sinusoidal wave from a 40 GHz signal generator. This RF signal was applied in conjunction with a DC reverse bias voltage, via a 50 GHz bias tee, to the modulator. The bias voltage was altered between -1 and -2 V in 0.2 V steps and the generated pulses were analysed at RF drive voltages from 2.5 to 3.7 Vpp in 0.3 Vpp increments. This characterisation was implemented over a wide wavelength range from 1540 to 1560 nm in 5 nm steps.

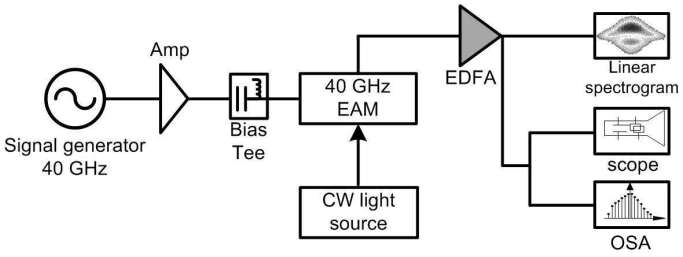

Fig. 3.6. Experimental setup used for 40 GHz pulse generation and subsequent characterisation

The output of an EAM was passed through a booster EDFA to overcome the insertion loss before being monitored by an OSA and a 50 GHz oscilloscope in conjunction with a 50 GHz photodetector. Due to the limited response time of the temporal detection system (scope and detector), it was difficult to obtain information about the characteristics of the generated pulses. In addition as the bias and modulation voltages applied to the EAM were varied, there were no noticeable changes on the oscilloscope (not even pulse width). Therefore a more sophisticated pulse characterisation technique was required to characterise not only the pulse width and shape, but also the phase. This characterisation was accomplished by using the linear spectrographic pulse measurement method outlined in section 2.4.5.

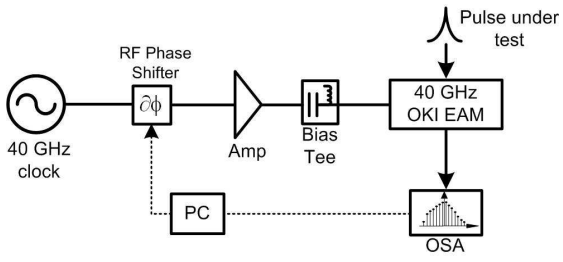

Fig. 3.7. 40 GHz linear spectrogram pulse measurement setup

The linear spectrogram setup used to retrieve the intensity and phase of the generated pulses is depicted in Fig. 3.7. A 40 GHz clock signal (which was referenced to the pulse carving clock) passed through a phase shifter before being amplified and applied to a commercially available 40 GHz OKI EAM, which performed the temporal gating. The relative delay between the input pulse train to be measured and the gate was modified with the voltage controlled phase shifter, which can introduce a delay sufficient enough to

cover the 25 ps time window. The spectrum of the pulse was recorded at each delay with an OSA which had a spectral resolution of 0.01 nm. A computer was used to control the phase shifter and to record the spectra of the gated pulse, to build up a spectrogram on a 128x128 grid. The intensity and phase of the generated pulses were then resolved by using a phase retrieval algorithm [17].

Fig. 3.8 illustrates the intensity and chirp profiles of the generated pulses at an operating wavelength of 1540 nm. For this characterisation the modulation voltage remained constant at 2.5 Vpp while the bias voltage was varied. From the figure it is evident that there is a large variation in pulse width, chirp sign and magnitude and extinction ratio. The pulse width varies from 7.1 to 5.4 ps, while the ER has a low value of 22 dB at -1 V, which gradually increases with greater bias voltage, reaching 26 dB at -2 V. More significantly, there is a large variation in the chirp sign and magnitude. For example, at a bias voltage of -1.4 V the chirp has a positive slope, however as the bias is increased by 0.2 V, the chirp sign flips and now has a negative slope. The reason for this can be understood by considering the small signal alpha parameter characterisation shown in Fig. 3.5. The alpha parameter passes through zero at a bias voltage of -1.2 V and changes from a positive to a negative value. As mentioned earlier, a negative value of alpha will result in a chirp with positive slope. This is extremely important when implementing the RZ transmitter in a long haul transmission system as this tuneable chirp can be used as a significant advantage in combating any residual dispersion that may be present in the dispersion map.

Fig. 3.9 displays the corresponding pulse characterisation at an operating wavelength of 1560 nm. The performance of the EAM, in terms of pulse width, contrast ratio and more importantly chirp, varies significantly at this wavelength in comparison to 1540 nm. The absorption experienced through modulation of the EAM is much lower than that at 1540 nm, as demonstrated in Fig. 3.3. Therefore while biased at -1 V, the gradient of the transmission profile is quite low, resulting in a poor extinction ratio of 8 dB. As the modulation voltage is relatively weak (2.5 Vpp), the off state is not fully reached. As a consequence the pulse intensity in sitting on a CW component and does not go to zero, further degrading the extinction. This value of extinction would be prohibitive in a long haul transmission system and would inevitably limit the achievable transmission distance. As the detuning energy at 1560 nm is greater than at 1540 nm, a lower amount of absorption is experienced; therefore the alpha parameter at this wavelength is larger. Consequently, a negative alpha value is only experienced at -1.9 V.

The pulses analyzed at these two wavelengths exhibit a large variance in performance even though the EAM driving conditions have remained constant. If the EAM was

implemented in a long haul transmission system, with constant driving voltage and bias, there would be a large inconsistency in performance at different wavelengths. Therefore, it is imperative to characterise the pulses at each wavelength, not only over a range of bias voltages but also as a function of modulation voltage. By recording the pulse duration, extinction and chirp at each permutation, an accurate performance map of the device can be obtained. This would allow for the selection of optimum EAM operating conditions at each wavelength, to suit the intended application of the device, whether that is pulse transmission or pulse processing.

To validate the EAM pulse characterisation, the generated pulses were analysed using a commercially available FROG (outlined in section 2.4.4) from Southern Photonics and a high speed PicoSolve optical sampling oscilloscope. The FROG measurement technique provided both the intensity and phase characteristics of the generated pulses, which were directly comparable to the linear spectrogram characterisation. Both the duration and chirp of the generated pulses, characterised as a function of operating wavelength and EAM drive conditions, agreed with our linear spectrogram characterisation. The only discrepancies between the two pulse measurement techniques were the optical extinction ratio of the pulses. This is a result of the poorer sensitivity realised with the FROG technique, which is inherent to the non-linear process. As a result of the poorer sensitivity, higher values of noise threshold were required to achieve convergence of the phase retrieval algorithm, which subsequently inhibited the extinction ratio measurement. Therefore, the linear spectrogram technique provided a more accurate measurement of the optical ER, to values of approximately 30-35 dB below the peak of the pulse.

The PicoSolve sampling oscilloscope was also employed to measure the duration of the optical pulses. It operated over the 1525 to 1565 nm wavelength range and had a temporal resolution of less than 1 ps, with an ultra-low timing jitter of less than 50 fs. As with the FROG characterisation, the high-speed sampling oscilloscope measured the duration of the generated pulses. The values of pulse width, recorded using the PicoSolve, agreed comprehensively with our linear spectrogram characterisation. The performance of the linear spectrogram characterisation has therefore been validated by employing these two commercially available pulse measurement tools and indicates that the linear pulse characterisation provides an extremely accurate depiction of the performance of the EAM based transmitter.

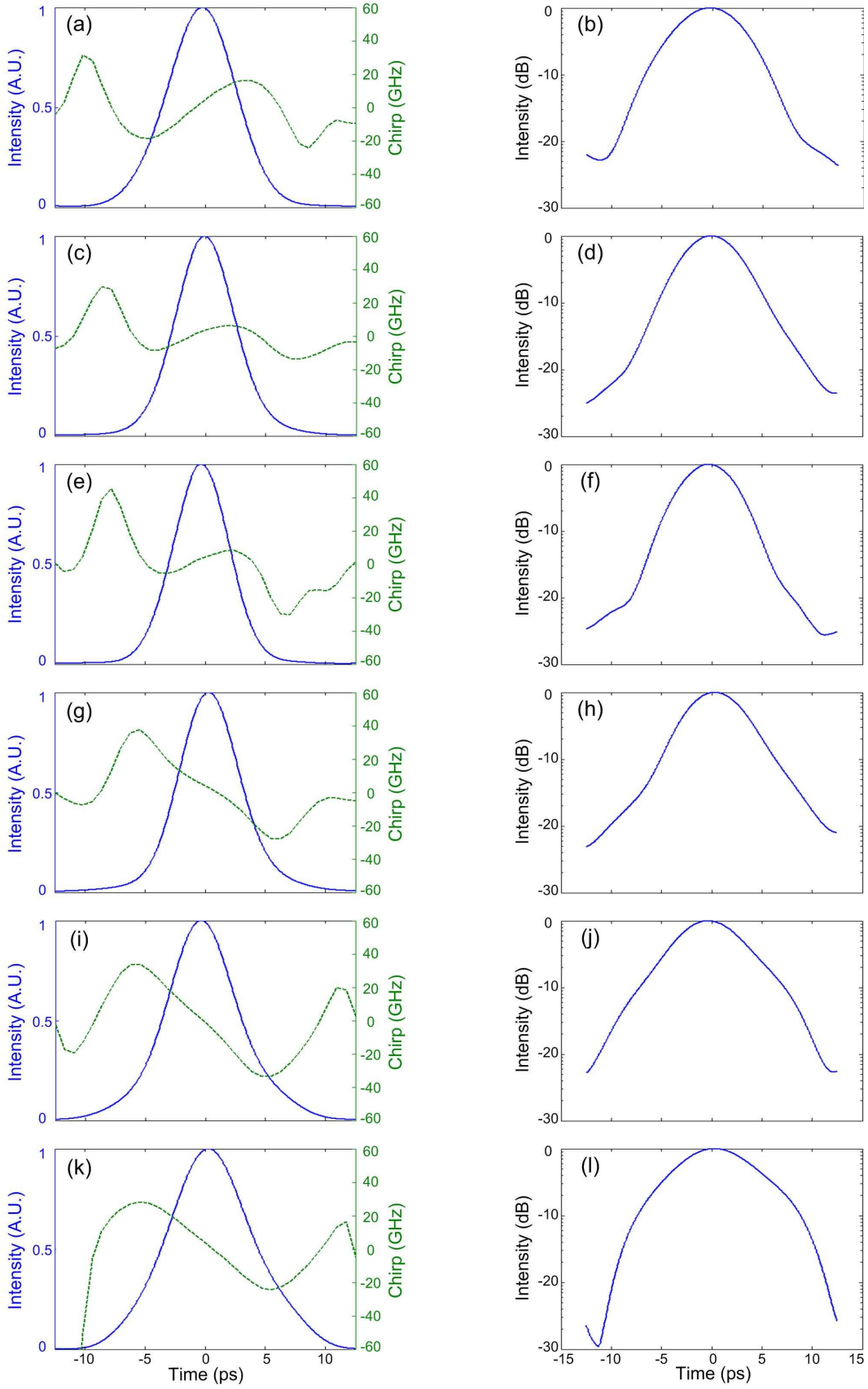

Fig. 3.8. Linear spectrogram measurement of the generated pulses at an operating wavelength of 1540 nm and a modulation voltage of 2.5 Vpp, as a function of bias voltage. (a-b) -1 V, (c-d) -1.2 V, (e-f) -1.4 V, (g-h) -1.6 V, (i-j) -1.8 V and (k-l) -2 V

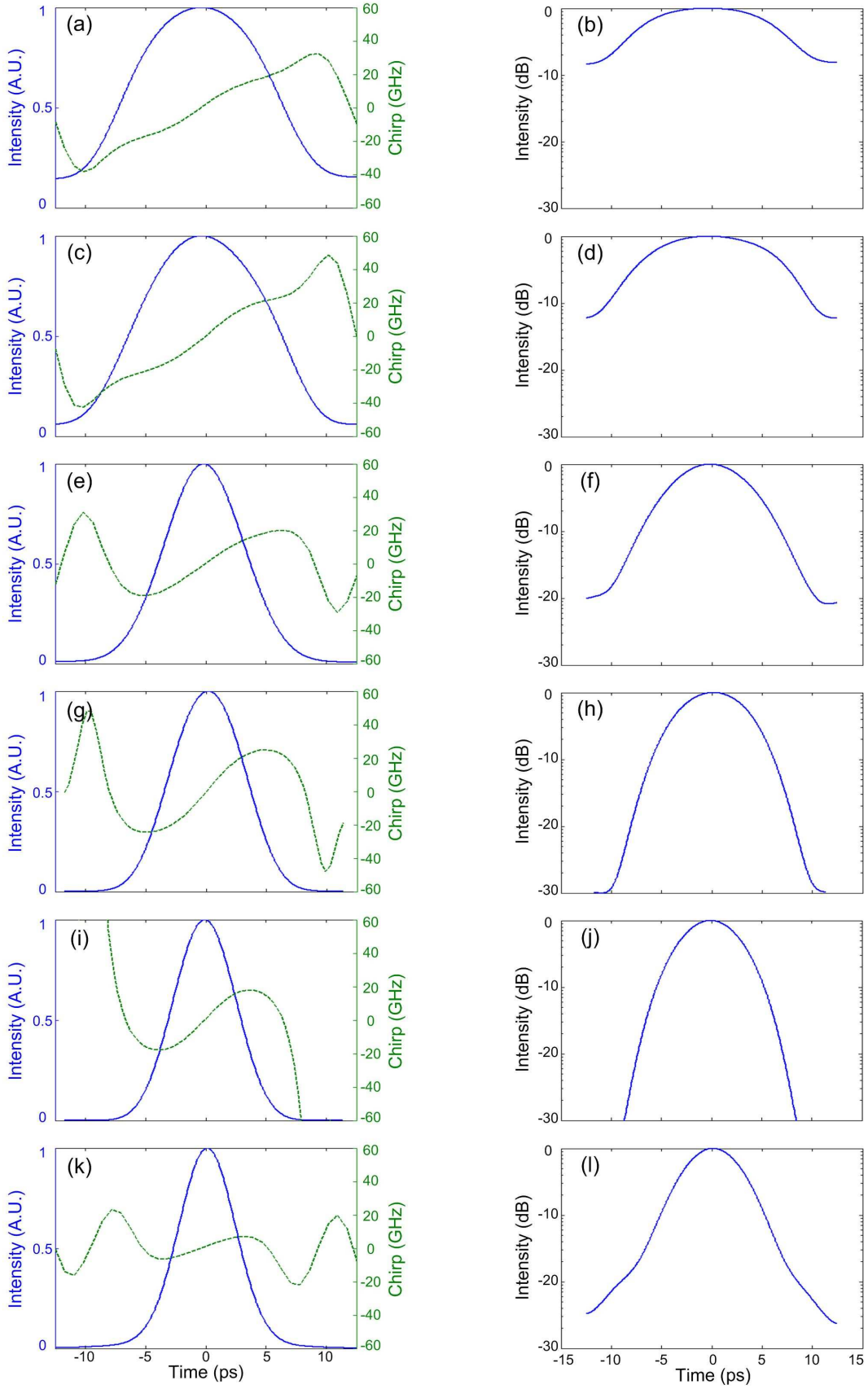

Fig. 3.9. Linear spectrogram measurement of the generated pulses at an operating wavelength of 1560 nm and a modulation voltage of 2.5 Vpp, as a function of bias voltage. (a-b) -1 V, (c-d) -1.2 V, (e-f) -1.4 V, (g-h) -1.6 V, (i-j) -1.8 V and (k-l) -2 V

3.4.2 Performance Map of EAM

Fig. 3.10 illustrates the performance map of our commercially available electro-absorption modulator while operating at two different wavelengths of 1560 and 1540 nm. The generated pulses at each wavelength are again analysed using the linear spectrogram measurement technique for a range of reverse bias and RF drive voltages. The bias voltage was altered between -1 and -2 V, while the RF modulation voltage was varied from 2.5 to 3.7 Vpp. A modulation voltage of 3.7 Vpp is large when considering the static transmission profile (Fig. 3.3b) of the device and would usually exceed the damage threshold. However the EAM response at 40 GHz was 5 dB lower than that obtained at lower frequencies, therefore slightly larger driving voltages are required to achieve maximum on-off contrast. For each permutation of bias and modulation voltage, the pulse width, extinction ratio and chirp slope were recorded for each wavelength.

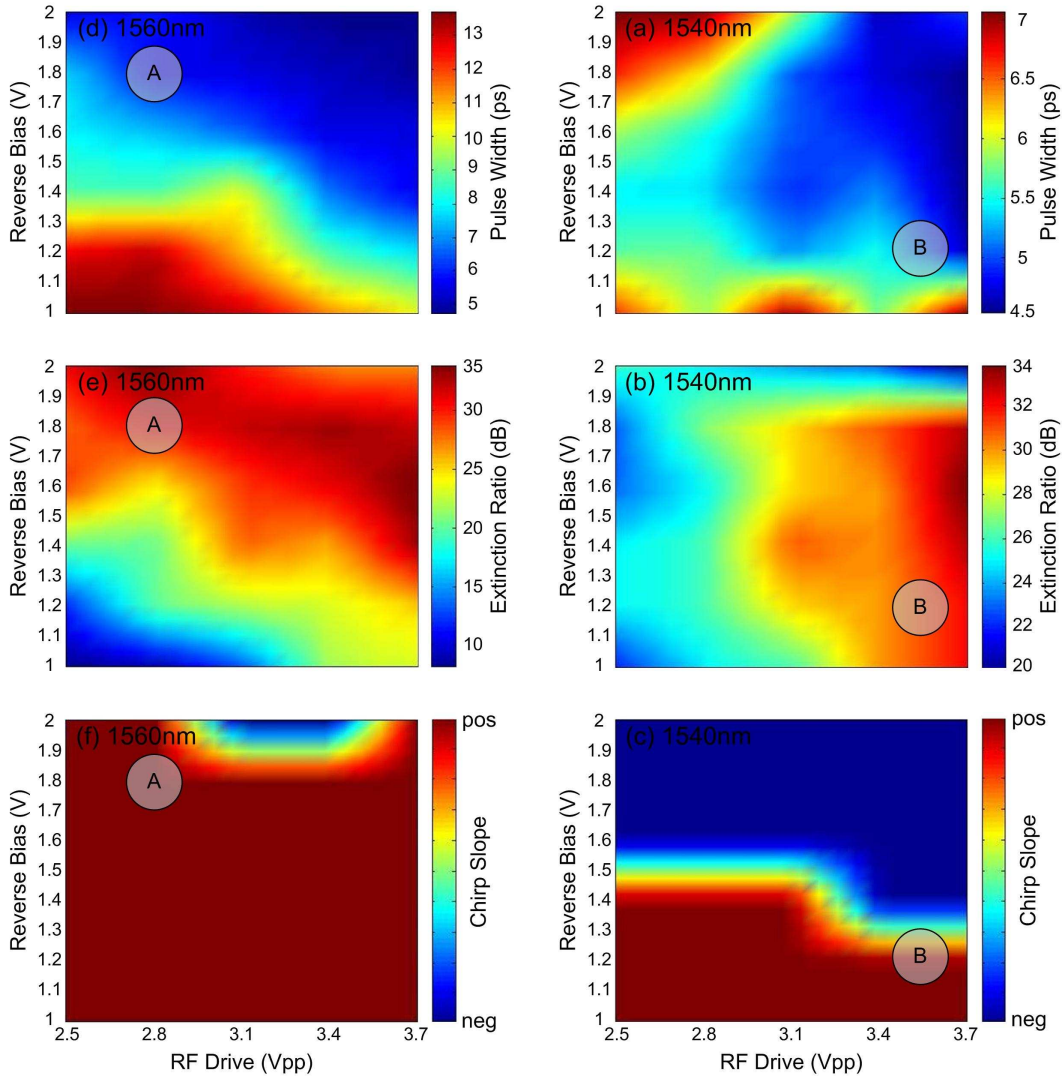

Fig. 3.10. Performance map of an EAM as a function of reverse bias and modulation voltage, for two wavelength channels. (a-c) 1560 nm and (d-e) 1540 nm

Fig. 3.10 (a-c) displays the EAM performance maps of the pulse width, extinction ratio and chirp slope respectively, at an operating wavelength of 1560 nm, while (d-f) illustrates the corresponding performance maps at 1540 nm. From this detailed characterisation, it is evident that there is a large variability in pulse characteristics between the two wavelength channels. For example, the shaded area marked A in the 1560 nm performance maps defines the optimum bias and modulation voltages that could be applied to the EAM, generating pulses that are ideal for long haul transmission systems that exhibit a net positive value of residual dispersion [18]. At point A, the bias voltage was set at -1.8 V, while a modulation voltage of 2.8 Vpp was applied to the EAM. The generated pulses had an approximate duration of 6 ps, a large ER of 30 dB and a positive chirp profile. In a reconfigurable optical network, WDM channels can be switched from one wavelength channel to another in order to accommodate fluctuating traffic patterns and to increase bandwidth in geographical areas where there is higher uptake in new services. Therefore if the EAM driving conditions remained constant and a WDM channel switching event occurred from 1560 to 1540 nm, there would be a significant impact on transmission performance.

While biased at -1.8 V at an operating wavelength of 1540 nm, the performance map indicates that the pulse duration would be slightly broader and the extinction ratio would be marginally reduced, in comparison to the values obtained at 1560 nm. However, more significantly the sign of the chirp slope would be opposite to that experienced at 1560 nm. If the transmission system had a net positive value of residual dispersion, this change in chirp slope would result in degradation in BER performance, inevitably leading to a shorter transmission reach. Therefore optimum bias and modulation voltages must be selected for this operating wavelength and are highlighted by the shaded area labelled B in Fig. 3.10 (d-f). If the sign of the residual dispersion changes across the wavelength range in a long haul transmission system, as illustrated in Fig. 2.11, it may be necessary to generate pulses with alternating signs of chirp slope. Therefore the optimum operation of the EAM can be adapted to obtain the highest level of transmission performance for a wide range of system designs.

It is extremely difficult to select one bias point and one modulation voltage that would give acceptable pulse characteristics over a wide wavelength range. Therefore it is imperative to utilise a control system that will automatically adjust the driving conditions of the EAM when a switching event in an agile optical network occurs. By doing this, an enhanced level of transmission performance can be achieved with a high degree of consistency across a large wavelength range. To demonstrate the effect of a non-

optimised EAM transmitter, the performance of a 42.7 Gb/s EAM based pulse source in a 1500 km transmission system is investigated in greater detail in the following section.

3.5 Wavelength Tuneable RZ Transmission

This section investigates the optimisation of a wavelength tuneable RZ transmitter, consisting of an EAM and a SG DBR tuneable laser, by implementing it in a 1500 km 42.7 Gb/s transmission system. The performance maps of the EAM constructed prior to transmission (as in 3.4.2) are employed to allow optimal selection of the bias and RF modulation voltages to be applied to the EAM at each operating wavelength. To achieve long haul transmission, a circulating loop configuration had to be utilised, which essentially mimics a terrestrial system comprising of a periodically amplified dispersion map. The 42.7 Gb/s transmission system was also simulated using the Virtual Photonics Incorporated (VPI) software package and good agreement between the experimental and simulated results was obtained.

3.5.1 Circulating Loops

With the advent of the EDFA over two decades ago, the potential for ultra-long haul, high bit-rate transmission systems became a reality and a great deal of research interest was placed on pulse propagation over transoceanic distances. Field trials achieving transmission distances over 2000 km at a data rate of 2.5 Gb/s were demonstrated [19], however, one drawback of such experimental setups was the requirement for extensive amounts of equipment such as EDFAs, spools of fibre and filters. Consequently a more feasible solution was required to enable lab based experiments with relatively modest amounts of equipment to simulate long haul dispersion compensated transmission systems. The solution to this problem was the circulating loop [20].

The circulating loop allows for the simulation of a long haul transmission system by reusing or re-circulating the optical data stream through an amplifier chain of modest length, ranging from tens to hundreds of kilometres [21]. Once a specified number of circulations have been completed the reused data is released from the loop and BER analysis is carried out. Fig. 3.11 illustrates the typical setup of a simple re-circulating loop configuration. The loop consists of a switching element that allows data to flow into the loop or indeed to allow data to re-circulate within the loop. A dispersion managed segment of fibre, which typically combines approximately 50 km of SSMF with a corresponding dispersion compensation module (DCM), is combined with an EDFA to overcome the fibre attenuation. Finally an optical band pass filter (OBPF) removes the out of band ASE and an isolator ensures single direction operation. It is important to open the switch for a period, τ, which should allow the loop to be sufficiently filled with data,

thus reducing EDFA transients. Therefore, one re-circulation is completed if the switch remains closed for τ and two round trips if it remains closed for 2τ and so on [22].

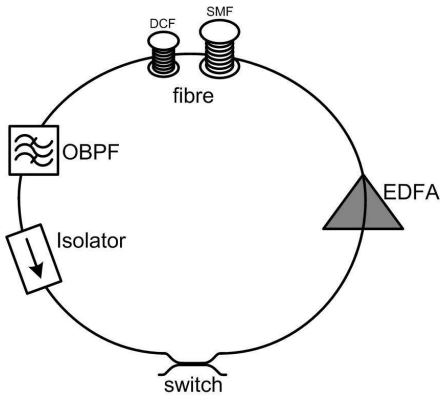

Fig. 3.11. Simple circulating loop configuration

Once the desired transmission distance has been achieved, by completing the required number of circulations, the switch toggles and allows the used data to exit the loop for bit error rate analysis. The key to BER analysis for a circulating loop is to synchronise the optical switch and the BER tester. This is also true for any other measurement equipment such as an OSA or digital communications analyser (DCA). Synchronisation can be achieved be using an electronic gate function that has a duration equal to an integer multiple of τ. This function can then be used to simultaneously trigger the BER tester. Therefore by counting the errors made on the Nth pass of the data around the loop, the BER is measured as a function of received optical power and transmission length [23].

3.5.2 42.7 Gb/s Transmission Test Bed

The experimental setup used to analyse the performance of our wavelength tuneable pulse source is depicted in Fig. 3.12. The pulse source was identical to that used in the preceding sections and again consisted of a 40 GHz CIP EAM and a commercially available widely tuneable SG DBR laser. The tuneable laser provided continuous wave light with an average power of 8 dBm to the sinusoidally driven EAM. A 42.7 GHz clock signal (40 GHz base rate with 7 % overhead required for FEC) from a pulse pattern generator (PPG) passed through a phase shifter and a gain-controlled electrical amplifier before being applied to the EAM via a bias tee. The gain-control on the electrical amplifier allowed for easy adjustment of the peak-to-peak modulation voltage applied to the modulator. A 42.7 Gb/s NRZ pseudorandom binary sequence of length 2^7-1 (which was limited by our ability to generate a true 42.7 Gb/s PRBS bit signal) was used to modulate the pulse train with the aid of a MZM via a polarisation controller. The phase shifter aligned the pulse train and the NRZ data, to ensure that the pulses remained in the centre of the NRZ bit slot. The resultant STM-256 RZ signal was then passed through an

EDFA operating in saturation and followed by a variable optical attenuator, to allow for an easily adjustable power level.

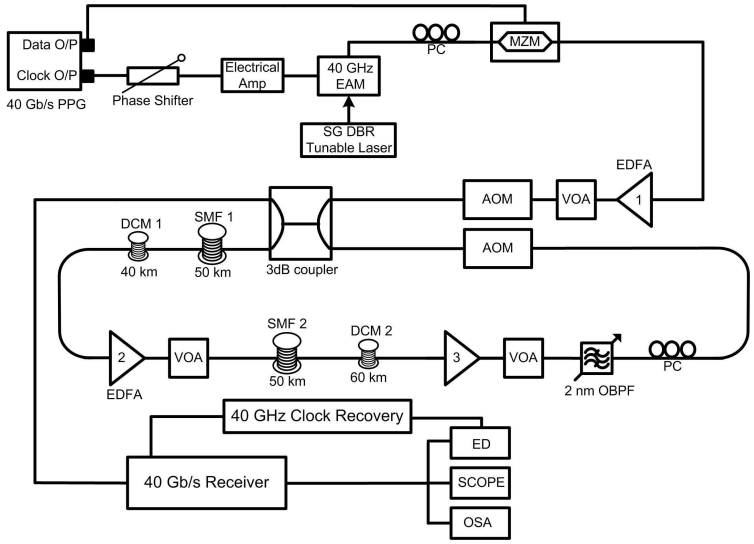

Fig. 3.12. 42.7 Gb/s Circulating Loop Transmission Test Bed

The transmission performance of the EAM-based pulse source was evaluated through a re-circulating loop. The loop has a round trip time (τ) of 600 µs and consisted of two 50 km spans of SMF and two dispersion compensating modules, approximately compensating for 40 and 60 km lengths respectively. The SMF exhibited a measured dispersion of 17.37 ps/nm.km and specified dispersion slope of 0.06 ps/km/nm^2 at 1550 nm, while the slope-matched DCM had a dispersion of -36 ps/nm.km and a dispersion slope of -0.12 ps/km/nm^2 at 1550 nm. The calculated residual dispersion per loop was 4.3 ps/nm at 1550 nm, such that self phase modulation was required to balance a portion of the net residual dispersion. An average launch power into the loop remained constant at 0 dBm as the operating wavelength of the pulse source was varied.

Two EDFAs with 5.5 dB noise figures were employed to overcome the accumulated attenuation of the fibre links whilst variable optical attenuators offered controllability over the power within the loop. An OBPF with a 3 dB bandwidth of 2 nm was placed in the loop primarily to minimise the accumulation of out of band ASE but is also believed to have provided a degree of pulse reforming in combination with self phase modulation in the transmission fibre [24]. A PC was adjusted to maintain an optimum state of polarisation by monitoring the BER performance. This optimisation was carried out at each of the operating wavelengths and for each number of loop circulations. This optimisation in effect, ensured that the impact of PMD on transmission performance was equalised (minimised) for all wavelengths.

The 40 Gb/s receiver consisted of two stages of optical amplification with each amplifier followed by a band pass filter to suppress ASE. Clock recovery was performed by using

an electronic phase locked loop (PLL) which was used to trigger the oscilloscope and error detector for received eye and BER analysis respectively. The BER was recorded as a function of the number of transmission loops, for each wavelength and EAM drive condition. An optical spectrum analyser and a high speed oscilloscope were used to monitor the pulse spectrum and received eyes respectively. All test equipment was gated using the loop timing signal to isolate the output after a given transmission distance.

3.5.3 Single Channel Transmission Performance

Initially, the RZ wavelength tuneable transmitter was employed in the re-circulating loop setup at an operating wavelength of 1560 nm. The conditions allowing the greatest number of re-circulations within the FEC limit were obtained by tuning the DC bias of the EAM between -1.4 and -2 V in 0.2 V steps and by tuning the peak-to-peak drive signal from 2.5 to 3.7 Vpp in 0.6 V steps.

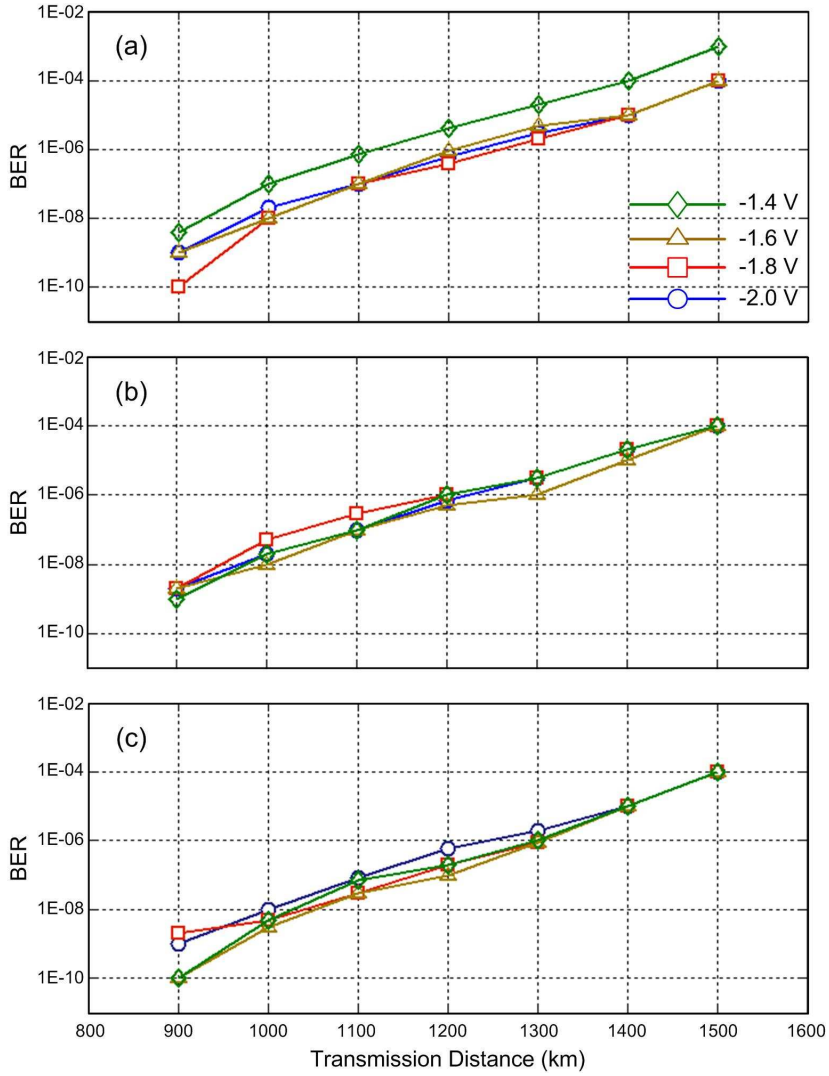

Fig. 3.13. BER as a function of transmission distance and reverse bias at an operating wavelength of 1560 nm, for three modulation voltages. (a) 2.5 Vpp, (b) 3.1 Vpp and (c) 3.7 Vpp

Fig. 3.13 illustrates the BER as a function of transmission distance measured over the range of bias and modulation voltages outlined above. When the modulation voltage is set at 2.5 Vpp (Fig. 3.13a) the transmission performance is consistent for each value of reverse bias, except for the case when the EAM was biased at -1.4 V. At this bias voltage the pulse duration was 9 ps and the extinction ratio was 18 dB. The slight degradation in performance (1400 km at BER of 10^{-4}) achieved at this bias voltage may be attributed to the large pulse width and poor optical extinction. As the chirp profiles of the generated pulses are positive at all bias voltages from -1.4 to -2 V, consistent performance was expected once critical pulse parameters, such as PW and ER, were maintained within acceptable values. The transmission performance of the pulses proved consistent at the remaining bias voltages, achieving a transmission distance of 1500 km at a BER of 10^{-4}, which is below the FEC limit to allow a slight margin for aging.

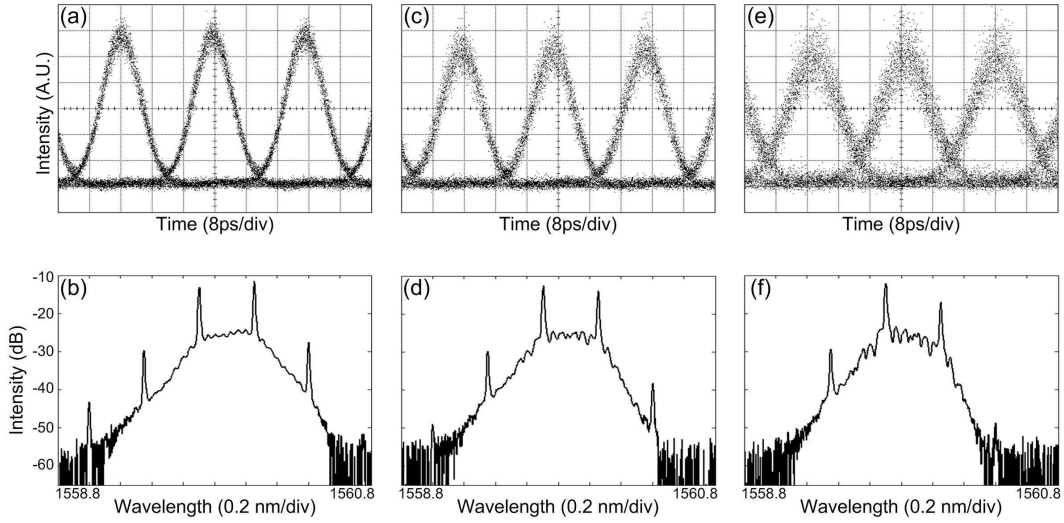

Fig. 3.14. Received eye diagrams and corresponding spectra at a modulation voltage of 3.1 Vpp and a reverse bias of -2 V at 1560 nm, after, (a, b) 0 km, (c, d) 500 km and (e, f) 1000 km

The transmission performance at the remaining two RF modulation voltages of 3.1 and 3.7 Vpp were similar, achieving a maximum transmission distance of 1500 km at a BER of 10^{-4}. The increase in modulation voltage lead to a larger ER and narrower pulse duration at a bias voltage of -1.4 V, therefore a more equalised level of BER performance was realised over the bias range. Fig. 3.14 displays the received eye diagrams and the corresponding spectra when a modulation voltage of 3.1 Vpp was applied to the EAM, which was biased at -2 V. Figures (a and b) show the received eye and spectrum for the back-to-back case, prior to transmission. The eye is open and exhibits a low level of temporal jitter, thus providing error free performance. After a transmission distance of 500 km (c, d) the received eye remained open with a slight increase in jitter but remained error free. The received eye after 1000 km exhibits a greater level of jitter and is slightly

closed with respect to the received eyes after 0 and 500 km and as a consequence generated a BER of 10^{-8}.

In order to maximise the obtainable transmission distance of our optical RZ pulses, the OBPF in the circulating loop was slightly detuned from the carrier frequency, producing a vestigial side-band (VSB) RZ signal. This is a simple, low cost method employed to increase the spectral efficiency of the generated pulses, therefore improving their fibre dispersion tolerance [25]. This filter detuning can be observed from the received spectra displayed in Fig. 3.14 (b, d, f) as a slight increase in magnitude of one of the sidebands relative to the central carrier frequency. Although the transmission performance of our RZ transmitter performed consistently while operating at one specific wavelength channel, it is imperative to analyse the performance over a wide wavelength range. As illustrated from the EAM performance maps, the generated pulse characteristics can vary significantly as a function of operating wavelength, which is expected to significantly affect transmission performance.

3.5.4 Transmission Performance Variation with Wavelength

Once again the RZ transmitter was implemented in the 42.7 Gb/s circulating loop test bed at an operating wavelength of 1560 nm. The bias and RF drive voltages were tuned to provide the greatest transmission reach within the FEC limit and values of -2 V and 2.5 Vpp were selected respectively. Both of these EAM drive conditions and the launch power (0 dBm) into the loop were held constant and the operating wavelength was varied. Fig. 3.15 (a) represents this non-optimised scenario, where the RF drive (2.5 Vpp) and the DC bias (-2 V) applied to the EAM remained constant for each operating wavelength (1540, 1550 and 1560 nm). The corresponding eye diagrams, recorded after 1000 km, are also illustrated in Fig. 3.15 (b).

As can be seen, a great variability in transmission performance was obtained with the error correctable maximum distance (a BER of 10^{-3}) varying from 1000 to over 1500 km, or equivalently the BER varying by over two orders of magnitude. At a BER of 10^{-4} a transmission distance of 1500 km was achieved when the tuneable laser in the RZ transmitter operated at 1560 nm, which decreased to 1000 km when operating at 1540 nm, representing a 33 % drop in transmission performance. Degraded performance is also realised when operating at 1550 nm, which achieves a transmission distance of 1350 km at a BER of 10^{-4}. Such a large variance in system performance illustrates that constant EAM driving conditions will lead to unacceptable levels of performance over a wide wavelength range, which would be unacceptable in a real system.

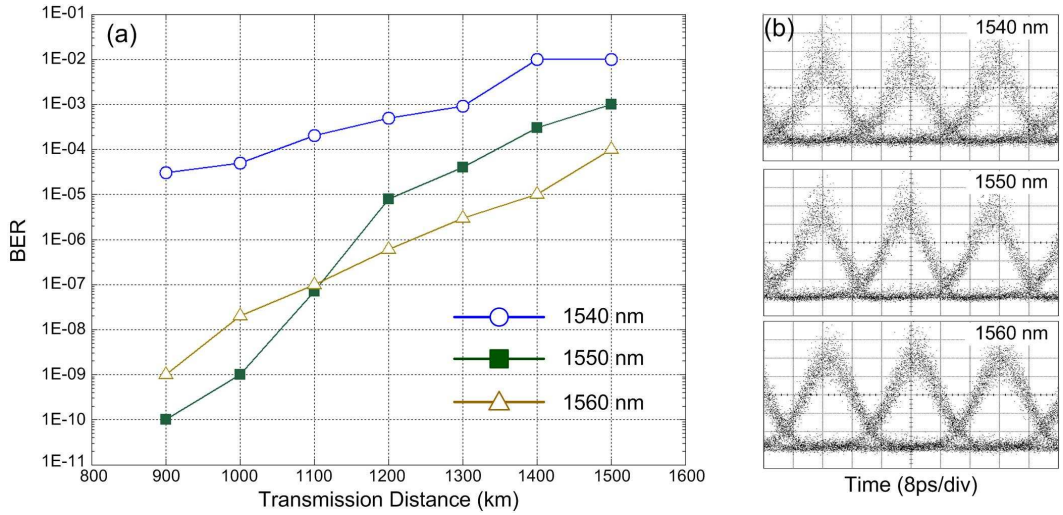

Fig. 3.15. (a) BER as a function of transmission distance for a non-optimised transmitter and (b) corresponding eye diagrams received after 1000 km for 1540, 1550 and 1560 nm respectively

To understand the discrepancies in performance over the wavelength range, the performance map of the EAM can be considered in order to identify the pulse characteristics that are leading to the transmission impairment. Fig. 3.16 illustrates the intensity and chirp profiles, measured using the linear spectrogram technique, for the pulses under the constant drive conditions. The temporal widths of the three pulses are 5.5, 5.3 and 6 ps respectively. It is anticipated that such variations would result in a negligible impact on transmission performance, whilst the measured extinction ratios (25 to 31 dB) would also result in a negligible change in transmission distance. However, the chirp magnitude and more specifically sign of the chirp changes distinctively from one pulse to another. At 1540 nm where the greatest degradation in transmission performance was realised, the chirp profile is negative across the centre of the pulse. At 1550 nm, the chirp flattens out and becomes positive across the centre of the pulse with a decrease in magnitude. Significantly, at 1560 nm, the chip is opposite to that experienced at 1540 nm and there is a positive chirp profile with a larger magnitude.

The fibre used in the circulating loop is slope matched and as mentioned in section 3.5.2 there was a measured net residual dispersion of 4.3 ps/nm.loop (at 1550 nm), therefore the positive chirp profile exhibited at an operating wavelength of 1560 nm best suits the given dispersion map of the transmission link, providing the greatest tolerance to the dispersive and non-linear effects during transmission. By comparing the intensity and phase information of the generated pulses at each wavelength, with the reference wavelength (1560 nm), an estimate can be made as to which drive conditions for the transmitter would achieve similar pulse profiles at each wavelength, thereby achieving extended transmission reach and greater performance uniformity over the wavelength tuning range.

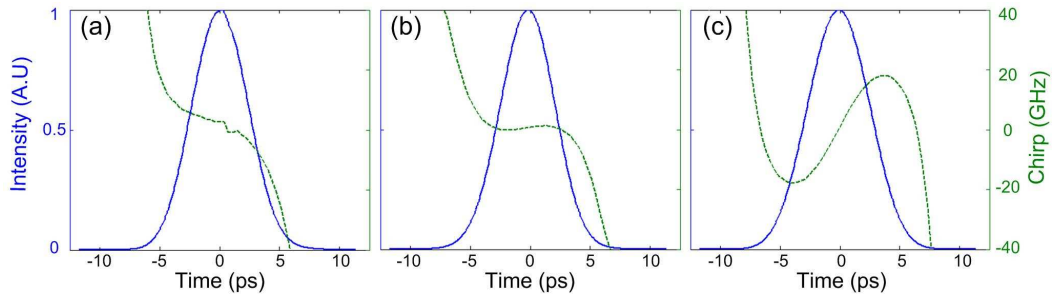

Fig. 3.16. Linear spectrogram characterisation of the non-optimised pulses with constant bias (-2 V) and RF drive (2.5 Vpp) applied to the EAM, for three different wavelengths, (a) 1540, (b) 1550 and (c) 1560 nm

An estimate of the optimum EAM driving conditions for each wavelength can be deduced by considering the performance maps of the device characterised in section 3.4.2. From the performance map the bias of the EAM must be adjusted to -1.4 V when operating at 1540 nm with a slightly larger modulation voltage of 3.1 Vpp. From Fig. 3.10 it is apparent that this will result in a pulse with a positive chirp profile, a larger extinction ratio and a slightly smaller duration. Similarly, when operating at 1550 nm, the bias must also be slightly reduced to -1.8 V and again driven with an increased RF driving voltage of 3.1 Vpp. The corresponding pulse intensity and chirp profiles at the new optimised EAM drive conditions for the three wavelengths are illustrated in Fig. 3.17.

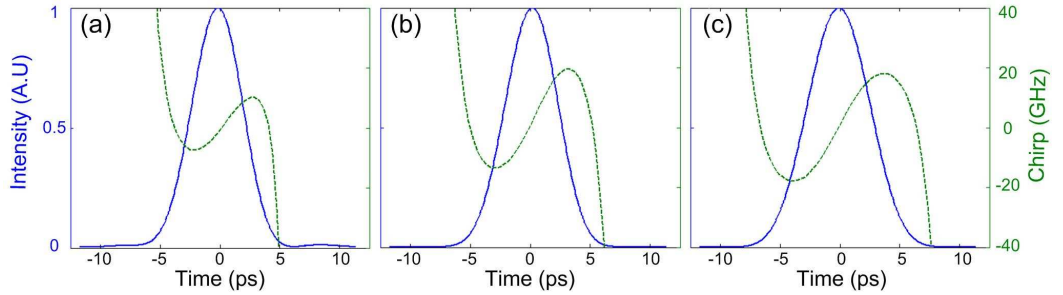

Fig. 3.17. Linear spectrogram characterisation of the optimised pulses for three different wavelengths, (a) 1540, (b) 1550 and (c) 1560 nm

The sign and magnitude of the pulse chirp profiles at all three wavelengths are now similar, therefore indicating that a more consistent level of performance may be achieved across the C-band. To verify this, the transmitter was again employed in the 42.7 Gb/s re-circulating transmission test bed to determine the performance of the optimised pulses at each wavelength. Fig. 3.18 illustrates the BER performance as a function of transmission distance, with the corresponding eye diagrams, recorded after 1000 km of SMF. By optimising the drive conditions of the EAM in our RZ tuneable transmitter, a greater transmission distance (within an error correctable level) has been achieved at 1540 and 1550 nm. A distance of 1400 km at a BER of 10^{-4} was realised while operating at 1540 nm, representing an improvement of 400 km, relative to the non-optimised scenario. At

1550 nm, there is an improvement of 150 km (relative to the non-optimised case), thereby ensuring a near consistent level of performance over the entire wavelength range. Extrapolation suggests that the error correctable maximum distances below 10^{-3} were 1500, 1600 and 1600 km at the operating wavelengths 1540, 1550 and 1560 nm respectively.

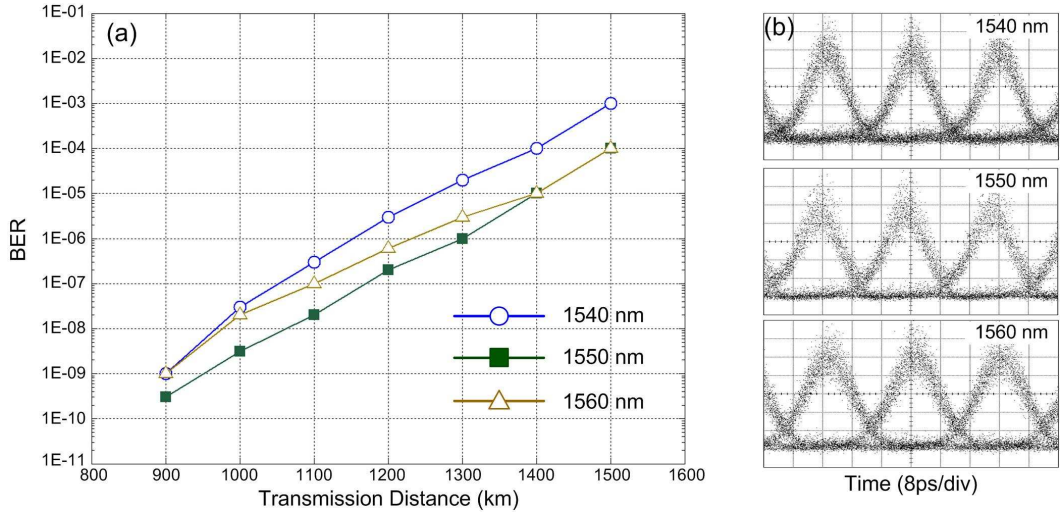

Fig. 3.18. (a) BER as a function of transmission distance for a non-optimised and (b) corresponding eye diagrams received after 1000 km for 1540, 1550 and 1560 nm respectively

By utilising the linear spectrogram technique to build up a performance map of the EAM over a wide wavelength range, optimal drive conditions could be selected for each wavelength on the ITU grid. This characterisation could be used to create a look-up table, comprising of a modulation voltage and DC bias for each ITU wavelength channel. Therefore, as the SG DBR tuneable laser is switched from one wavelength channel to another, the drive conditions of the EAM would be altered simultaneously, thereby achieving the ideal pulse profile for transmission, ensuring consistent performance is maintained over the entire wavelength range.

3.5.5 Wavelength Tuneable Transmitter Comparison

To quantify the performance of our EAM based wavelength tuneable transmitter, it was compared to a commercially available SHF 44 Gb/s MZM based transmitter. This transmitter consisted of two mach-zehnder modulators that had 3 dB bandwidths of 30 GHz. Both of the chirp free lithium niobate modulators were thermally controlled and individual amplifiers were used to control the applied peak-to-peak modulation voltages. To obtain 33 % RZ pulses the first MZM was modulated at $2V\pi$ with the 42.7 GHz clock signal from the PPG and were subsequently fed straight into the second modulator which was driven at $V\pi$ with the 42.7 Gb/s NRZ data signal. This transmitter essentially replaced the EAM and MZM components in the test bed illustrated in Fig. 3.12. The BER

was recorded as a function of the greatest obtainable transmission reach within an error correctable maximum distance. Fig. 3.19 (a) illustrates the BER performance of the commercially available MZM based transmitter for three different wavelengths, 1540, 1550 and 1560 nm. The corresponding eye diagrams received after 10 loop re-circulations (1000 km) are illustrated in Fig. 3.19 (b).

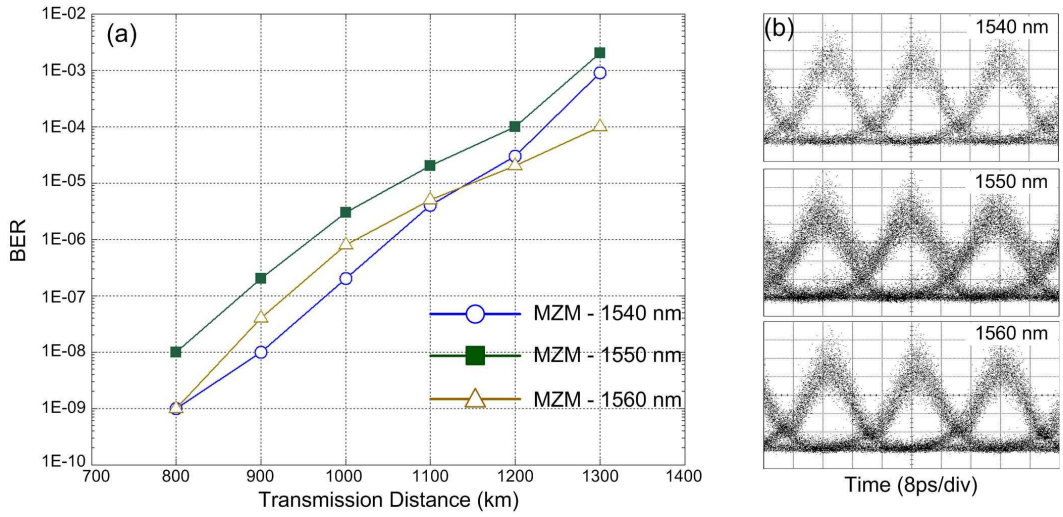

Fig. 3.19. (a) BER as a function of transmission distance and wavelength for an MZM based pulse source and (b) corresponding eye diagrams received after 1000 km for 1540, 1550 and 1560 nm respectively

As seen from the figure, the transmission performance of the MZM based source was consistent across the 20 nm wavelength range. While operating at 1540 nm a transmission distance of approximately 1230 km was achieved at a BER of 10^{-4}. At 1550 nm there was a slight degradation in performance as only 1200 km was realised at this wavelength and this was also evident from the higher amount of jitter seen in the received eye diagram. There was an improvement in transmission performance of 100 km when the tuneable laser was switched to 1560 nm. The consistency of this device was expected as the MZM has a weak dependency on wavelength and has an alpha parameter approximately equal to zero, therefore the generated pulses exhibit almost zero chirp and are transform limited. The performance of this transmitter is inferior to the EAM based source as the greatest transmission reach was as much as 20 % less than that achieved with the EAM. The extended transmission reach of the EAM was due to the tuneable chirp profile exhibited by this device, combined with smaller pulse durations and slightly high ER. This is illustrated in Table 3.2, which outlines the non-optimised and optimised EAM based transmitter performance and the MZM source performance as a function of wavelength.

Not only does the performance of the EAM based transmitter exceed that of the MZM in achievable transmission reach, the peak-to-peak voltages required for each device differ substantially. The EAM generally requires a maximum modulation voltage of 3.7 Vpp,

however to achieve 33 % RZ pulses from an MZM, it must be driven at 2Vπ which generally requires a voltage of approximately 10 Vpp. Secondly, the MZM based pulse source was inherently sensitive to the state of polarisation and hence a PC was required for constant adjustment of polarisation. Conversely the EAM was polarisation insensitive, thereby providing more simple and stable operation. Finally, the integrability of the EAM is much higher than that of a MZM and when combined with its lower power consumption and extended transmission capability, provides the ideal platform for a low cost, small form factor wavelength tuneable RZ transmitter ideal for implementation in future long haul reconfigurable WDM networks.

	EAM - non-optimised			EAM - optimised			MZM
Wavelength	Bias	RF Drive	TX Distance	Bias	RF Drive	TX Distance	TX Distance
1540 nm	-2 V	2.5 Vpp	1000 km	-1.4 V	3.1 Vpp	1400 km	1230 km
1550 nm	-2 V	2.5 Vpp	1350 km	-1.8 V	3.1 Vpp	1500 km	1200 km
1560 nm	-2 V	2.5 Vpp	1500 km	-2 V	2.5 Vpp	1500 km	1300 km

Table 3.2. Transmission performance for both the non-optimised and optimised EAM based transmitter and the MZM based transmitter for the three wavelength channels

3.5.6 Simulated 42.7 Gb/s Transmission System

To confirm the performance of our EAM based transmitter over a wide wavelength range, the circulating loop transmission test bed described in section 3.5.2 was simulated using the VPI transmission maker software package. The complete transmission system is illustrated in Fig. 3.20. Continuous wave light with an average power of 7 dBm was applied to a sinusoidally driven EAM. The EAM model contained both the static transmission and alpha parameter profiles for each wavelength that were experimentally obtained in section 3.3. An initial pulse characterisation was performed for a number of reverse bias and modulation voltages for several wavelengths from 1535 to 1565 nm. The pulse duration, extinction ratio and chirp magnitude and sign were recorded. This was necessary as it would give an indication as to the optimum bias conditions of the EAM, similar to the performance maps that were constructed experimentally.

Once this characterisation was complete the generated pulses were then modulated with a 42.7 Gb/s PRBS of length 2^7-1, with the aid of an ideal amplitude modulator. A power combiner was used to add white Gaussian noise to the generated pulses to emulate more realistic system performance. The pulses were subsequently amplified before entering a re-circulating loop that consisted of two 50 km reels of SMF and two compensation modules, compensating for lengths of 40 (DCF 1) and 60 km (DCF 2) respectively. Two 5.5 dB noise figure EDFAs overcame the accumulated attenuation of the fibre links and a 2 nm OBPF was used to suppress the out of band ASE. Once the desired number of

circulations was complete the signal passed through a 40 Gb/s receiver. This receiver was similar to that employed in the experimental setup and consisted of two low noise EDFAs and two band-pass filters with 3 dB bandwidths of 3.5 and 1 nm respectively. Clock recovery was performed and BER measurements were recorded as a function of transmission distance for each EAM drive condition and from 1535 to 1565 nm in 5 nm steps. A scope and an OSA monitored the received eyes and the corresponding spectra.

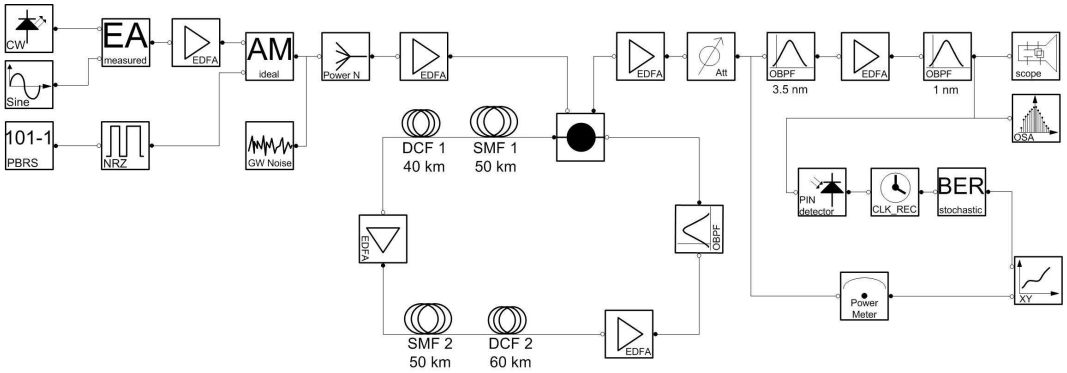

Fig. 3.20. 42.7 Gb/s VPI transmission model

As in the experimental procedure the RZ wavelength tuneable transmitter was initially employed in the circulating loop simulation model at a wavelength of 1560 nm. The conditions allowing the greatest number of re-circulations within the FEC limit were obtained by tuning the DC bias of the EAM between -1 and -2.2 V in 0.2 V steps. As the EAM model had an infinite electrical bandwidth response, the modulation peak-to-peak voltage was altered from 1 to 2.6 Vpp in 0.4 V steps. Once the greatest transmission distance was achieved, the bias and RF drive voltages and the launch power (0 dB) were held constant as the operating wavelength was varied. The optimal values were -1.4 V reverse bias and a modulation voltage of 1.4 Vpp. This is, as in the experiment, referred to as the non-optimised scenario and is illustrated in Fig. 3.21 along with sample received eye diagrams at 1540, 1550 and 1560 nm.

As can be seen, a great variability in transmission performance was obtained with the error correctable maximum distance varying from 1000 to 1500 km. At a BER of 10^{-4} a transmission distance of approximately 1500 km was achieved when the transmitter operated at 1560 nm, which decreased to 1100 at 1540 nm, representing a 30 % drop in transmission performance. The shortest transmission reach achieved at a BER of 10^{-4} was 950 km at 1535 nm. As previously mentioned, such a large variance in system performance over the C-band wavelength range illustrates that constant EAM drive conditions, in the transmitter will lead to un-acceptable levels of performance over a wide wavelength range.

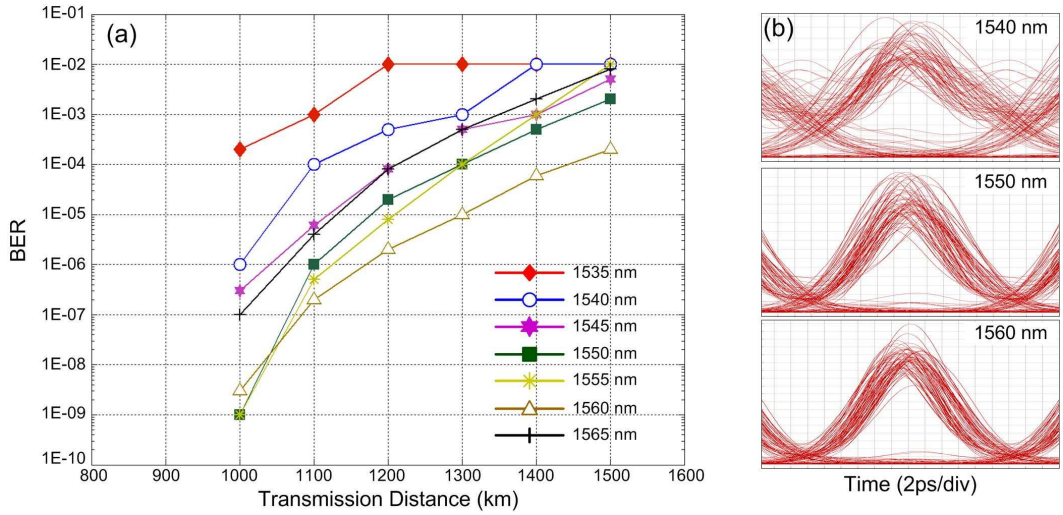

Fig. 3.21. (a) Simulated BER as a function of transmission distance for a non-optimised EAM at wavelengths from 1535 to 1565 nm and (b) sample eye diagrams received after 1000 km for 1540, 1550 and 1560 nm respectively

To understand the varying levels of performance achieved as a function of operating wavelength the intensity and chirp profiles (as measured in VPI) were analysed. Fig. 3.22 (a-c) displays the intensity and chirp profiles of the generated pulses under the constant EAM drive conditions (-2 V bias and 1.4 Vpp clock signal). At 1540 nm where one of the poorest levels of transmission performance was realised, the chirp profile is negative across the centre of the pulse. At 1550 nm however, the sign of chirp has flipped and is now positive, while at 1560 nm the sign of chirp is also positive, although with a slightly larger magnitude. This change in chirp sign is in good agreement with the experimental results and gives an accurate indication as to the affect the pulse chirp has on transmission. At 1535 nm, there is a large degree of negative chirp and when combined with the net positive dispersion of the loop results in degraded transmission performance. Another limiting factor is a low ER of 12 dB that is exhibited at this wavelength under the application of a small reverse bias. This value of extinction ratio and the slightly broader pulses also contributed to the degraded transmission reach (950 km at a BER of 10^{-4}) achieved at this wavelength channel.

By comparing the intensity and phase of the generated pulses, with the reference wavelength (1560 nm), an estimate can be made as to which drive conditions for the transmitter would achieve a similar pulse profile at each wavelength, thereby achieving extended transmission reach and greater performance uniformity over the tuning range. At 1540 nm for example the DC bias of the EAM was adjusted to -1.4 V and the modulation voltage was increased to 2.2 Vpp. Similarly, at 1550 nm, the bias voltage was decreased to -1.8 V and the EAM was again driven with a peak-to-peak voltage of 2.2

Vpp. The optimised pulse profiles at these two wavelengths are illustrated in Fig. 3.22 (d-f).

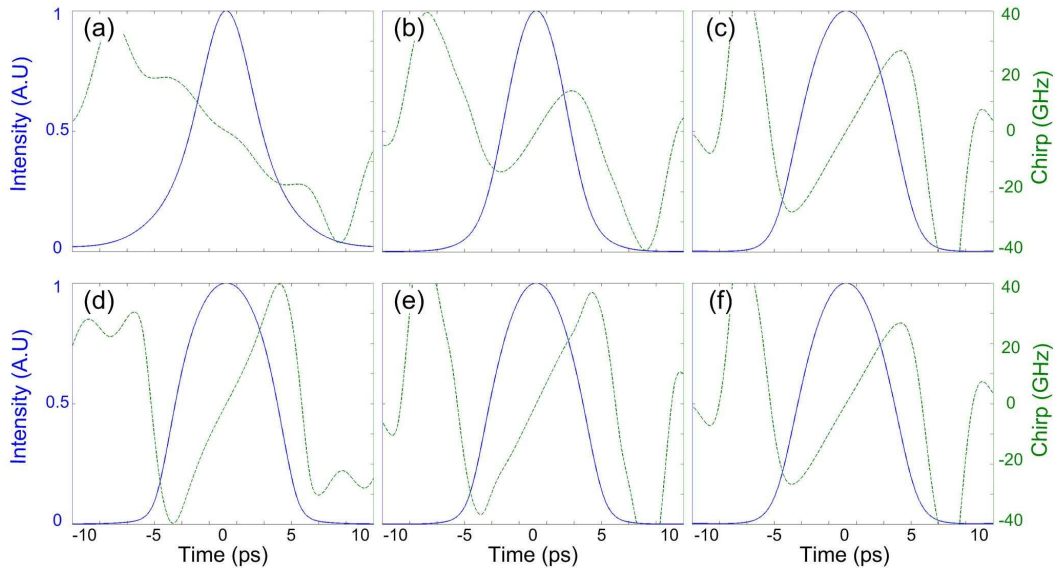

Fig. 3.22. (a-c) Intensity and chirp profiles for non-optimised scenario at wavelengths 1540, 1550, and 1560 nm and (d-e) corresponding intensity and chirp profiles for the optimised scenario

This selection of bias and drive voltages was completed for all wavelengths until the sign and magnitude of the pulses were similar. The optimised transmitter was again employed in the 42.7 Gb/s circulating loop simulation model to verify if a greater level of performance uniformity over the C-band could be achieved. Fig. 3.23 illustrates the optimised transmission performance, again with the corresponding eye diagrams at 1540, 1550 and 1560 nm, received after 1000 km. By adjusting the bias conditions of the EAM, a greater transmission distance has been achieved at all wavelengths. A distance of 1450 km at a BER of 10^{-4} was realised while operating at 1535 nm, representing an improvement of 500 km, relative to the non-optimised transmitter. At 1550 nm, an improvement of 150 km was achieved. The increased level of performance at 1540 nm is visually apparent by comparing the received eye diagrams for both EAM scenarios. The eye for an optimised transmitter contains a lower level of temporal jitter and exhibits a greater eye opening, both of which contribute to increased BER performance.

Table 3.3 displays the achieved transmission reach within a BER of 10^{-4} for the non-optimised transmitter, where constant DC bias and modulation voltages were applied to the EAM. The corresponding optimised EAM drive conditions are also shown with the improved transmission reach, obtained over the entire wavelength range. The simulation results are in good agreement to the experimental results outlined in section 3.5.4 and demonstrate that the wavelength tuneable transmitter has the capability to operate over the entire C-band wavelength range. Consistent performance was achieved by generating

pulses with similar pulse width, shape, extinction and most importantly chirp sign. The same chirp sign was desired at all operating wavelengths in the experiment and simulation because for both cases there was a net positive residual dispersion in the fibre link across this waveband. If the dispersion map was similar to that shown in Fig. 2.11, then opposing chirp signs would be required for wavelengths on the opposite ends of the spectrum. This is an important issue, but further demonstrates the dynamic capabilities of EAM based RZ transmitters as both positive and negative signs of chirp can be achieved by simple adjustment of the reverse bias and modulation voltages. Therefore RZ transmitters based on an EAM and SG DBR tuneable laser are a viable option for future long haul reconfigurable WDM networks.

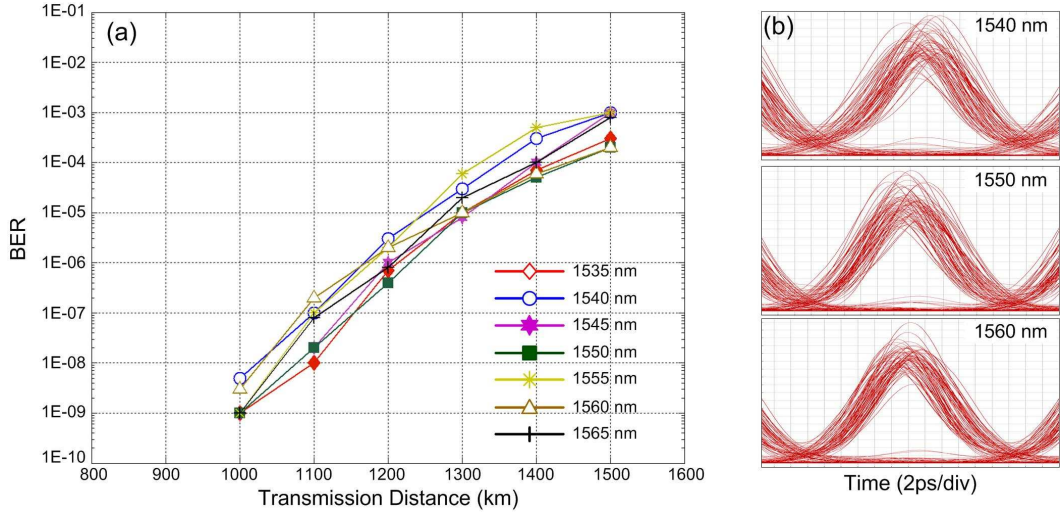

Fig. 3.23. (a) Simulated BER as a function of transmission distance for an optimised EAM at wavelengths from 1535 to 1565 nm and (b) sample eye diagrams received after 1000 km for 1540, 1550 and 1560 nm respectively

	Non-optimised Scenario			Optimised Scenario		
Wavelength	Bias	RF Drive	TX Distance	Bias	RF Drive	TX Distance
1535 nm	-2 V	1.4 Vpp	950 km	-1.2 V	2.4 Vpp	1450 km
1540 nm	-2 V	1.4 Vpp	1100 km	-1.4 V	2.2 Vpp	1400 km
1545 nm	-2 V	1.4 Vpp	1200 km	-1.6 V	2.6 Vpp	1400 km
1550 nm	-2 V	1.4 Vpp	1300 km	-1.8 V	2.2 Vpp	1500 km
1555 nm	-2 V	1.4 Vpp	1300 km	-1.8 V	2.4 Vpp	1400 km
1560 nm	-2 V	1.4 Vpp	1500 km	-2 V	1.4 Vpp	1500 km
1565 nm	-2 V	1.4 Vpp	1200 km	-2.2 V	1.6 Vpp	1400 km

Table 3.3. EAM bias and drive conditions for each operating wavelength and corresponding transmission reach for both the optimised and non-optimised transmitter scenarios

3.6 Summary

An electro-absorption modulator, when combined with a widely tuneable laser such as an SG DBR TL, provides an excellent source for high speed wavelength tuneable pulses that are ideal for implementation in future reconfigurable core optical networks. As the

characteristics of an optical pulse, generated using an EAM device, are highly dependant on operating wavelength, reverse bias and modulation voltage, it is important to carry out pre-transmission characterisation. Such a pulse characterisation can be advantageous as it allows the pulse parameters (specifically chirp) to be tuned to match the given dispersion map of a core network. The complete pulse characterisation of a commercially available EAM has been completed for a number of wavelength channels across the C-band wavelength range. This lead to the construction of performance maps for the chirp, ER and PW as a function of bias and modulation voltages for each wavelength. It has been demonstrated that the optimisation of the EAM drive conditions is imperative when employed in a long haul wavelength tuneable optical network. An extended transmission reach of up to 30 % (1540 nm) was achieved in the experimental re-circulating loop setup and improvements of up to 50 % (1535 nm) were demonstrated in the corresponding VPI simulation model. This transmission performance comparison illustrates the importance of EAM optimisation, if such a RZ transmitter was employed in a long haul network. The advantages associated with a tuneable chirp profile are also significant in combating the alternating signs of residual dispersion associated with the dispersion map of long haul networks.

REFERENCES

[1] B. Mason, “Electroabsorption modulators,” in WDM Technologies: Active Optical Components, Academic Press, Elsevier Science, 2002.

[2] J.C. Cartledge and B. Christensen, “Optimum operating points for electroabsorption modulators in 10 Gb/s transmission systems using nondispersion shifted fiber,” IEEE/OSA J. Lightwave Technol., vol. 16, no. 3, pp. 349-357, Mar. 1998.

[3] E. Lach et al., “Application of electroabsorption modulators for high-speed transmission systems,” J. Opt. and Fiber Comms. Reports, vol. 2, no. 2, pp. 140-170, Jun. 2005.

[4] J. Calaway, “Optical absorption in an electric field,” Phys. Rev., vol. 130, no. 2, pp. 549-553, Apr. 1963.

[5] P. Bhattacharya, “Optical Processes in semiconductors,” in Semiconductor Optoelectronic Devices: Second Edition, Prentice Hall, 1997.

[6] Y.A. Akulova et al., “Widely tunable electroabsorption-modulated sampled-grating DBR laser tranmitter,” IEEE J. Sel. Topics in Quant. Electron., vol. 8, no. 6, pp. 1349-1357, Nov./Dec. 2002.

[7] G.B. Morrison et al., “Electroabsorption modulator performance predicted from band-edge absorption spectra for bulk, quantum-well, and quantum-well-intermixed InGaAsP structures,” Elsevier, Solid-State Electronics, vol. 51, no. 1, pp. 38-47, Jan. 2007.

[8] D.S. Chemka et al., “Electroabsorption by Stark effect on room-temperature excitons in GaAs/GaAlAs quantum well structures,” Appl. Phys. Lett., vol. 42, no. 10, pp. 864-866, May. 1983.

[9] T.H. Wood et al., “131 ps optical modulation in semiconductor multiple quantum wells (MWQ’s),” IEEE J. Quant. Electron., vol. 21, no. 2, pp. 117-118, Feb. 1985.

[10] F. Koyama and K. Iga, “Frequency chirping of external modulators and its reduction,” IEE Electron. Lett., vol. 21, no. 23, pp. 1065-1066, Nov. 1985.

[11] C.H. Henry, “Theory of the linewidth of semiconductor lasers,” IEEE J. Quant. Electron., vol. 18, no. 2, pp. 259-264, Feb. 1982.

[12] F. Koyama and K. Iga, “Frequency chirping in external modulators,” IEEE/OSA J. Lightwave Technol., vol. 6, no. 1, pp. 87-92, Jan. 1988.

[13] N. Nagai et al., “Field-induced modulations of refractive index and absorption coefficient in a GaAs/AlGaAs quantum well structure,” IEE Electron. Lett., vol. 22, no. 17, pp. 888-889, Aug. 1986.

[14] M.K. Chin and W.S.C. Chang, “Theoretical design optimization of multiple-quantum-well electroabsorption modulators,” IEEE J. Quant. Electron., vol. 29, no. 9, pp. 2476-2488, Sep. 1993.

[15] F. Devaux et al., “Simple measurement of fiber dispersion and of chirp parameter of intensity modulated light emitter,” IEEE/OSA J. Lightwave Technol., vol. 11, no. 12, pp. 1937-1940, Dec. 1993.

[16] B. Christensen et al., “Simple dispersion measurement technique with high resolution,” IEE Electron. Lett., vol. 29, no. 1, pp. 132-134, Jan. 1993.

[17] D.J. Kane, “Real-time measurement of ultrashort laser pulses using principle component generalised projections,” IEEE J. Sel. Topics in Quant. Electron., vol. 4, no. 2, pp. 278-284, Mar./Apr. 1998.

[18] A.H. Gnauck et al., “Dispersion penalty reduction using an optical modulator with adjustable chirp,” IEEE Photon. Technol. Lett., vol. 3, no. 10, pp. 916-918, Oct. 1991.

[19] S. Saito et al., “Coherent transmission experiment over 2223 km at 2.5 Gbit/s using erbium-doped fibre amplifiers,” IEE Electron. Lett., vol. 26, no. 10, pp. 669-671, May 1991.

[20] T. Widdowson and D.J. Malyon, “Error ratio measurements over transoceanic distances using recirculating loop,” IEE Electron. Lett., vol. 27, no. 24, pp. 2201-2202, Nov. 1991.

[21] N.S. Bergano, “Undersea amplified lightwave systems design,” in Optical fiber telecommunications IIIA, Academic Press, 1997.

[22] D.J. Maylon et al., “Demonstration of optical pulse progagation over 10000km of fibre using recirculating loop,” IEE Electron. Lett., vol. 27, no. 2, pp. 120-121, Jan. 1991.

[23] N.S. Bergano et al., “Bit error rate measurements of 14000 km 5 Gbit/s fibre-amplifier transmission systems using circulating loop,” IEE Electron. Lett., vol. 27, no. 21, pp. 1889-1890, Oct. 1991.

[24] T. Widdowson and A.D. Ellis, “20 Gbit/s soliton transmission over 125 Mm,” IEE Electron. Lett., vol. 30, no. 22, pp. 1866-1868, Oct. 1994.

[25] M. Suzuki and N. Edagawa, “Dispersion-managed high-capacity ultra-long-haul transmission,” IEEE/OSA J. Lightwave Technol., vol. 21, no. 4, pp. 916-929, Apr. 2003.

Chapter 4 – Pulse Generation using Gain-Switching Technique

4.1 Introduction

As discussed in Chapter 3, the return-to-zero modulation format is favoured for long haul transmission in the core optical network as it offers enhanced transmission performance over the conventional NRZ scheme due to its increased robustness to fibre dispersive and non-linearity effects. For metro networks, the NRZ format is normally employed due to its low cost and simplicity of operation. However, as the line rates and indeed the transmission distances spanned by metro networks continue to increase, the RZ format may be required in the future to maintain optimal system performance. As the metro network is shared among fewer customers than the core network, more cost effective solutions must be utilised, such as directly modulated sources or arbitrary fibre types. Gain-switching is one of the most cost efficient and simple techniques to generate picosecond optical pulses from a directly modulated laser.

This chapter explores the process of gain-switching in dept and discusses the detrimental characteristics exhibited by the generated pulses, such as SMSR degradation and large timing jitter. Some of the most common techniques employed to increase the spectral and temporal purity of gain-switched pulses are also explored, with particular attention placed on self-seeding of a semiconductor laser. A novel self-seeding scheme to generate short picosecond pulses, which exhibit low jitter and high SMSR, from a gain-switched FP laser is presented and a discussion on how to adapt the RZ transmitter for implementation in a WDM based reconfigurable network is also presented.

4.2 Gain-Switching Principle of Operation and Rate Equations

A basic description of the gain-switching pulse generation technique was outlined in section 2.3.3 and was illustrated in Fig. 2.6. It was shown that if a current step was applied to a semiconductor laser below threshold, the output power of the laser will initially increase and then undergo a number of oscillations before a steady state value is reached. The oscillations observed in the carrier density are due to the time delay between the build up of the gain in the active region and the generation of photons. Under the application of an electric current step, the carrier density increases in the absence of a sizeable amount of stimulated emission. Once the gain within the laser cavity overcomes the accumulated losses, the photon density will begin to increase due to stimulated emission. As the photon density rises, the carriers are depleted faster than the level at

which they are injected, therefore the carrier population decreases, thus leading to a collapse in the free carrier density, eventually below that of the threshold level. The net result is a decrease in the gain within the cavity and a corresponding decrease in the electromagnetic field intensity. As the photon density decreases there is a subsequent increase in the carrier density and the cycle starts over again [1].

The idea of gain-switching came from the observation of this carrier density oscillation. It was demonstrated that by cutting off the applied electric step just before the onset of the second carrier density oscillation, an optical pulse could be emitted. Another interesting demonstration illustrated that the generated pulse duration was considerably shorter than that of the applied electrical pulse. The most common techniques employed to achieve gain-switching are to either apply a large electrical pulse, typically from a SRD [2] or a large RF sinusoidal wave [3], to a DC biased laser, thus switching the optical gain through the modulation of the driving current.

The dynamics of a gain-switched FP laser can be understood by considering two multi-mode rate equations [4]. The differential rate equations illustrate the relationship between the electron (or hole) density N and the photon density P. Eqs. 4.1 and 4.2 define the change in carrier and photon densities as a function of time for the m^{th} longitudinal mode of a gain-switched multimode laser, where N is the carrier density, J(t) is the applied current density, q is the electronic charge, d is the thickness of the active region, v_g is the group velocity, g_m is the optical material gain and τ_n and τ_p are the carrier and photon lifetimes respectively. The carrier density and photon densities are represented by N and P_m respectively, while β_{sp} and Γ are the spontaneous emission factor and the confinement factor.

$$\frac{dN}{dt} = \frac{J(t)}{qd} - \sum_m v_g g_m P_m - \frac{N}{\tau_n} \tag{4.1}$$

$$\frac{dP_m}{dt} = \Gamma g_m P_m - \frac{P_m}{\tau_p} + \frac{N}{\tau_n}\beta_{sp} \tag{4.2}$$

$$J(t) = j_b + j_a \sin 2\pi ft \tag{4.3}$$

$$\Delta\tau = \tau_p + \frac{1}{g_m N_i} \tag{4.4}$$

From the differential rate equations it is clear that the carrier and photon densities are dependant on the modulation frequency and amplitude of the applied electric current. Eq. (4.3) defines the injected carriers as a function of j_b and j_a which are the DC bias and modulation current densities respectively. It has been demonstrated from simple rate equation analysis, that if the modulation frequency is too low, multiple optical pulses will be generated within the same modulation period. This is due to the carrier density

relaxation oscillations. However, if the modulation frequency is increased, the number of generated pulses within the same modulation window will decrease until eventually single pulse operation is achieved. A further increase in the modulation frequency will result in a reduction of the pulse amplitude and therefore indicates the cut-off frequency [5]. Therefore to generate pulses in the MHz frequency range, an electrical pulse generator is typically required to gain-switch a laser; however at higher repetition rates in the GHz regime a RF sinusoidal wave can be used.

If the laser is electrically pumped by a very short optical pulse, such that the initial inversion carrier density (Ni) is much larger than the carrier density at transparency, an approximation of the optical pulse width can be made from Eq. 4.4. From this equation it is evident that a large differential gain (which is the change in gain as a function of carrier density) as well as a higher level of excited carriers and a lower photon lifetime will lead to the generation of a pulse with small duration [6]. A good approximation of the shape and duration of a gain-switched pulse can therefore be made from the carrier and photon density rate equations. The dynamics of gain-switched pulses will be discussed in greater detail in the following section.

4.3 Important Parameters Associated with Gain-Switched Pulses

As mentioned in the introduction, pulses generated through the gain-switching process can suffer from a number of inherent characteristics that limit their usefulness in high speed optical transmission. Such characteristics include asymmetric pulse shape, large duration, SMSR and jitter degradation and large frequency chirp. Therefore, in order to improve the purity of the generated pulses, these effects and the causes of such effects must be discussed in greater detail. This section explores the underling mechanisms that determine the characteristics of a gain-switched pulse.

4.3.1 Pulse shape and Duration

A gain-switched pulse can be described as the combination of two exponential curves with time constants τ_r (rising edge) and τ_f (falling edge). Without careful optimisation of the laser DC bias, gain-switched pulses are generally asymmetric in shape with fall times approximately equal to 1.5 to 2 times the rise time [7]. The rise time of the optical pulse is proportional to the maximum level at which the non-equilibrium carrier density is driven above the carrier density at transparency and is therefore inversely proportional to the net charge transferred to the active medium by the electric pulse. The decay time (falling edge) is dependant on how far down below threshold the carrier density is pulled during the emission of the pulse and consequently has a dependency on the bias level of the laser [8].

At low DC bias a gain-switched laser diode will generate a broad optical pulse with relatively low amplitude and will be pedestal free. The disadvantages associated with a low DC bias are larger pulse duration, a longer turn on delay time and a subsequently large timing jitter. As the DC bias is increased the pulse width becomes shorter, while the peak power increases, with the shortest duration corresponding to the greatest peak power. However if the bias level of the laser is increased to the threshold level of the device or greater, pedestals begin to form on the trailing edge of the pulse. These pedestals are created if the carrier density is not pulled down far enough below the lasing threshold of the device and can cause extremely poor levels of TPSR (< 10 dB), which would limit the performance of a high speed OTDM system due to intersysmbol interference. It has been demonstrated that the optimum bias point for the operation of a gain-switched laser is approximately half the threshold current (I_{th}) [9].

Fig. 4.1 illustrates a gain-switched commercially available DFB laser diode. A 10 GHz 28 dBm sinusoidal signal was applied to the laser via a bias tee. The laser diode had a threshold current of 15 mA. Fig. 4.1 (a) displays the generated pulse when the laser has a DC bias of 35 mA and (b) shows the corresponding pulse profile when the laser was at a DC bias of 60 mA. The first pulse is more symmetric, has a smaller duration and is pedestal free (as observed on a sampling scope). However, due to the lower bias voltage, a larger turn on delay time is experienced and therefore the pulse jitter is slightly higher. When the bias current is increased, the carrier density is not pulled down far enough below threshold and a large pedestal forms. The higher bias however provides greater peak power and a lower value of jitter, although these improvements are nullified as the low TPSR would render this pulse useless for high speed transmission.

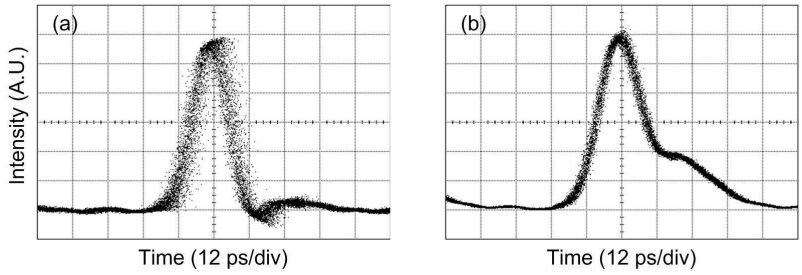

Fig. 4.1. Gain-switched DFB laser diode with (a) low bias and (b) high bias

From Eq. 4.4 it is evident that a lower photon lifetime will result in a smaller pulse FWHM. A shorter photon lifetime can be realised by decreasing the length of the laser cavity. It has been demonstrated that the gain-switched pulse widths decrease linearly with shorter cavity lengths [10]. A disadvantage to cavity shortening is that it suffers from difficulties in device handling, including wire bonding and mounting. Therefore an alternate way of reducing the photon lifetime is to apply anti-reflection coating to one of

the laser facets. The second term in Eq. 4.4 that has a contributing factor to pulse width is the differential gain. A higher differential gain will reduce the pulse duration, however this factor is difficult to increase as it is dependant on the material and structure of the laser device. The pulse duration can also be reduced by obtaining a larger overshoot in carrier density, which can be achieved by employing a laser diode that can endure a high level of current pumping without incurring significant leakage. If a larger carrier overshoot is realised, the peak power of the pulse will increase, resulting in a smaller duration.

Finally the nonlinear gain compression can also have an effect on the generated pulse width as it has a detrimental impact on the small signal resonance peak of lasers frequency response at high power [11]. It imposes a limit on the photon density by damping the large frequency oscillation, thus reducing the peak power and hence increasing the pulse width. Again, as with the differential gain, gain compression is dependant of the device structure. There are many parameters that can determine both the pulse shape and the duration of a gain-switched optical pulse, however once the fabrication process is complete, only adjustment of the bias, RF drive voltage and repetition rate may be used to obtain the smallest pulse duration with the largest TPSR.

4.3.2 Frequency Chirping

As discussed in section 3.2.3, the Kramers-Kronig relations indicate that if the gain (or loss) that is due to the imaginary part (k) of the refractive index is varied, then the real part (n) will undergo some modulation. The real and imaginary parts of the refractive index are related to each other through the Henry alpha factor or the linewidth enhancement factor (LEF) [12]. In a gain-switched laser, the applied current injection causes a substantial change in the carrier density within the device, which causes a corresponding variation in refractive index. This variation in refractive index alters the effective guided mode index, which subsequently changes the phase of the frequency components of the optical pulse and hence results in frequency chirp.

The linewidth enhancement factor is related to the change in refractive index through Eq. 4.5. Due to the free carrier plasma effect, the change in effective index as a function of carrier density is negative; therefore the alpha parameter is positive. Pulse chirp has a detrimental effect on high speed transmission as it combines with fibre dispersion leading to intersymbol interference. Another inherent problem associated with frequency chirp is the longitudinal linewidth broadening. For a single mode laser the spectral width of the dominant mode will increase, while for a multi-mode laser such as a FP, each longitudinal mode will broaden. Linewidth broadening can be detrimental in a WDM transmission system as it causes interchannel interference between neighbouring WDM

signals, thus it is imperative to restrict the extent of the spectral broadening in a gain-switched pulse source in order to mitigate this transmission impairment [7]. As spectral broadening is inherent to the gain-switching technique, the generated pulses are far from transform limited and consequently limit the usefulness of such pulses in medium to long haul transmission.

$$\alpha = -\frac{4\pi}{\lambda}\left(\frac{dn/dN}{dg/dN}\right) \tag{4.5}$$

From the equation above, it is evident that a high differential gain will result in a lower alpha factor and hence a smaller chirp profile. As mentioned in the previous section, the differential gain is dependant on the device structure and can be increased by using smaller cavity lengths. Conversely the magnitude of the electrical pulse could be reduced, thereby effectively reducing the change in carrier density. However this reduction in chirp comes at the cost of short pulse duration and high pedestal suppression, therefore rendering this option unrealistic for substantial chirp reduction. Finally the chirp can also be reduced by external injection into the laser cavity, because the injected photons decrease the threshold gain of the laser longitudinal mode, whose frequency coincides with the frequency of the injected photons [13]. This essentially lowers the inversion point and causes a reduction in the random fluctuation in the carrier density, hence limiting changes in the laser refractive index, resulting in lower chirp.

4.3.3 Timing Jitter

The timing jitter inherent to gain-switching can be broken into two sub-categories, correlated and uncorrelated jitter. Correlated jitter is mainly caused by the drive circuitry of the laser diode and the RF source, therefore if low noise electronics are employed this type of jitter can be reduced to a very low value [14]. Un-correlated timing jitter is due to the variation in the turn on delay time of the generated pulse. The delay time is equal to the interval between the onset of the electrical pulse and the emission of an optical pulse. Due to the fact that pulse generation in a gain-switched laser diode is dependent on random fluctuations of the spontaneous light in the cavity, the turn on delay time of the pulse jitters in a random manner, both in the generation of single pulse and from pulse-to-pulse. This random phase variation leads to noise on the pulse and is known as timing jitter [15].

The extent of timing jitter on a gain-switched pulse can be quite large and differs whether the laser diode is multi-mode or single-mode. The jitter exhibited by a gain-switched single-mode laser is larger than that of a multimode laser by a factor ranging from 3-5. The reason for the difference in timing jitter for each source depends on the photon density. For a single-mode laser the photon density contribution is contained within one

dominant mode, however for a multi-mode laser the photon density is a convolution of the single-mode photon numbers of all the modes in the lasers gain spectrum. Therefore, a higher photon density is realised in a multi-mode laser, thus reducing the turn on delay time, resulting in a corresponding decrease in jitter [16].

The timing jitter of a gain-switched pulse can be improved by increasing the bias level above threshold to generate a larger photon number, by using a laser with a broad gain spectrum (such as a multi-mode laser) or by using a laser with a large differential gain. All three techniques contribute to reducing the turn on delay time of the generated pulse and therefore decreases the temporal jitter. However, the reduction in jitter comes at the cost of other detrimental pulse characteristics. For example by increasing the DC bias, poor TPSR and a large PW will be realised, while a gain-switched multi-mode laser is not suitable for long haul transmission. Therefore another pulse improvement technique is required to increase the temporal and spectral purity of gain switched pulses and this will be discussed in more detail later in the chapter.

4.3.4 Side Mode Suppression Ratio

The side mode suppression ratio of a gain-switched pulse source is substantially degraded due to the large fluctuation in photon density as the laser is pulled below threshold, which strongly excites the side modes. There is also a large spectral broadening of the modes within the laser cavity, coupled with a spectral shift due to the large frequency chirping. Side mode excitation is not considered a problem in multi-mode laser diodes as the generated pulses are already supported by a number of spectral modes. However for single-mode lasers, SMSR degradation can have a substantial effect on transmission performance, especially when considered for WDM based optical networks [17].

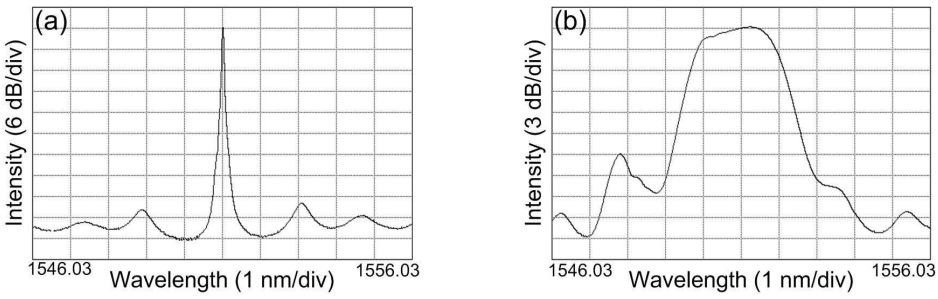

Fig. 4.2. SMSR of a DFB laser diode under (a) CW operation and (b) gain-switched operation

Fig. 4.2 illustrates the SMSR of a commercially available distributed feedback laser under CW and gain-switched conditions. In Fig. 4.2 (a) the laser is free running in CW operation and exhibits a large SMSR of 43 dB, while the spectral width is extremely small (beyond the resolution of the OSA). From Fig. 4.2 (b), it is evident that there is a large degradation in SMSR after the DFB is gain-switched, with the pulse exhibiting a

value of 18 dB. There is also a substantial broadening in the laser spectrum in comparison to when the laser operates in CW mode.

4.3.5 Extinction Ratio

The optical extinction of a gain-switched pulse is the ratio between the pulse on level and the off level. It is different to the TPSR which typically measures the ratio between the pulse peak and the most significant pulse pedestal. However the pulse ER is closely related to the TPSR in a gain-switched source and can have an equally detrimental impact on transmission performance, especially in a high speed OTDM system [18]. The on-off contrast of a gain-switched pulse can be increased by maximising the differential gain, carrier density overshoot and by reducing gain compression damping. The ER can also be maximised through careful adjustment of the operating conditions of the laser diode. If the DC bias is maintained below the threshold current, an optimum zero level can be obtained, while the magnitude of the modulation signal determines the maximum one level. If the bias level is increased above, I_{th}, the ER will be seriously degraded.

4.4 Optical Injection, Pulse Compression and Tuneability

Although gain-switching is a simple and cost effective pulse generation technique, the poor temporal and spectral characteristics of the generated pulses make them inadequate for optical transmission. As discussed in the previous section, gain-switched pulses exhibit large temporal jitter, high frequency chirp, poor SMSR and optical extinction and also have large pulse widths from 10 to 30 ps. Therefore, in order to implement such a source in a high speed system, the temporal and spectral purity of the pulses must be increased. This can be achieved by injecting light back into the laser cavity through self-seeding or external injection. Such techniques can also be adapted to provide a degree of wavelength tuneability.

4.4.1 Self-Seeding

Self-seeding is a cost efficient technique employed to increase the temporal and spectral quality of gain-switched pulses. It is achieved by using a wavelength selective device to filter out one lasing longitudinal mode, which is then re-injected back into the laser cavity, essentially seeding the optical pulse spectrum [19]. Fig. 4.3 illustrates the typical experimental setup for a gain-switched FP laser that is self-seeded using a wavelength selective external cavity. An amplified sinusoidal wave is applied to a DC biased laser. The output pulses pass through a polarisation controller before being split into two signals using a 50:50 coupler. One arm goes to a wavelength selective device, which filters out one longitudinal mode and reflects it back into the laser cavity. The PC is then adjusted to ensure that the injected light is aligned with the optical axis of the laser. However, it is

imperative to tune the length of the external cavity to ensure that the re-injected light returns during the build up time of an optical pulse. This can be achieved by either tuning the repetition rate of the signal generator or by employing a tuneable optical delay line in the feedback loop. This is a major drawback of the self-seeding technique and reduces the flexibility of the device. Therefore a novel self-seeding scheme is discussed in greater detail later in this chapter.

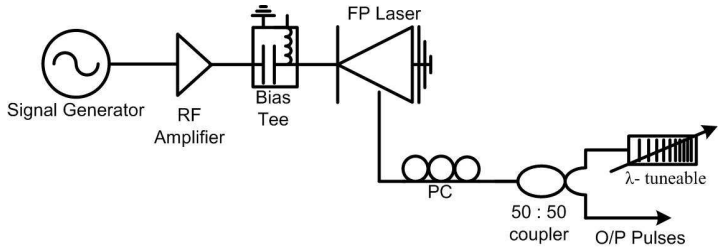

Fig. 4.3. Typical self-seeded gain-switched setup

For an un-seeded gain-switched laser diode, the temporal jitter of the generated pulses is caused by the random fluctuation of the photon density generated by spontaneous emission. This jitter, known as turn on jitter (TOJ), can be substantially reduced through self-seeding. In a self-seeded arrangement, the optical field inside the laser cavity is no longer determined by the spontaneous emission, but by the optical feedback. Therefore this excitation reduces the random fluctuation of the photon density and hence the TOJ. The output of the laser diode reaches a steady state condition after approximately 10 to 15 round trips of the external cavity and the pulses are now single-moded and exhibit a low value of temporal jitter [20, 21]. Fig. 2.1 illustrates a gain-switched pulse without and with self-seeding and there is a clear reduction in jitter, while Fig. 4.4 displays the corresponding spectra with the self-seeded pulse exhibiting a large SMSR of 48 dB.

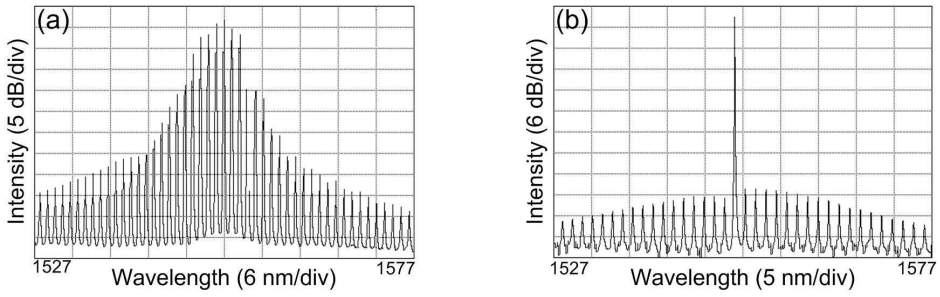

Fig. 4.4. (a) Spectrum of gain-switched FP laser and (b) corresponding spectrum with self-seeding injection

The chirp of the gain-switched pulses is also reduced by injecting light back into the laser. With the injection of light, the threshold gain of the mode whose frequency coincides with the frequency of the injected photons decreases, which causes a corresponding decrease in the carrier concentration. Thus the peak inversion level is

reduced; therefore the gain variations during the emission of a pulse are also reduced, resulting in a lower frequency chirp and a narrower spectral width, albeit with a slight increase in pulse width [22]. Therefore, single-mode pulse generation with low jitter, high SMSR and reduced chirp can be obtained through the self-seeded gain-switched (SSGS) technique. However due to the need for cavity length tuning, an alternative seeding method has been explored, known as external injection.

4.4.2 External Injection

Although self-seeding of a gain-switched laser diode substantially improves the temporal and spectral quality of the generated pulses, the requirement of the repetition frequency to be maintained at an integer multiple of the external cavity round trip time limits the flexibility of the source. This is because the re-injected light is not a continuous signal, but is also pulsed. Therefore, if the pulse transmitter was operated at an arbitrary frequency, the external cavity would have to be continuously tuned for optimum injection. To overcome this limitation another seeding technique has been extensively investigated and is known as external injection [23]. This scheme is similar to the self-seeding technique except a second laser diode is employed to provide a CW source for injection. Wavelength selectivity is obtained by tuning the emission wavelength of the CW laser to match that of the gain-switched source. As the second laser diode provides a continuous signal, the affects of the injection are immediate, unlike self-seeding which takes a short time to reach steady state.

The advantage of external injection is that the repetition rate of the directly modulated laser can be set at an arbitrary value and due to the fact that the injected light is continuous, the need to tune the cavity length is negated. Therefore the same improvements in pulse characteristics achieved through self-seeding are also obtained with external injection, in addition to enhanced transmitter flexibility. This flexibility is essential for implementation in future reconfigurable metro networks that must be transparent to repetition rate and modulation format. One drawback to the external injection technique is the necessity for an additional laser diode, which adds a substantial cost to the pulse source. Therefore, a more cost efficient device that is capable of achieving the same level of performance is desired and one such technique capable of achieving this is discussed later in the chapter.

4.4.3 Pulse Compression

As gain-switched pulses typically have durations in the region of 10 to 30 ps, they are only suitable for serial transmission at 10 or even 20 Gb/s. However, the performance of gain-switched pulse sources in such transmission systems is also greatly impaired due to

the large frequency chirp, resulting in pulses that are far from transform limited. Therefore, the chirp exhibited by gain-switched pulses is a serious problem associated with this technique, although it can be used as an advantage. If the generated pulses are passed through a length of dispersion compensating fibre, the chirp is compensated by the negative dispersion, thus compressing the pulse [24]. A similar compression scheme that utilises the chirp to reduce the pulse duration and to obtain transform limited pulses, employs a linearly chirped FBG that has a chirp sign opposite to that of the generated pulses. By using a reflective grating the pulse source can become quite efficient, as pulse compression and self-seeding can be performed simultaneously [25].

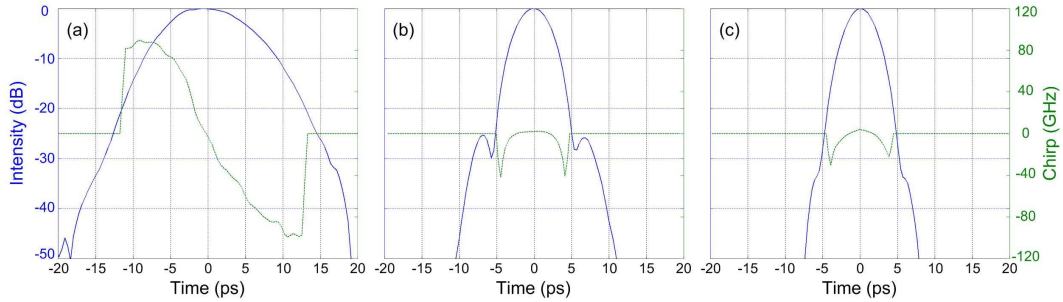

Fig. 4.5. (a) Intensity and chirp profile of a gain-switched DFB laser, (b) corresponding profile after linear pulse compression and (c) after non-linear pulse compression

However, as the chirp of a gain-switched pulse in linear across its centre, but significantly non-linear in the wings, linear compression leads to the formation of pedestals due to the non-ideal compensation of the non-linear chirp. When implemented in an OTDM setup the poor TPSR limits system performance due to interferometric noise caused by pulse overlapping [26]. There have been many experiments carried out to increase the TPSR after compression but such schemes inevitably increase the complexity of the transmitter, thus increasing form factor and cost [27].

An alternative method that can be employed to compress gain-switched pulses, while simultaneously maintaining a large TPSR, is to apply non-linear chirp compensation. This entails characterising the pulse chirp and fabricating a FBG with the exact opposite chirp profile. Fig. 4.5 illustrates an externally injected gain-switched DFB laser at 10 GHz. From figure (a) it is evident that the 10.5 ps pulse obtains a large frequency chirp, resulting in a large time bandwidth product. If linear compression is applied (Fig. 4.5 b) to the pulse, the duration is reduced to 3.6 ps, although pedestals form 23 dB below the peak of the pulse due to the non-optimised compensation of the non-linear chirp. Such a level of pedestal suppression would have a detrimental impact on an OTDM system. However, when non-linear compensation is applied a large TPSR of 33 dB can be maintained, thus increasing the temporal purity of the transform limited pulses, as seen in Fig. 4.5 (c). Such a large TPSR may not be a requirement for serial transmission, but

when implemented in an OTDM system, significant improvements in performance can be achieved [28, 29].

4.4.4 Wavelength Tuneability

To implement a gain-switched pulse source in a reconfigurable metro based WDM network a high degree of wavelength tuneability is required. Wavelength tuneability of a gain-switched multi-mode laser can be achieved by using a tuneable optical filter to provide a high degree of longitudinal mode selectivity. By tuning the filter, a number of different modes can be seeded, thus providing a cost efficient wavelength tuneable pulse source [30, 25]. The tuning time of such a source is determined by the time it takes for the filter to be tuned, combined with the 10-15 round trips of the external cavity the pulses must traverse before a steady state output is required.

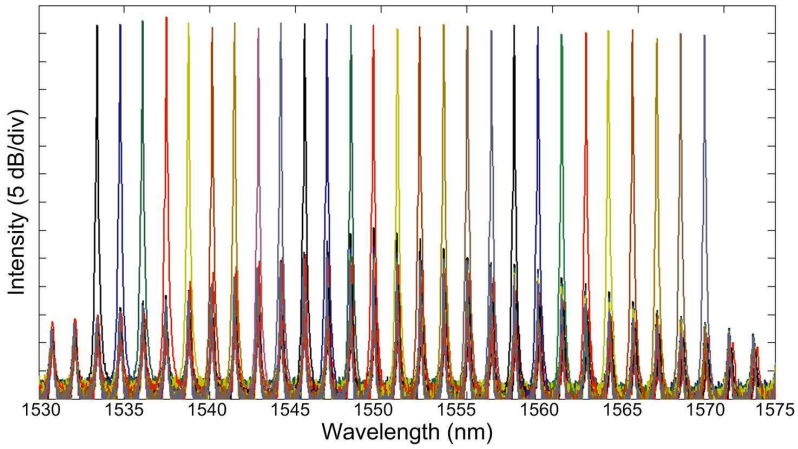

Fig. 4.6. Externally injected gain-switched FP laser with single-moded tuneability over the C-band

An alternative technique to obtain wavelength tuneability is to employ a widely tuneable laser to externally inject the gain-switched laser diode. This technique provides extremely fast tuning times, which are completely dependant in on the switching time of the tuneable laser. Fig. 4.6 illustrates the spectrum of an externally injected gain-switched FP laser. A widely tuneable laser was used to inject light into a number of longitudinal modes across the C-band wavelength range. It is shown that an SMSR of greater that 30 dB can be obtained over the wide wavelength range, illustrating the prevalence of such a source for a metro based WDM network. For an even greater tuning range, multiple FP lasers can be cascaded to provide wavelength tuneable pulse generation over a 70 nm range [31]. One drawback of the external injection technique however, is the high cost associated with an extra laser source.

4.5 Cavity Length Independent SSGS FP Laser

Section 4.4 discussed the merits of both optical injection techniques used to improve the spectral and temporal quality of gain-switched pulses. Both self-seeding and external

injection achieve this goal, but the value of each technique is diminished somewhat by two key disadvantages. For self-seeding, the cavity length must be equal to an integer multiple of the round trip time of the external cavity, while for external injection the cost of an extra laser diode would be prohibitive for cost efficient metro networks. Therefore this section focuses on a novel self-seeding scheme that allows continuous repetition rate tuning, without degrading the pulse quality. This is achieved by employing a highly chirped FBG to perform the optical injection. The high positive dispersion associated with the grating combines with the negative pulse chirp to spread out the generated pulses to an extent that a CW like feedback is obtained. As the re-injected light is continuous in its nature, the need to tune the external cavity length or the pulse repetition rate is negated.

4.5.1 FBG Characterisation

The linearly chirped FBG (LC FBG) used for self-injection locking of a gain-switched pulse source had a central wavelength of 1545.13 nm at 25° C, with a 3 dB reflection bandwidth of 0.128 nm and a peak reflectivity of 85.1 %. The grating was 131 mm in length with a rejection ratio greater than 30 dB and exhibited a dispersion of 4957.8 ps/nm. The experimental setup used to characterise the reflection profile of the FBG is illustrated in Fig. 4.7 (a). An ASE source supplied broadband light to the chirped FBG via a circulator. As the grating operated in reflection, the third port of the circulator was monitored using an OSA with a spectral resolution of 0.05 nm. Fig. 4.7 (b) displays the measured reflection profile and the specified group delay profile of the grating. A rejection ratio of 37.65 dB and a measured 3 dB reflection bandwidth of 0.128 nm are displayed. The group delay exhibited over the filter band-pass was 634.6 ps (from the data sheet).

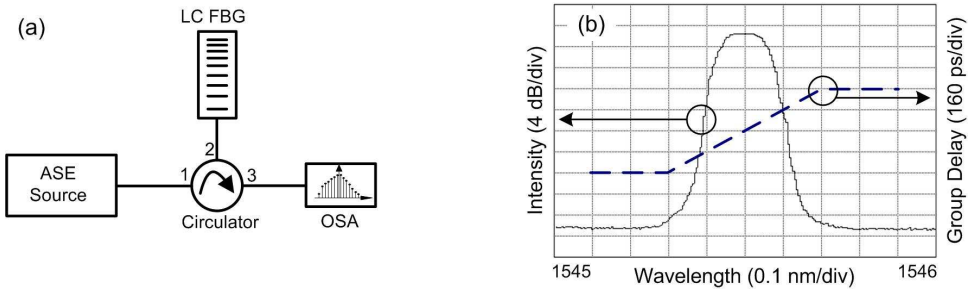

Fig. 4.7. (a) Experimental setup to characterise dispersive FBG and (b) reflection and group delay profile of FBG

4.5.2 SSGS Experimental Setup

The experimental setup used to realise the cavity tuning independent self-seeded gain-switched pulse source is illustrated in Fig. 4.8. The FP laser used was a commercially

available 1.5 µm InGaAsP device manufactured for use in 10 Gb/s systems, with a threshold current of 10 mA and a longitudinal mode spacing of 1.2 nm. The laser output power, at a bias of 50 mA, was measured to be 6 mW after being coupled via a GRIN lens fibre pigtail. Gain-switching of the FP laser was achieved by applying a dc bias of 50 mA in conjunction with a 28 dBm sinusoidal signal at a repetition rate of 10 GHz, via a bias tee. This provided a current swing of 250 mA to the input to the board that the laser was mounted on, which is sufficient to bring the laser below threshold, thus providing a good on-off extinction ratio. Self-seeding of the gain-switched laser diode was accomplished using an external cavity (length of cavity: 4 m) containing a PC, a 3 dB optical coupler and the LC FBG.

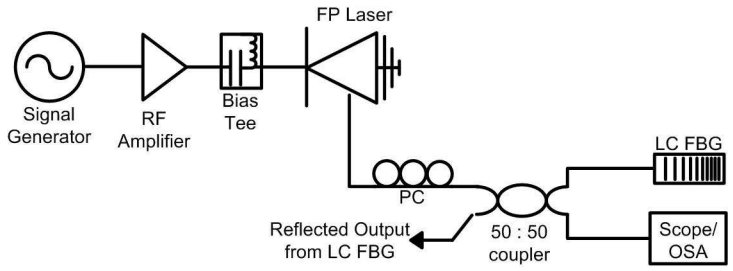

Fig. 4.8. Experimental Setup

In order to achieve optimum SSGS pulse generation, the peak emission wavelength of the FP laser was temperature tuned to the corresponding reflection wavelength of the grating. The target wavelength of 1545.13 nm was achieved by temperature tuning the FP to 22° C. The SSGS pulses were characterised using an optical spectrum analyser and a 50 GHz pin photodetector in conjunction with a 50 GHz digitising oscilloscope. The reflected pulses, which were dispersed by the grating and fed back to the gain-switched laser, were monitored at the second input arm of the 50:50 coupler (as shown in Fig. 4.8). The SMSR and temporal duration of the generated pulses were subsequently analysed as the repetition rate of the applied sinusoidal signal was varied.

4.5.3 Results and Discussion

The repetition rate was tuned from 10 down to 2.5 GHz (in 500 MHz steps) in order to verify the cavity length independence under self-seeding with the LC FBG. Fig. 4.9 shows the spectra of the SSGS pulses at various repetition rates (2.5, 5 and 10 GHz). These figures clearly illustrate the fact that the SSGS pulses still portray an acceptable SMSR of approximately 30 dB [32] at each of the repetition rates. It is important to note that the frequencies mentioned are exact values and not frequencies tuned to a sub-harmonic of the inverse cavity roundtrip time. In all previous work carried out on SSGS lasers, the repetition frequency or the cavity length was altered in order to remain within the limits of the feedback time window, to ensure optimum pulse generation.

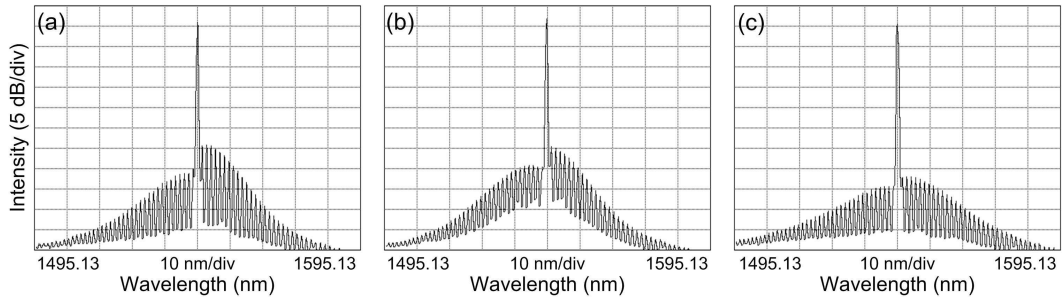

Fig. 4.9. Single-moded spectra at varied repetition rates of (a) 2.5, (b) 5 and (c) 10 GHz

Combined with a constant SMSR, the temporal duration of the gain-switched pulses remained almost constant over the entire repetition rate tuning range of 7.5 GHz. Fig. 4.10 illustrates the corresponding optical pulses, again at repetition rates of 2.5, 5 and 10 GHz. The measured widths (full-width at half-maximum) of the pulses were 31, 30 and 30 ps respectively. The 3 dB spectral width was measured to be 0.58 nm and when combined with a pulse width of 30 ps, yields a TBP of 2.2. Therefore the pulses are far from transform limited and indicate that they are heavily chirped. This chirp should enable the pulses to be compressed to less than 10 ps and ensure that they are also transform limited (as discussed in section 4.4.3).

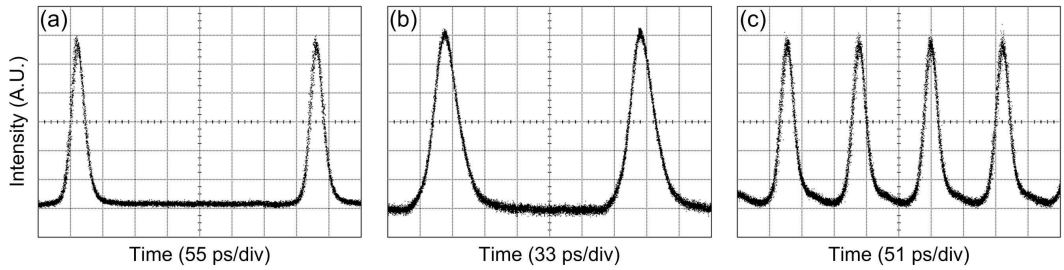

Fig. 4.10. SSGS pulses at a repetition rate of (a) 2.5, (b) 5 and (c) 10 GHz

The averaged oscilloscope traces of the reflected (feedback) signal from the highly chirped FBG at two different rates of 2.5 and 10 GHz are shown in Fig. 4.11 (a) and (b), respectively. The average signal powers fed back at 2.5 and 10 GHz were -9 and -10 dBm. The high dispersion factor associated with the LC FBG is responsible for the broadening of the optical pulses, which caused a high degree of temporal overlap between them. As can be seen from Fig. 4.11, this overlap produces a CW-like feedback into the gain-switched laser cavity. The degree of overlap between the dispersed pulses is much higher when the repetition rate is at 10 GHz rather than 2.5 GHz. This is essentially due to the 10 GHz period being much smaller (100 ps) than the 2.5 GHz period (400 ps). The ripples observed in the feedback signal cause minor fluctuations in the width and SMSR of the output pulses. However, within the range of the repetition rates used (2.5 to 10 GHz), it is important to note that the SMSR is always greater than 30 dB and the pulse duration less than 32 ps.

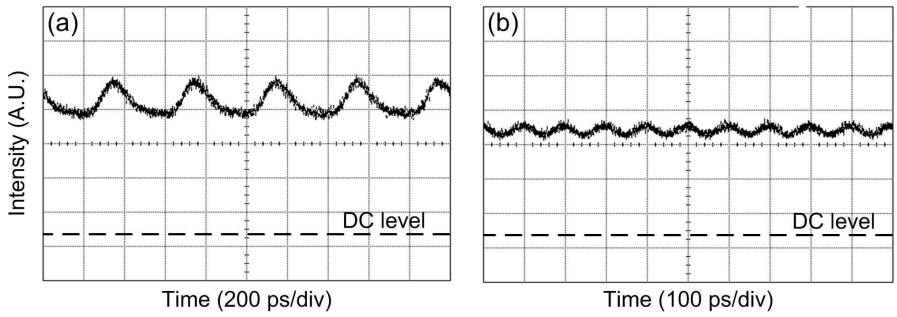

Fig. 4.11. Optical feedback from LC FBG (a) 2.5 and (b) 10 GHz

The variation of the SSGS pulse suppression ratio and width as a function of repetition rate have been plotted in Fig. 4.12. The SMSR remains relatively stable over the entire frequency range. More importantly, it remains above 30 dB at all repetition rates, which is deemed adequate for high speed WDM communication systems. The pulse duration also remains approximately constant, demonstrating that the pulse source operates consistently across the entire repetition frequency tuning range. This directly modulated pulse source is ideal for metro based optical networks, which require such sources for more cost efficient transmission than that of the core network.

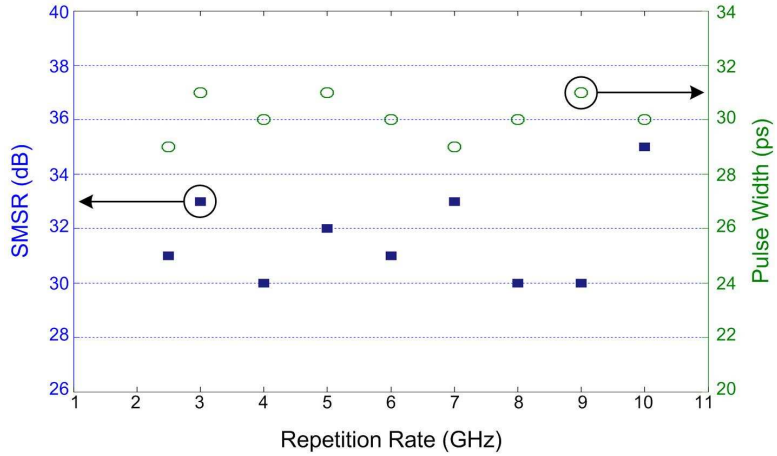

Fig. 4.12. SMSR and pulse width as a function of repetition rate

Further development of the source could include a wavelength tuneable grating to achieve optimum pulse generation over a wide wavelength range. Thus, if the FP laser cavity was carefully fabricated the longitudinal mode spacing could be a multiple integer of 100 GHz, therefore equalling the specified ITU channel spacing in a WDM system. Slight temperature tuning of the device would allow for the absolute wavelength calibration. The gain-switched source could also be integrated with the multi-wavelength grating, providing a cost efficient, small form factor device. Finally, if the transmission distance required did not necessitate the RZ modulation scheme, this self-seeding technique could be applied to the NRZ modulation format.

4.6 Summary

Self-seeded gain-switched pulse sources are ideal for implementation in future reconfigurable metro WDM networks, due to the low cost and high spectral and temporal purity of the generated pulses. To overcome the cavity length dependence of current self-seeding schemes, a novel technique that incorporated a highly chirped FBG was implemented to disperse the generated pulses, thus providing a CW-like feedback into the gain-switched laser cavity. This CW feedback, mimicking an external injection scenario, overcomes the cavity length limitation associated with the self-seeding technique. Hence, by using the proposed method the potential of continuously tuning the repetition rate, while simultaneously maintaining optimum pulse generation, can be realised without changing the cavity length. Experimental results obtained show that pulses exhibiting 30 dB SMSR and 30 ps widths are generated over a wide range of modulation frequencies. Further development of this source may be achieved by utilising a wavelength tuneable grating, therefore enhancing the ability of the source to operate in reconfigurable metro based WDM network. The cost, footprint and power consumption of the transmitter could also be reduced by integrating the FP laser and FBG.

REFERENCES

[1] T. Amand and X. Marie, “Pulses semiconductor lasers,” in Femtosecond Laser Pulses: Principles and Experiments, Second Edition, Springer 2005.

[2] P-L. Liu et al., “Picosecond pulse generation from InGaAsP lasers at 1.25 and 1.3 µm by electrical pulse pumping,” IEEE J. Quant. Electron., vol. 17, no. 5, pp. 671-674, May 1981.

[3] J.AuYeung, “Picosecond optical pulse generation at gigahertz rates by direct modulation of a semiconductor laser,” Appl. Phys. Lett., vol. 38, no. 5, pp. 308-310, Mar. 1981.

[4] T.K. Yee and D. Welford, “A multimode rate-equation analysis for semiconductor lasers applied to the direct intensity modulation of individual longitudinal modes,” IEEE J. Quant. Electron., vol. 22, no. 11, pp. 2116-2122, Nov. 1986.

[5] H. Ito et al., “Generation of picosecond optical pulses with highly RF modulated AlGaAs DH laser,” IEEE J. Quant. Electron., vol. 17, no. 5, pp. 663-670, May 1981.

[6] Y. Arakawa et al., “Picosecond pulse generation (< 1.8 ps) in a quantum well laser by a gain-switching method,” Appl. Phys. Lett., vol. 51, no. 17, pp. 1295-1297, Oct. 1987.

[7] P. Vasil’ev, “Gain and Q-switching in diode lasers,” in Ultrafast Diode Lasers: Fundamentals and Functions, Artech House, Boston.

[8] P.M. Downey et al., “Picosecond dynamics of a gain-switched InGaAsP laser,” IEEE J. Quant. Electron., vol. 23, no. 6, pp. 1039-1047, Jun. 1987.

[9] H.F. Liu et al., “Gain-switched picosecond pulse (< 10 ps) generation from 1.3 µm InGaAsP laser diodes,” IEEE J. Quant. Electron., vol. 25, no. 6, pp. 1417-1425, Jun. 1989.

[10] G.J. Aspin et al., “The effect of cavity length on picosecond pulse generation with highly RF modulated AlGaAs double heterostructure lasers,” Appl. Phys. Lett., vol. 39, no. 11, pp. 860-861, Dec. 1981.

[11] K.Y. Lau and N.B. Chaim, “High-speed operation of single-quantum-well lasers with large gain compression,” IEEE Photon. Technol. Lett., vol. 4, no. 2, pp. 118-120, Feb. 1992.

[12] C.H. Henry, “Theory of the linewidth of semiconductor lasers,” IEEE J. Quant. Electron., vol. 18, no. 2, pp. 259-264, Feb. 1982.

[13] S. Mohrdiek et al., “Chirp reduction of directly modulated semiconductor lasers at 10 gb/s by strong CW light injection,” IEEE/OSA J. Lightwave Technol., vol. 12, no. 3, pp. 418424, Mar. 1994.

[14] M. Jinno, “Correlated and uncorrelated timing jitter in gain-switched laser diodes,” IEEE Photon. Technol. Lett., vol. 5, no. 10, pp. 1140-1143, Oct. 1993.

[15] E.H. Bottcher et al., “Turn-on delay time fluctuations in gain-switched AlGaAs/GaAs multiple-quantum-well lasers,” J. Appl. Phys., vol. 63, no. 7, pp. 2469-2471, Apr. 1988.

[16] A.G. Weber et al., “Measurement and simulation of the turn-on delay time jitter in gain-switched semiconductor lasers,” IEEE J. Quant. Electron., vol. 28, no. 2, pp. 441-446, Feb. 1992.

[17] L.P. Barry and P. Anandarajah, “Effect of side-mode suppression ratio in the performance of self-seeded gain-switched optical pulses in lightwave communications systems,” IEEE Photon. Technol. Lett., vol. 11, no. 11, pp. 1360-1362, Nov. 1999.

[18] S. Bouchoule et al., “High speed gain-switched laser as very simple 4x10 Gbit/s and up to 8x10 Gbit/s OTDM source,” in Proc. of European Conference on Optical Communication (ECOC), vol. 1, pp.215-216, Sep. 1998.

[19] T. Anderson et al., “Generation of single-mode picosecond pulses by injection locking of an AlGaAs semiconductor laser,” Appl. Phys. Lett., vol. 41, no. 1, pp. 14-16, Jul. 1982.

[20] M. Schell et al., “Jitter and dynamics of self-seeded fabry-perot laser diodes,” IEEE J. Sel. Topics in Quant. Electron., vol. 1, no. 2, pp. 528-534, Jun. 1995.

[21] L.P. Barry et al., “Simple technique to improve the spectral quality of gain-switched pulses from a DFB,” IEE Electron. Lett., vol. 30, no. 25, pp. 2143-2145, Dec. 1994.

[22] S. Mohrdiek et al., “Chirp reduction of directly modulated semiconductor lasers at 10 Gb/s by strong CW light injection,” IEEE/OSA J. Lightwave Technol., vol. 12, no. 3, pp. 418-424, Mar. 1994.

[23] P. Anandarajah et al., “High frequency pulse generation using a gain-switched commercial semiconductor laser with strong injection,” IEEE High Speed Postgraduate Student Colloquium, pp. 121-126, 2000.

[24] K.A. Ahmed et al., “Nearly transform-limited pulse (3.6 ps) generation from gain-switched 1.55 µm distributed feedback laser by using fibre compression technique,” IEE Electron. Lett., vol. 29, no. 1, pp. 54-56, Jan. 1993.

[25] S. Li et al., “Simultaneous chirp compression and single-mode operation of a self-seeded gain-switched semiconductor laser with a linearly chirped fibre Bragg grating,” in Proc. of The Pacific Rim Conference on Lasers and Electro-Optics (CLEO/Pacific Rim), pp. 922-923, Aug./Sep. 1999.

[26] J. Zhang et al., “Interferometric noise in optical time division multiplexing transmission system,” IEEE/OSA J. Lightwave Technol., vol. 20, no. 8, pp. 1329-1333, Aug. 2002.

[27] W. Chang et al., “Complete characterisation of the generation of a 2.8 ps pedestal-free optical pulse using a gain-switched laser and a compressing nonlinear amplifying loop mirror,” in Proc. of European Conference on Optical Communication (ECOC), paper We4, pp. 757-758, Sep. 2005.

[28] R. Maher et al., “Complete performance analysis of a 3.5 ps pulse source consisting of a gain-switched laser diode followed by a non-linearly chirped grating,” in Proc. of Conference on Lasers and Electro-Optics (CLEO), paper CThR6, May 2008.

[29] P.M. Anandarajah et al., “System-performance analysis of optimized gain-switched pulse source employed in 40- and 80-Gb/s OTDM systems,” IEEE/OSA J. Lightwave Technol., vol. 25, no. 6, pp. 1495-1502, Jun. 2007.

[30] S. Lundqvist et al., “Generation of tunable single-mode picosecond pulses from an AlGaAs semiconductor laser with grating feedback,” Appl. Phys. Lett., vol. 43, no. 8, pp. 715-717, Oct. 1983.

[31] A.M. Clarke et al., “Generation of widely tunable picosecond pulses with large SMSR by externally injecting a gain-switched dual laser source,” IEEE Photon. Technol. Lett., vol. 16, no. 10, pp. 2344-2346, Oct. 2004.

[32] P. Anandarajah et al., “Performance issues associated with WDM optical systems using self-seeded gain switched pulse sources due to mode partition noise effects,” IEEE Photon. Technol. Lett., vol. 14, no. 8, pp. 1202-1204, Aug. 2002.

Chapter 5 – Direct Modulation of a SG DBR Tuneable Laser

5.1 Introduction

While Chapter 3 and Chapter 4 focused on the development and characterisation of tuneable RZ transmitters for the core and metro optical networks, this chapter investigates the feasibility of a directly modulated tuneable laser for implementation in short reach applications, specifically the access network. Tuneable lasers are of great interest for future reconfigurable agile optical networks and are a requirement for the dynamic operation of all of the sub-systems outlined in section 1.5. The technology is not only considered as a cost efficient technique to reduce inventory, but as one of the key components in future communications systems. There are many tuneable lasers available that can offer tuning over a large wavelength range, while maintaining high SMSR and output power. The SG DBR is an ideal candidate for reconfiguration applications due to its large tuning range (40 nm), high output power (> 10 dBm), high side mode suppression (> 30 dB) and simplicity of integration. This tuneable laser is therefore utilised in all of the experimental work in this chapter and will be discussed in greater detail in section 5.5.

The access network is the most expensive part of the communications infrastructure because it is provided on a unique basis to each customer, therefore transmitter cost is of paramount importance. The cost efficiency and simplicity of the NRZ modulation format, combined with the wide tuning range of a TL, offer the capability of a fast switched dynamic short reach NRZ transmitter. The importance of tuneable lasers in WDM-PON architectures for dynamic bandwidth provisioning has been outlined by Banerjee et al. [1]. Hence, to develop a cost efficient solution, the performance of a directly modulated SG DBR laser is investigated to verify its usefulness for such applications. However, direct modulation of a lasers gain section causes a time dependant frequency drift. This shift in operating frequency is characterised and its effect on the performance of a WDM system is also demonstrated. To overcome this inherent drawback of the direct modulation scheme, a frequency drift compensation technique, which reduces the magnitude of the frequency drift, is also investigated.

5.2 Tuneable Laser Applications and Requirements

Tuneable laser applications span many diverse fields from agile WDM optical communication systems, to sensor applications or spectroscopy. The main initial driver for tuneable lasers in communications networks has been sparing and inventory

reduction. Although this poses as quite an unglamorous application for TLs, the savings are finite and have paved the way for increased source development [2]. Future applications will include network reconfiguration, however before large volumes of tuneable laser deployments are realised for current and future WDM networks, their performance requirements must at least equal to, if not exceed that of their single wavelength counterpart, the DFB laser diode.

5.2.1 Sparing and Inventory Reduction

In current WDM networks, wavelength specific line cards are required to supply the digital data at each operating wavelength, therefore dozens of fixed frequency laser sources must be manufactured. An additional corresponding amount of laser sources are also required as spares, so component failure within the network can be easily rectified. The sparing and inventory of these wavelength specific line cards account for a large percentage of the total component costs and therefore pose as a significant overhead. The introduction of tuneable lasers offers a competitive alternative to fixed frequency devices. As a widely tuneable laser can access any channel across the C-band ITU grid, it can be deployed as a replacement to any one of the wavelength specific transponders. Therefore huge savings in inventory costs can be made as the quantity of spares can be reduced by an order of magnitude [3].

Tuneable lasers also allow for one time provisioning of wavelength independent transponders. This is similar to current fixed wavelength applications, except the single frequency sources are replaced with tuneable lasers. The advantages associated with one time provisioning of tuneable lasers include, reduced forecasting and planning, subsequent inventory reduction and streamlined manufacturing processes. By utilising tuneable lasers in all of the network transponders, the lasers can be forecasted on volume alone, as apposed to a frequency-by-frequency basis. For one time provisioning to become a reality, the cost of commercially available widely tuneable lasers must become comparable to fixed frequency sources or at least offer only a modest increase in component cost [4]. Currently, TLs are approximately one and a half to two times more expensive than single frequency devices. This is due to increased manufacturing complexity, extra component testing and low volume demand. However, as tuneable laser applications become more widespread the volume of lasers being manufactured will increase, which should drive costs down.

5.2.2 Network Reconfiguration

More interesting and advanced applications for tuneable lasers are in the areas of optical switching, light-path rerouting and dynamic provisioning. Tuneable lasers can be

employed in all-optical wavelength convertors and tuneable transponders, within network nodes and in each transmitter/receiver subsystem. Thus, as traffic is routed through an optical network, certain wavelengths may already be in use on certain transmission links, therefore the wavelength must be switched to an alternate unused channel to avoid contention. This problem can be easily overcome using one of the key switching components in an optical network, the ROADM. This switching device was discussed in section 1.5.3 and uses AWG demultiplexers and multiplexers to separate the WDM signal into the constituent channels. The tuneable laser, which is a complementary component to a ROADM, provides the optical switching or wavelength conversion. Such switching nodes provide a greater degree of flexibility and can usually be controlled remotely, therefore negating the need for any manual intervention. The deployment of a dynamically reconfigurable network allows for quick provisioning of available bandwidth and less cumbersome introduction of new services, thus resulting in fewer lost revenue opportunities and less network management [5].

Such systems are known as circuit-switched, where the source to destination optical paths are pre-determined and subsequently maintained for long periods of time. Therefore the switching speed required for reconfiguration can be over a number of seconds. This can reduce the complexity of a tuneable transponder as fast wavelength locking control may not be required. However, new optical network architectures such as burst switching and packet switching, which transmit the data in bursts or short packets, will require dramatically shorter switching times. This is because each packet or burst does not have a specific pre-determined destination and must therefore be dynamically switched throughout the network, thus requiring switching speeds in the nanosecond timescale, making the fast switched tuneable laser a fundamental component in these systems. The accuracy and stability of the tuneable laser, in terms of wavelength tuning, will be critical making some implementation of wavelength locking control a necessity.

5.2.3 Requirements

The specific performance requirements that widely tuneable lasers must adhere to prior to implementation in a DWDM system will vary from one application to the next. They should however provide similar performance to the fixed frequency devices used in current WDM systems. Table 5.1 illustrates a summary of the desired specifications for tuneable lasers that was outlined by Buus and Murphy in 2006 [6]. It is important to have a large output power from the tuneable laser to overcome the losses associated with external modulators, coupling and other related semiconductor devices, while the differences in power between channels should be as close to zero as possible for consistent performance uniformity. The electrical power dissipation should also be as low

as possible to reduce operational expenditure, while the number of components within the laser module is irrelevant, once it meets both energy and footprint demands. The switching speed of < 10 ms applies primarily to circuit switched networks; however this tuning time must be much faster for burst of packet switched schemes.

Attribute	Desired Specification
Output power	+ 13 dBm
Power variation over wavelength	± 0.1 dB to ± 0.5 dB
Electrical power dissipation	2 W to < 8 W
# of components in package	not important
Package dimensions	pluggable (XCVR or SPF)
Switching speed	< 1 ms to < 10 ms
Tuning range	C or C+L
Tuning type	quasi-continuous
SMSR	> 30 dB
Fabrication and characterisation	low cost mass production

Table 5.1. Desired tuneable laser requirements for DWDM networks

The laser must also be able to tune over a wide wavelength range of at least the C-band, but preferably both the conventional and long bands. As mentioned previously an SMSR of greater that 30 dB is a prerequisite for WDM systems to avoid crosstalk with adjacent channels. Low cost mass manufacturing is also important to reduce component cost. Another additional requirement that is important for tuneable lasers is dark tuning. As the laser tunes between two WDM channels many spurious modes can be generated. Thus the laser output must be isolated from the network to avoid uncontrolled emissions that could be severely detrimental to system performance. This tuning problem can be negated however by placing an SOA at the output of the laser, which is zero biased during a switching event, effectively acting as a wavelength blocker [7]. Although this is an effective blocking technique, it adds to the device complexity and cost. There are many other laser specifications that have not been outlined in the table above but will be discussed in greater detail later in the chapter. These include wavelength stability, accuracy, tuning speed and latency.

5.3 Laser Diode Tuning

To understand the basic tuning mechanisms of a laser, we must first consider the simple laser diode structure, illustrated in Fig. 5.1. As current is injected into the active section of the laser diode, the carriers are initially converted into photons due to spontaneous emission. Mirrors placed at either end of the cavity, reflect the photons back into the active region to be amplified by stimulated emission, generating more photons with the same phase and frequency. Lasing occurs when the overall gain within the cavity exceeds the combined losses. Above this gain threshold, any additional carriers are converted

directly to photons by stimulated emission. The laser diode oscillator operates simultaneously over a number of closely spaced longitudinal modes, yielding a comb mode emission spectrum (as in Fig. 4.4 a). The central emission wavelength of the device is defined as the longitudinal mode closest to the peak of the laser gain curve (frequency that experiences the cavity loss minimum). The side comb modes, spaced at an integer multiple of Δf (where Δf=c/2nL, c is the speed of light, n is the refractive index of the material and L is the length of the cavity), also carry a significant amount of the total output power, making the laser multi-moded. Single moded operation can be achieved by making the mirror loss wavelength dependant [8].

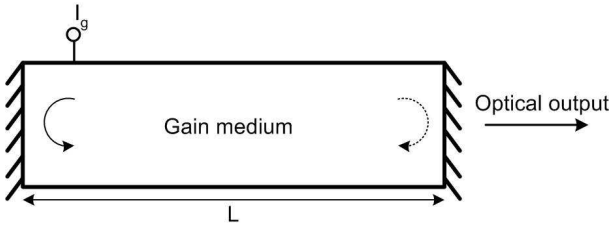

Fig. 5.1. Basic laser diode structure

The central wavelength of the laser diode can be tuned in three different ways, by varying the amplitude condition of the laser (achieved by shifting the cavity gain curve), by adjusting the phase condition of the laser (achieved by spectrally shifting the longitudinal modes), or through a combination of both. The tuning method used will define the frequency range of a tuneable laser and also to what extent each discrete frequency can be accessed. There are three tuning types that generally define the operation of a tuneable laser and they are continuous, discontinuous and quasi-continuous [9].

Fig. 5.2 (a) illustrates continuous tuning. In this scheme, the wavelength is adjusted smoothly and in small discrete steps, while maintaining the same lasing longitudinal mode. Therefore the laser output can remain single moded over a moderate tuning range by simply adjusting the effective length of the cavity and without changing the frequency of the minimum cavity loss [10]. Due to the stringent requirement of single longitudinal mode tuning, simultaneous control of the cavity gain peak and the comb mode spectrum is required [11].

Greater tuning ranges can be obtained if the central longitudinal mode is allowed to change. This is achieved when the longitudinal mode at the loss minimum of the laser cavity is initially tuned continuously. The change is frequency is linear until an adjacent longitudinal mode suddenly experiences a lower loss within the cavity and thus becomes the dominant lasing mode. During this transition the single mode frequency jumps to that of the new longitudinal mode frequency, therefore representing a discontinuity in the tuning, as seen in Fig. 5.2 (b). Through this technique, tuning ranges of up to 100 nm

have been achieved, however it is impossible to access all wavelengths within the same range [12].

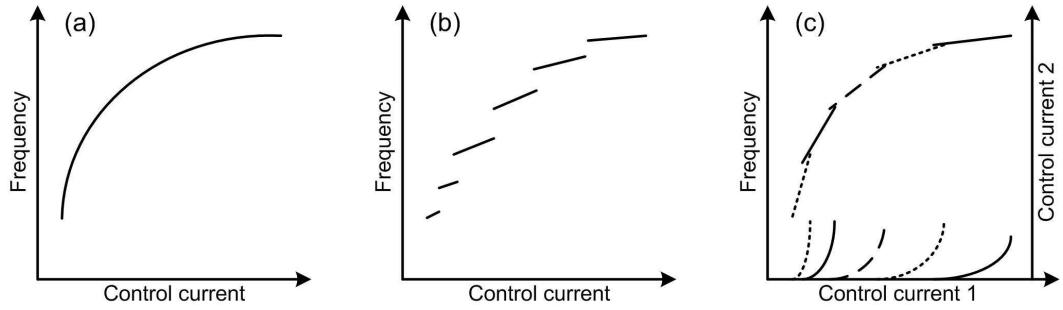

Fig. 5.2. Emission frequency versus control current for (a) continuous tuning, (b) discontinuous tuning and (c) quasi-continuous tuning

Another mechanism is required to provide tuning over a wide wavelength range that is continuous in nature and still allows access to discrete wavelength channels. This tuning scheme is known as quasi-continuous and is depicted in Fig. 5.2 (c). Quasi-continuous tuning enables high wavelength channel selectivity using different longitudinal modes. The general operation involves tuning the cavity modes and the gain curve synchronously over a range equal to the longitudinal mode spacing. Therefore continuous tuning is used to access the discrete frequencies held within the mode hops experienced through discontinuous tuning. The application of these tuning mechanisms are discussed in greater detail by considering the operation of the distributed Bragg reflector (DBR) laser and the SG DBR tuneable laser.

5.4 Distributed Bragg Reflector Laser

One of the most common single mode laser structures is the distributed Bragg reflector (DBR) laser and it is illustrated in Fig. 5.3. The laser consists of three electrically controlled sections, comprising of a gain section, a passive phase section and a Bragg grating section. The active (gain) region, which is similar to the generic laser outlined in Fig. 5.1, controls the optical gain and output power of the laser, through the application of a single current I_g. The Bragg section exhibits a wavelength selective loss and therefore has the ability to determine the emission wavelength and hence the position of the gain curve of the laser. As the period of the grating is set during the fabrication process of the device, the refractive index remains as the only adjustable parameter. Therefore, in order to tune the emission wavelength of the laser diode, the refractive index must be altered accordingly. The most common method to achieve this is through free carrier injection [9]. The passive phase section separates the Bragg grating and the active region. It has a larger bandgap than the active region to avoid absorption of the incident photons. Current

injection into this section allows for the independent adjustment of the comb mode spectrum.

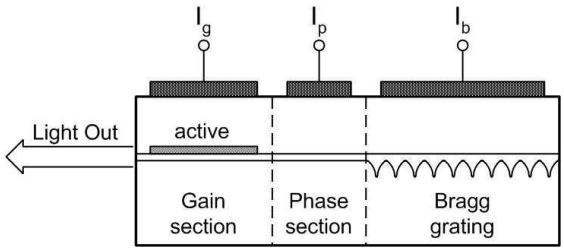

Fig. 5.3. Three section DBR laser structure

Therefore by injecting carriers into the Bragg grating section, the position of the laser gain curve can be manipulated. This leads to discontinuous wavelength tuning. Conversely current injection into the passive phase section provides continuous tuning of the comb mode spectrum. Through the mutual control of the injection currents to each section, continuous tuning ranges of ~ 4 nm can be achieved [13], while quasi-continuous tuning ranges of ~ 10 nm [14] and dis-continuous tuning of ~ 20 nm can be obtained [15]. The upper limit on the continuous tuning of a DBR laser is limited by the maximum obtainable phase shift is the passive section. The range of the discontinuous tuning scheme is limited by the maximum change in the Bragg wavelength, which is related to the maximum effective refractive index change achievable by carrier injection through the following equation:

$$\frac{\Delta\lambda_B}{\lambda_0} = \frac{\Delta n'_B}{n_{g,B}} \tag{5.1}$$

where $\Delta\lambda_B$ and $\Delta n'_B$ are the changes is Bragg wavelength and the effective refractive index of the grating section under current injection and λ_0 and $n_{g,B}$ are the initial wavelength and refractive index without tuning. Although three section DBR lasers can exhibit quasi-continuous tuning, the wavelength range over which they operate is limited by the maximum change in refractive index [16] and it can therefore only cover a portion of the available EDFA amplifying bandwidth. Consequently, more advanced tuning mechanisms are required to obtain wide wavelength tuneability. The principles of such techniques generally rely on the adjustment of the refractive index difference of the material, rather than the refractive index itself. One such method is known as the Vernier effect and it is utilised in the SG DBR laser.

5.5 Sampled Grating Distributed Bragg Reflector Laser

The SG DBR laser is one of the most promising candidates for implementation in future reconfigurable optical networks due to its large quasi-continuous tuning range (> 40 nm), high output power (> 10 dBm), high SMSR (> 45 dB) and simplicity of integration. For a

reconfigurable network, the ability to access each channel on the ITU grid is not the only requirement, as the speed at which each channel is accessed is also extremely important. Therefore the tuning speed, latency and stability of an SG DBR laser are discussed in this section.

5.5.1 Device Structure and Vernier Tuning

The typical device structure of a SG DBR tuneable laser, with an additional amplifier section, is shown in Fig. 5.4. The laser consists of three passive sections (front mirror, phase section and back mirror) and one active gain section. Each of the laser sections are individually controlled by an injected current. The front and back mirror reflectors are initially identical to conventional Bragg gratings, but are subsequently multiplied by a sampling function, which removes a portion of the grating elements in a periodic fashion. A schematic of the grating sampling technique is outlined in Fig. 5.5.

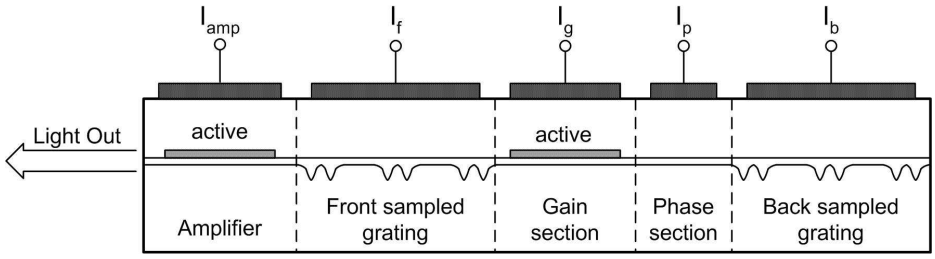

Fig. 5.4. SG DBR device structure with additional amplifier section

The uniform Bragg grating with period, Λ, which is set to give a central Bragg wavelength (Eq. 5.2) of 1550 nm, is multiplied by a sampling function with a period Λ_s. The sampling results in several sections of interrupted gratings with period Λ_g. The side comb frequencies of the reflection spectrum from the grating are spaced equally by Eq. 5.3, where n_g is the group refractive index of the material [17]. The peak amplitude of the comb frequencies are unequal and symmetrically reduce in power from the maximum reflection, which occurs at the central wavelength. This roll off in reflectivity strength limits the available tuning bandwidth of the laser device. A good indication of the available number of subsidiary reflection peaks can be deduced from the FWHM of the roll of envelope, expressed in Eq. 5.4. The envelope width of the reflectivity peaks can be increased by reducing Λ_g/Λ_s. Therefore, small duty cycle gratings are required for a large number of useable reflection peaks. However, this increase in the number of comb reflections comes at the expense of an overall decrease in reflectivity for the comb modes. Therefore a trade-off exists between a large number of reflection combs and high reflectivity.

In an SG DBR laser, two sampled grating are used to provide comb shaped reflectivity from each side of the laser structure. The two gratings have slightly different periods, Λ_s

and Λ_r, thus allowing only one set of reflection peaks to come into alignment within the wavelength range of interest. Frequencies that reside within a narrow spectral region defined by the product of the two reflection spectra will experience minimum cavity loss. Thus, by placing a single longitudinal mode within the defined reflection peak, it will experience minimum cavity loss and begin to laze at the expense of the remaining longitudinal modes. This process is known as the Vernier effect and is illustrated in Fig. 5.6. The phase section of the SG DBR laser is used for accurate alignment of the longitudinal mode and the comb reflectivity.

$$\lambda_B = 2n_g\Lambda \tag{5.2}$$

$$\Delta\lambda_s = \frac{\lambda^2}{2n_g\Lambda_s} \tag{5.3}$$

$$BW_{FWHM} = \frac{\Lambda_s}{\Lambda_g}\Delta\lambda_s \tag{5.4}$$

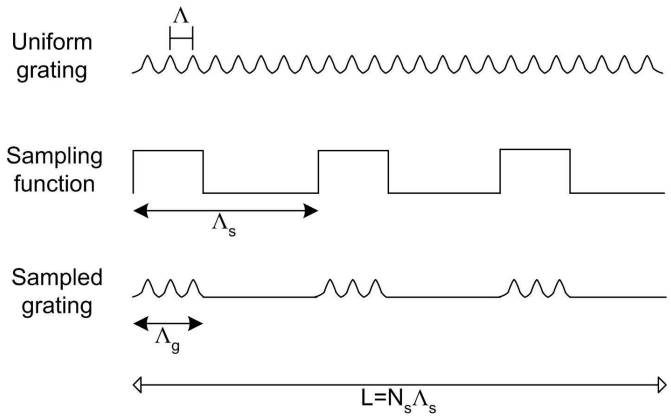

Fig. 5.5. Sampled Bragg grating

The tuning range of an SG DBR laser is generally limited by the repeat mode spacing, $\Delta\lambda_{rep}$. The repeat mode spacing is defined as the wavelength interval between which sampled grating maxima are aligned. Although the repeat mode occurs at a lower point in the spectral envelope roll-off, a second significant reflection peak is experienced, as shown in Fig. 5.6 (b). When one of the reflection combs is tuned by, $\Delta\lambda_{rep}$, relative to the other, the repeat mode can become dominant due to its position in the laser gain curve. Another detrimental effect is a severely reduced SMSR, as two longitudinal modes will co-exist within with the laser cavity. Therefore, the repeat mode spacing limits the tuning range of the device and should be maintained as large as possible.

In an SG DBR laser, the sampled gratings are at either end of the device structure. Therefore, as the output light passes through the front reflector, upon exiting the laser cavity, significant free carrier absorption occurs [18]. This loss can vary as a function of injected current and consequently as a function of operating wavelength. As a result the

output power of a SG DBR laser can vary by up to 6 dB across the intended wavelength range. To overcome this limitation a SOA can be monolithically integrated on the same chip as the tuneable laser (as in Fig. 5.4). This power variation can also be overcome by using gain control during tuning, however as variations in gain current also lead to a shift in operating frequency it is desirable to utilise an external control for power adjustment. Therefore a SOA is the favoured option to maintain a low power variation between WDM channels [19].

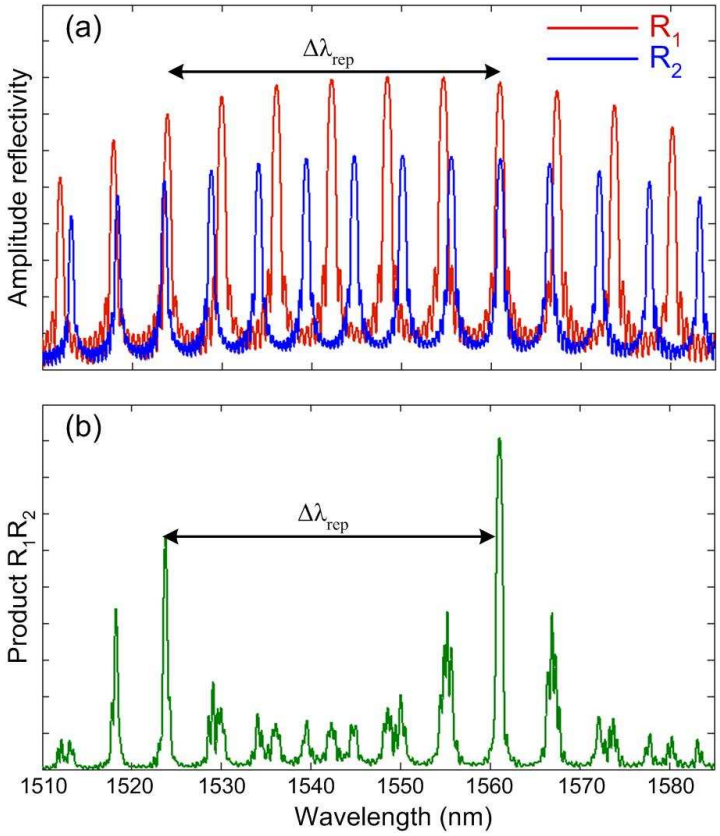

Fig. 5.6. (a) Reflection spectra from a SG DBR laser illustrating repeat mode tuning limitation and (b) product of reflection spectra with multiple peaks

5.5.2 Tuning Speed and Latency

An important aspect of a tuneable laser is the time it takes to switch from one ITU channel to another. The required switching time of a laser is dependent on the application and can vary substantially for different network designs (circuit or packet switched for example). The total tuning time of a tuneable laser is outlined in Fig. 5.7 and consists of latency and switching. The latency time associated with a tuneable laser refers to the time it takes the digital wavelength request to be translated into a change in actual control currents. This time is usually attributed to the switch processing time and the electronics used in the control module. The switching time is referred to as the time it takes the laser to switch from the initial channel ($\lambda_{initial}$) to within a tolerable frequency of the desired

channel (λ_{target}). An SOA can also be employed to blank out the laser output during this time to limit the transmission of spurious modes. The combination of both timing parameters equals the total tuning time of the device and must be taken into account during the system design process. Usually, tuneable lasers are encapsulated within control modules, which specify the tuning currents and also process switching requests. Such modules can also incorporate wavelength locking devices to increase the total switching times and is discussed in more detail in section 5.5.4.

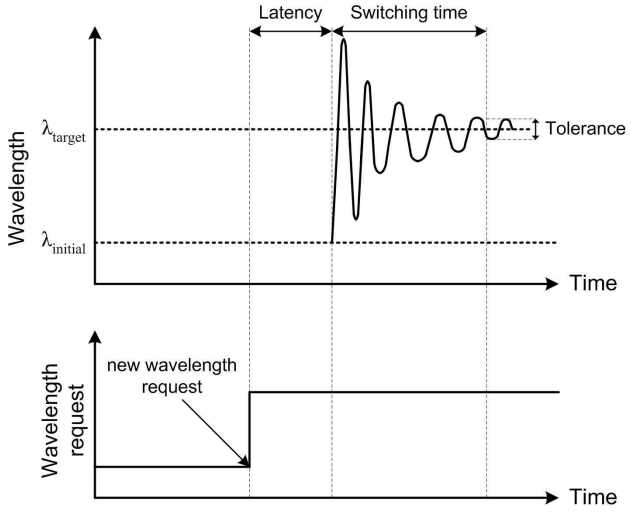

Fig. 5.7. Total wavelength switching time

5.5.3 Tuning Accuracy and Stability

Tuning accuracy and stability are very important aspects of tuneable laser operation and can have severe implications on WDM transmission performance. In a WDM system the laser must tune to and stay within ±5 % of the channel frequency to accommodate source frequency drift and drift from frequency-selective components such as filters and ROADMs. Wavelength lockers can again be employed to reduce frequency drift caused by component aging or environmental effects. Consistent side mode suppression and minimal power variation across the entire tuning range are also important factors and must be closely regulated.

5.5.4 Tuneable Laser Module

To ensure acceptable levels of tuning speed, wavelength accuracy and stability, commercially available tuneable lasers are commonly provided with automatic control systems within one single laser module. An SG DBR laser requires a number of different control currents to achieve single-mode operation which must be accurately adjusted when the tuneable transmitter is required to switch operating wavelength. Therefore a look-up table consisting of phase, front and back mirror currents, required to obtain a specific ITU channel, is always needed. To provide such accurate current supply, a

common control interface that contains a microprocessor and the look-up table is incorporated in the TL module. Once a switching request is made, the current values for each section is read from the look-up table and are then amplified before being applied to the laser.

To ensure that the new ITU channel stays within ±5 % of the channel frequency, a wavelength locker is also commonly implemented within the laser module. Fig. 5.8 illustrates a typical wavelength locker employed to maintain wavelength switching stability [20]. An optical tap is used to split the output of the laser and a portion of the light enters the wavelength locker. The signal is again split into two using a Y-branch coupler, with one arm being fed directly to a photodetector while the second arm passes through a filter, such as a FP etalon. The filter is designed to provide a periodic interference pattern as the input wavelength is changed and also exhibits a free spectral range (FSR) equal to the channel spacing of the laser [21]. The locker thus produces two control parameters, one of which is dependant on power (PD1) and one which is dependant on wavelength (PD2), which are used to generate an error signal. The error signal is then applied to the laser phase section to provide fine tuning of the operating wavelength.

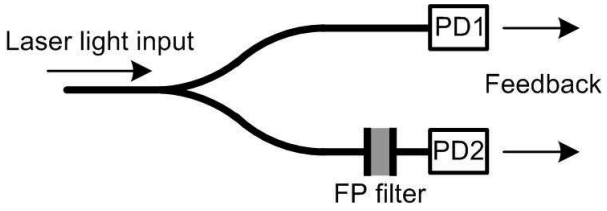

Fig. 5.8. Tuneable laser wavelength locker

As the wavelength locker also detects the laser output power, it can be used to maintain a constant laser output as a function of wavelength. Therefore the measured output power can be used independently to generate a second error signal, to be applied to an integrated SOA for amplitude control. The use of an SOA for this function is highly desirable, because if the current to the gain section is altered for amplitude adjustment, the output wavelength would also experience some variation [2].

5.6 Characterisation of a SG DBR Tuneable Laser

In order to generate a look-up table for a tuneable laser it is essential to first characterise the performance of the device as a function of the control currents applied to the phase and mirror sections. This can be achieved by compiling performance tuning maps of the laser, which provide an accurate indication of the lasers operation in terms of SMSR, output power and wavelength.

5.6.1 Performance Tuning Maps

The static characterisation of an SG DBR tuneable laser can be performed to illustrate a visual representation of the Vernier tuning function and can be obtained using an OSA and a power meter. Fig. 5.9 shows the performance tuning maps for a commercially available SG DBR laser from Agility Communications (specification sheet in Appendix II), which is used in the experimental work in section 5.8 of this chapter. The operating wavelength and SMSR of the device were recorded using an OSA, as a function of the front and back mirror currents. The gain current remained constant, while the current applied to the phase section was 0 mA. The output power from the laser was subsequently recorded using a power meter, as a function of the same current range.

From the conventional wavelength contour map (Fig. 5.9 a), the two fundamental channel transitions, super-mode and longitudinal mode changes are visible. Super-mode jumps are a result of the realignment of the mirror reflection spectra peaks and constitute a shift in operating wavelength of approximately 5 nm. They occur when one mirror section is tuned relative to the other and their boundaries result in a fan like layout on the plot. Longitudinal mode changes are observed within the super-mode boundaries and occur when a new longitudinal cavity mode experiences minimum loss. Longitudinal changes of approximately 0.3 nm can realised when the two mirror currents are tuned simultaneously, however this function is usually achieved by fine tuning the current applied to the laser phase section [22].

The SMSR and power contours are shown in Fig. 5.9 (b) and (c) respectively. The output power as a function of mirror currents exhibits characteristic saddle points. The peak reflectivity states of the front and back mirror sections are located at these saddle points and if the lasing wavelength coincides with the reflection peaks a high SMSR is obtained. The control currents provided by the TL module ensure that the laser operates at a saddle point, while the phase control current fine tunes the longitudinal mode spectrum to ensure that the saddle point coincides with the desired operating wavelength [23].

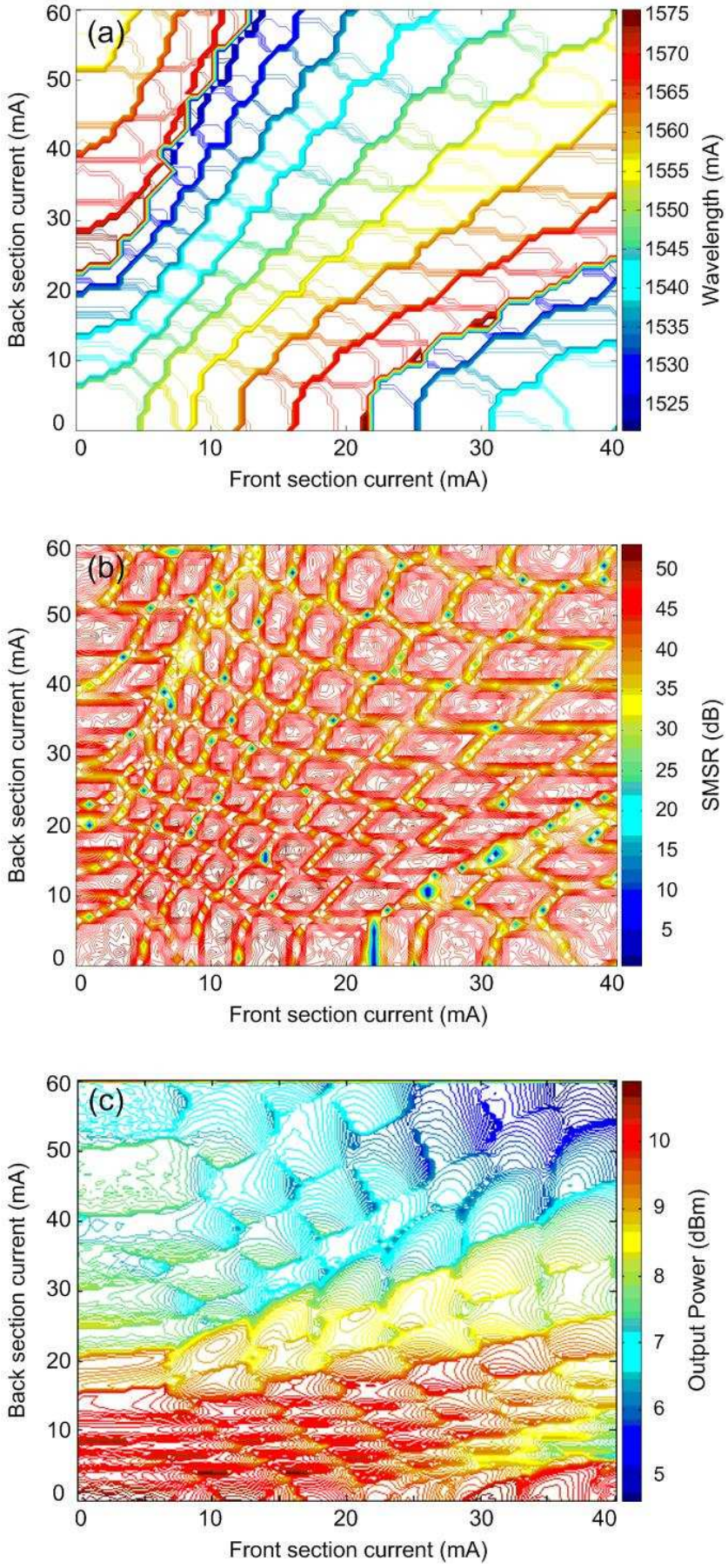

Fig. 5.9. SG DBR tuneable laser tuning maps, (a) wavelength, (b) SMSR and (c) output power

5.7 Frequency Drift Due to Direct Modulation

Although a directly modulated tuneable laser is an ideal short reach transmitter for implementation in a low cost, remotely reconfigurable access based optical network, there are some inherent drawbacks which may limit the usefulness of this technique. The most detrimental impairment, as with the gain-switching technique, is the frequency fluctuation (chirp) imposed on the signal. This frequency drift can impair the overall performance of a WDM system in two ways; either by drifting out of the receiving filters bandwidth and/or by drifting into the neighbouring channels filter bandwidth thereby causing cross channel interference. In this section the magnitude and settling time of the frequency drift of a directly modulated SG DBR TL module from Intune Networks is characterised. In addition the detrimental effect the frequency drift has on DWDM system performance, when the modulated channel is passed through a narrow OBPF, is also investigated.

5.7.1 Sloped Frequency Discriminator

It is imperative to accurately characterise the magnitude of the TL frequency drift in order to quantify the detrimental effect it may have on a high speed WDM network. There have been many techniques proposed to resolve the fluctuating chirp caused by fast channel switching or direct modulation of a widely tuneable laser [24, 25]. One of the most simple frequency drift characterisation techniques utilises a detuned optical band pass filter, as seen in Fig. 5.10. This in essence creates a sloped frequency discriminator, allowing the frequency drift exhibited by the TL to be converted into an intensity fluctuation. The directly modulated signal is passed into an optical coupler, with one arm being directly detected before an oscilloscope, while the second arm is passed through a detuned OBPF before detection. It is important for the filter to exhibit a sharp transfer function to obtain large amplitude fluctuations for a given frequency variation (as in Fig. 5.10 b).

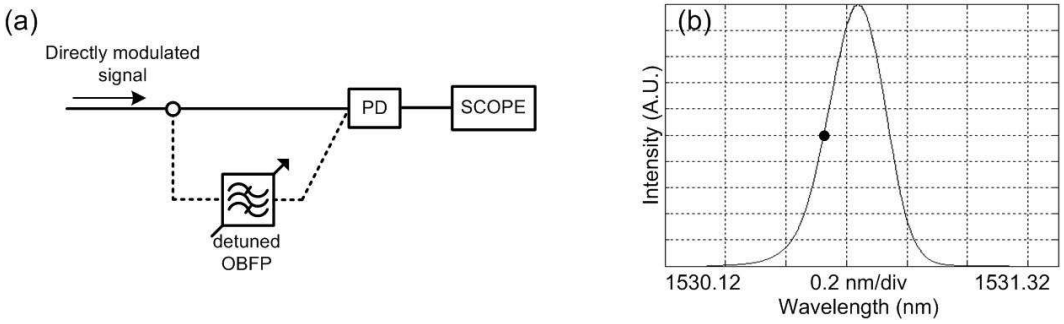

Fig. 5.10. (a) Sloped frequency discriminator and (b) detuned OBPF transfer function

The TL output power is measured on the oscilloscope after passing through the detuned filter, thus providing a time resolved trace of the power profile. A second, reference power signal taken without the filter, is subsequently subtracted to ensure that the power variation monitored on the scope is due solely to the frequency fluctuation of the device.

From the filter profile the power transmission as a function of frequency is known, therefore a power to frequency conversion can be performed on the recorded power trace, resulting in the frequency variation as a function of time [26].

5.7.2 Frequency Drift Characterisation

The two-stage experimental setup used to characterise the frequency drift of a tuneable laser is shown in Fig. 5.11. The commercially available TL module from Intune Networks used in this work was built around a SG DBR-SOA chip with an integrated wavelength locker. The SOA was zero biased during wavelength switching and provided 35 dB of power suppression. It also minimised the power variation (±1 dB) between the 83 ITU channels spaced 50 GHz apart. The typical CW output power was approximately 8.5 dBm and a SMSR of greater than 40 dB was realised over the 40 nm tuning range (C-band). The module also featured a custom made high speed RF input, attached to the gain section of the device, thus enabling direct modulation. The modulation bandwidth of the device under test was characterised to be approximately 1 GHz and this limitation was mainly due to the non-optimised electronic circuitry.

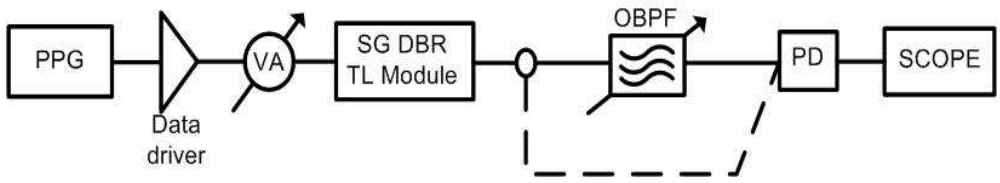

Fig. 5.11. Frequency drift characterisation setup

The TL was operated in static mode and the emission wavelength was set to channel 38 (1550.4 nm – 193.35 THz) on the ITU grid and was subsequently directly modulated at 1 Gb/s with the aid of a pulse pattern generator. A modulator driver amplifier in conjunction an electrical variable attenuator were placed between the PPG and the TL module to vary the direct intensity modulation index through values of 0.1 to 0.6, which corresponded to peak-to-peak voltages of 0.5 to 3 V respectively. An initial power reference measurement, denoted by the dotted line in the characterisation setup, was recorded where the modulated signal was directly detected using a high speed photodetector and a high speed sampling oscilloscope. A second power measurement was recorded by passing the modulated output of the TL through an OBPF with a 3 dB bandwidth of 26.5 GHz, detuned by 0.1 nm (as seen in Fig. 5.10 b), thus providing a sloped frequency discriminator.

By detuning the filter the set ITU frequency was made to lie on a portion of the filter characteristic with a higher rejection (lower power). On the application of the modulated signal, the frequency of the TL is offset towards the lower rejection side of the filter

transmission function, resulting in a higher amount of optical power being detected. Subsequently, a smaller output power from the filter is recorded as the in built wavelength locker drags the output signal back to its target frequency. As discussed in section 5.7.1, the power reference measurement is subtracted from the filtered power measurement to mitigate any intensity variation due to the direct modulation, thus ensuring that the remaining intensity profile is solely due to the frequency fluctuation of the TL module. This intensity variation was subsequently converted into a frequency variation as a function of time using the filter profile.

Fig. 5.12 (a) illustrates the frequency drift and settling time of the directly modulated TL when the modulation index was set at 0.2. The negative frequency values on the y-axis indicate a drift from the set ITU frequency towards lower frequencies. The frequency drift is defined as the maximum offset caused by the direct modulation during the presence of a logical one. The settling time is defined as the time the wavelength locker takes to counter-act the frequency offset caused by the direct modulation to within ± 2.5 GHz of the target ITU frequency. From the figure it is evident that the magnitude of the frequency drift was approximately 15 GHz. It is important to note that the settling time depends on the pattern length used (number of consecutive ones), therefore to measure the worst case scenario (the maximum settling time) a programmed sequence of 30 ones followed by 30 zeros was used. The channel frequency is within the specified ± 2.5 GHz range after approximately 11 ns. If an alternating pattern was used to directly modulate the TL, the presence of a logical one would result in an offset based on the index of modulation, while a logical zero would bring the signal back to its target frequency.

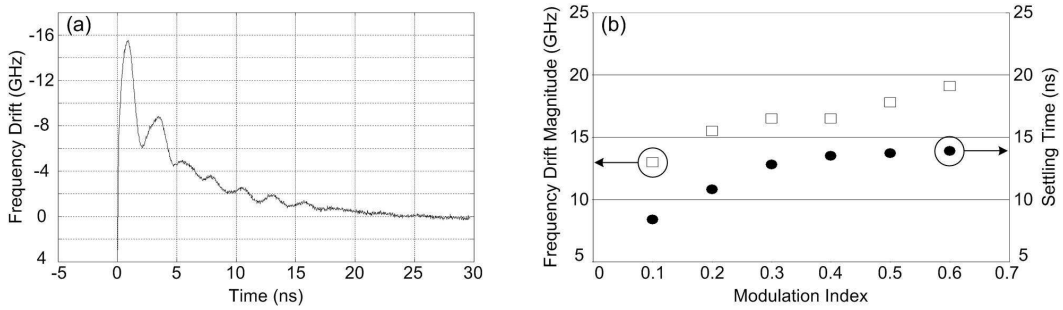

Fig. 5.12. (a) Frequency drift caused by direct modulation with an index of 0.2 and (b) frequency drift magnitude and settling time as a function of modulation index

Fig. 5.12 (b) shows the variation of both the magnitude and settling times of the frequency drift as a function of modulation index. This figure clearly shows that the frequency drift magnitude and the settling time increase with an increased modulation index. The maximum frequency offset was 19 GHz at a modulation index of 0.6 and reduced progressively to 13 GHz at an index of 0.1. The cause of the frequency drift can

be attributed to refractive index changes in the gain section (due to modulation), leakage currents into other sections and thermal effects.

5.7.3 BER Degradation Due to Optical Filtering

To examine the detrimental effects of this frequency drift, the directly modulated TL module was employed in a back-to-back system that mimicked a DWDM receiver, which incorporated a narrow band optical filter. BER performance could then be carried out with and without the filtration element. The experimental setup is illustrated in Fig. 5.13. The TL was again set at channel 38 on the ITU grid and modulated with a 1 Gb/s NRZ pseudorandom bit sequence of 2^7-1 and the modulation index was set at 0.2. An optical attenuator incorporated with an in-line power meter (P_{rec}) monitored the varied received power falling on the pre-amplified receiver. The BER was measured with the aid of an error detector under three different scenarios namely: with no filter in the receiver (dotted line), with the 26 GHz filter centred at the specified ITU frequency (193.35 THz) and finally with the filter centred at the average of the frequency shifted signal upon direct modulation (193.343 THz). Eye diagrams were also recorded with the aid of a 50 GHz sampling oscilloscope for each of the receiver arrangements.

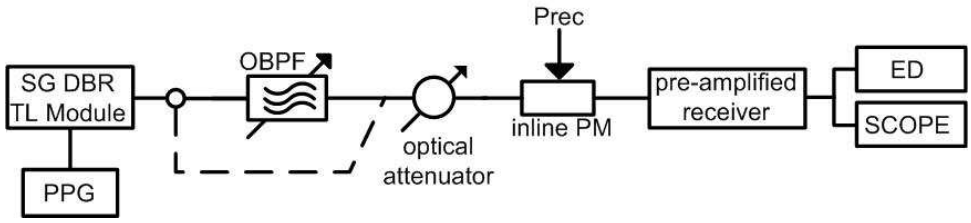

Fig. 5.13. Experimental setup to measure the effects of the frequency drift on WDM BER performance

The effect of the frequency drift on the performance of a typical DWDM system is highlighted by the BER versus received power plot shown in Fig. 5.14. The case where no filter is used acts as a performance reference (●). Alternatively, when the directly modulated signal is filtered with the filter centred at the target frequency of channel 38 on the ITU grid, the frequency fluctuations caused by the modulation are converted into intensity variations. These intensity fluctuations caused a degraded level of performance relative to the un-filtered scenario, reflected by the incurred power penalty of 6.7 dB at a BER of 10^{-9} (■). A slight improvement in performance of 1.64 dB at a BER of 10^{-9}, was obtained when the centre frequency of the filter was tuned to match the average shifted frequency of the TL module under direct modulation (Δ)

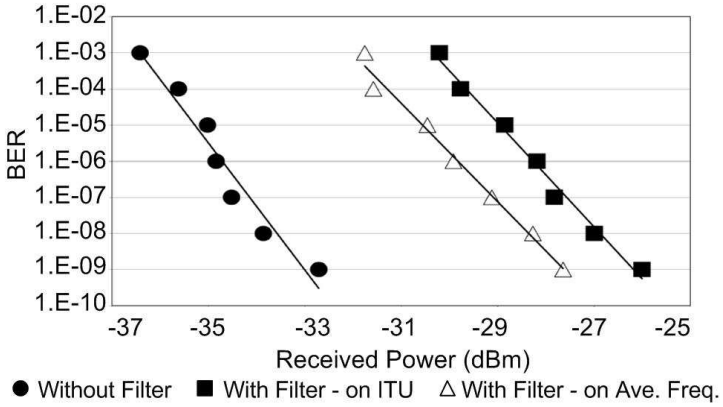

Fig. 5.14. BER versus received optical power

The corresponding received eye diagrams are illustrated in Fig. 5.15 (a-c) and reaffirm the BER degradation described above. Fig. 5.15 (a) shows the optical eye diagram for the scenario when the directly modulated signal is received without a filter. It is clearly seen that the eye is open and supports the excellent performance with received powers in the order of -33 dBm required to achieve a BER of 10^{-9}. This excellent performance could be attributed to the fact that even though the frequency drift exists, it does not manifest as intensity fluctuations when detected in the absence of a frequency discrimination medium, such as a band pass filter. However, when the filter is present in the DWDM receiver and centred at the target ITU frequency, the intensity fluctuations result in a partially closed eye (Fig. 5.15 b). It is important to note the comparative difference between these two eyes even though the closed eye is recorded at a higher received power of -30 dBm. Fig. 5.15 (c) illustrates the eye at the same received power (-30 dBm), but when the filter was centred at the average shifted frequency. A clear improvement in performance is observed.

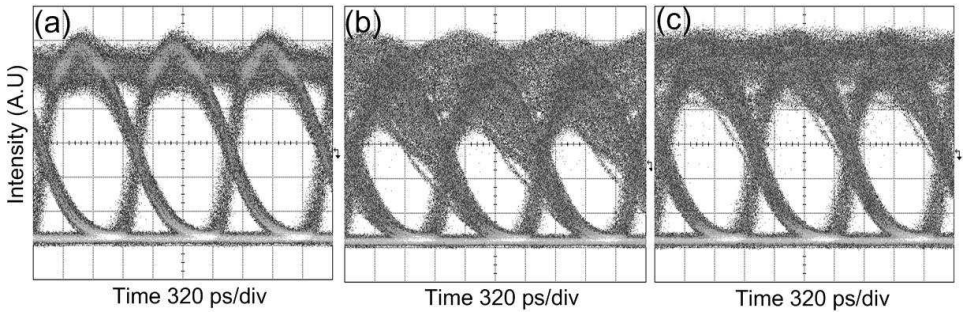

Fig. 5.15. Received eye diagrams (a) without filter, (b) with filter cantered at ITU frequency and (c) with filter centred at the average shifted frequency

Although a slight improvement in performance (1.64 dB) was realised when the filter was tuned to match the average shifted frequency of the TL module, this adjustment would be unrealistic in a conventional reconfigurable WDM network. The reason for this is that each filter in the entire access network (including AWGs) would have to be adjusted or

re-fabricated to improve the systems performance. Therefore alternative mechanisms must be implemented before directly modulated TLs can become a viable option as a short reach NRZ transmitter. The modulation index of the electrical signal applied to the device could be reduced in order to limit the extent of frequency drift, thus reducing the amount of power fluctuations when filtered in a DWDM receiver. This solution may reduce the magnitude of the frequency drift but comes at the cost of optical extinction.

Another solution would be to increase the filter bandwidth in the receivers, thus again minimising the intensity variations that lead to poor BER performance. This solution would require reduced channel spacing and thus impact the overall obtainable capacity of the network. An alternative approach would be to counter-act the frequency variation of the directly modulated TL prior to transmission. If this was achieved the viability of a directly modulated source would be vastly increased for implementation in future reconfigurable short reach applications. The following section outlines one such compensation technique.

5.8 Frequency Chirp Compensation Scheme

From the previous section it is apparent that the frequency drift impairment incurred by a directly modulated tuneable laser would overshadow the advantages of this scheme and prevent service providers from adopting such a technique. This section focuses on a corrective compensation technique that consists of the simultaneous modulation of both the gain and phase sections of a commercially available SG DBR laser from Agility Communications. The direct modulation of the laser phase section produces a corresponding frequency variation, but more importantly with a sign opposite to that produced through modulation of the gain section, thus reducing the inherent chirp associated with such modulation schemes.

5.8.1 Static Phase Section Characterisation

An initial static characterisation of the laser phase section was required before direct modulation could be applied. The experimental setup for this characterisation is shown in Fig. 5.16 (a). The SG DBR laser used for this experiment was the same commercially available device from Agility Communications that was used for the performance tuning map characterization in section 5.6.1. It was a temperature controlled fibre pigtailed device contained within a butterfly package. In comparison to the Intune Networks TL module used for the previous frequency drift measurement, this laser allowed access to all four sections and there was also no integrated SOA or wavelength locker. The temperature was set at 22° C and remained constant throughout the experiment. The back mirror (I_b), gain (I_g) and front mirror (I_f) currents were initially set at 55.03, 79.29 and

0.53 mA respectively, which resulted in a lasing wavelength of 1554.5 nm (λ_c) and a side mode suppression ratio of 45 dB.

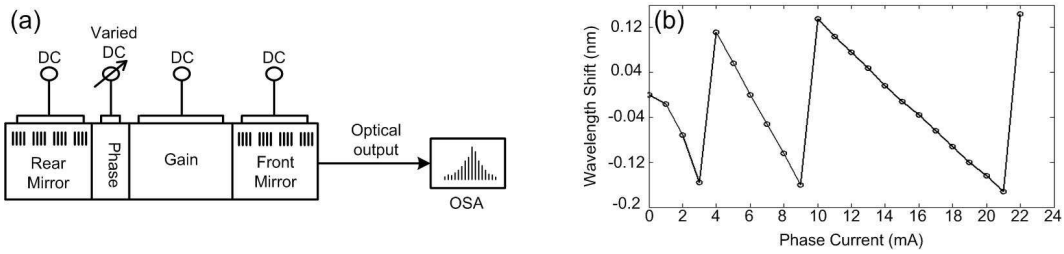

Fig. 5.16. (a) Setup for static characterisation of phase section and (b) wavelength shift as a function of phase current, relative to central wavelength at zero bias (1554.5 nm)

The static analysis of the phase section was obtained by applying a varied DC bias in 1 mA steps to the device and simultaneously recording the central lasing wavelength. The corresponding shift in wavelength relative to λ_c, as a function of phase current, is illustrated in Fig. 5.16 (b). As can be seen, the wavelength slowly decreases with an increase in the injection current until a longitudinal mode jump is experienced, after which the cycle is repeated. From this result we can see that by biasing the phase section around 15 mA and applying a peak-to-peak modulation of 10 mA, a maximum frequency shift without incurring a mode hop can be achieved.

5.8.2 Complex Spectral Analysis of a Directly Modulated TL

To obtain a qualitative analysis of the compensation scheme, the direct modulation induced frequency chirp was analysed for both the gain and phase sections individually. This was achieved by analysing the directly modulated TL with the aid of a commercially available complex OSA that had a spectral resolution of 20 MHz, as seen in Fig. 5.17. Using this device, both the intensity and phase information of the signal could be retrieved. However, a requirement for the phase measurement on the complex OSA, limited us to using a four bit patterned sequence of 1100 to directly modulate the TL at a clock rate of 2.5 Gb/s. Additionally, the bandwidth of the laser gain section (1.5 GHz) also restricted the upper limit of the data rate.

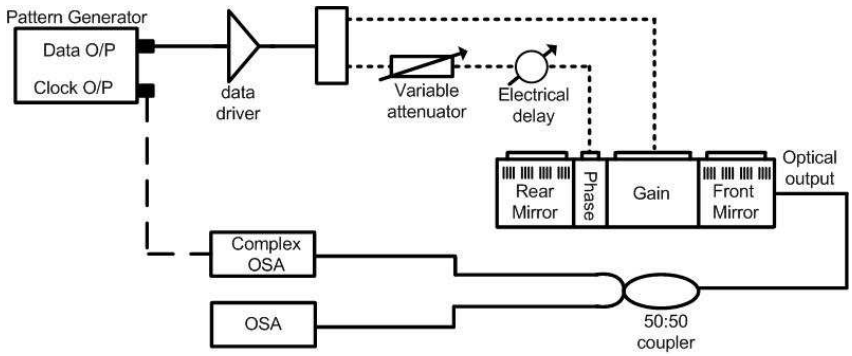

Fig. 5.17. Experimental setup for frequency chirp compensation scheme

The repeated pattern of 1100 was amplified and split into two paths. One arm consisting of a variable electrical attenuator and a bias tee was connected to the phase section of the laser, while the second arm which consisted of only a bias tee was connected to the gain section. The frequency chirp due to direct modulation was recorded using the complex OSA when the phase section was connected only, for a number of modulation voltages. This characterisation was repeated for the gain section of the device, therefore providing an accurate representation of the chirp magnitude and sign for both sections individually, therefore enabling the selection of optimum operating points for both laser sections to achieve a competent level of chirp compensation, as seen in Fig. 5.18. The chirp profile spanning from 0.4 to 1.2 ns corresponds to a time when two 1-bit symbols were present. By comparing the respective chirp profiles, optimum drive voltages were devised.

The compensation scheme is enabled by the fact that the frequency chirp profiles exhibited by both sections have opposing signs when directly modulated by an identical bit sequence. As expected, current injection into the passive phase section leads to a negative change in the refractive index and therefore results in a blue shift in frequency due to the free carrier plasma effect [27]. Conversely, carrier injection into the gain section causes a transient chirp on the leading and trailing edges of the modulated optical signal, with some intermittent adiabatic chirp [28]. However, it is important to note that if the modulation rate is high enough the transient frequency chirp will dominate, resulting in a frequency chirp profile opposite to that imposed by the phase section. This is the principle by which this chirp compensation scheme operates.

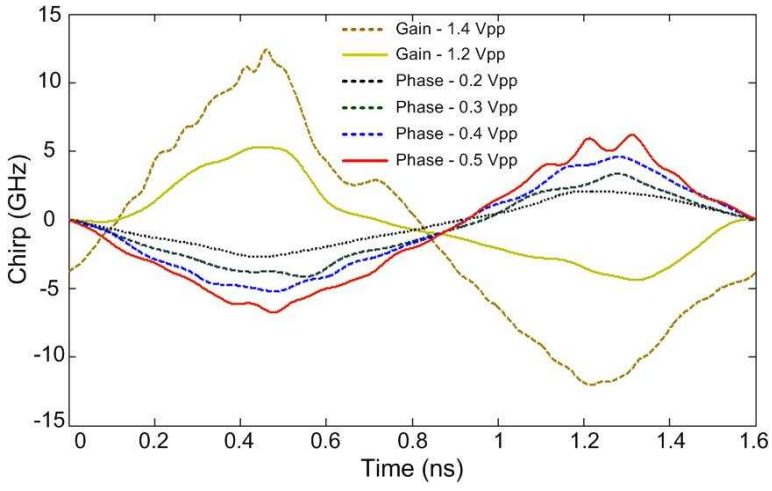

Fig. 5.18. Chirp profiles of both the gain and phase sections for a number of drive voltages

5.8.3 Frequency Chirp Compensation Scheme

For the frequency chirp compensation scheme, both sections of the device are modulated simultaneously. Therefore the electrical path lengths to both sections of the laser were matched in order to ensure an optimum bit-by-bit compensation. The output of the laser

was again monitored with the complex OSA. Fig. 5.19 illustrates the intensity and chirp profiles of the directly modulated SG DBR laser, measured using the complex OSA, for the two scenarios. Firstly, modulation was applied to the gain section of the device with the phase section DC biased at 15 mA (Fig. 5.19 a). The figure shows two 1-bits corresponding to 800 ps with a large frequency chirp of 25 GHz. Fig. 5.19 (b) displays the intensity and chirp profile of the laser output when both sections are modulated. There is a dramatic improvement in the level of frequency chirp and this reduction is due to the gain and phase sections exhibiting opposite chirp profiles under direct modulation as discussed in section 5.8.2. The chirp exhibited by the NRZ data stream is now approximately zero with nearly complete compensation. The minor fluctuations are a result of the non-ideal matching of the chirp profiles.

The corresponding spectra of the directly modulated SG DBR laser under the two different scenarios are illustrated in Fig. 5.20 (a) and (b). The broadened spectrum in Fig. 5.20 (a) clearly shows the direct modulation induced frequency offset, while figure (b) displays the compensated spectrum which was achieved through the simultaneous modulation of both gain and phase sections. The narrowing in the spectrum mirrors the reduction in chirp illustrated in Fig. 5.19 (b) and reaffirms the frequency chirp compensation technique. The compressed spectrum will dramatically reduce the effect of cross channel interference and will also ensure that the effects of fibre dispersion are minimised.

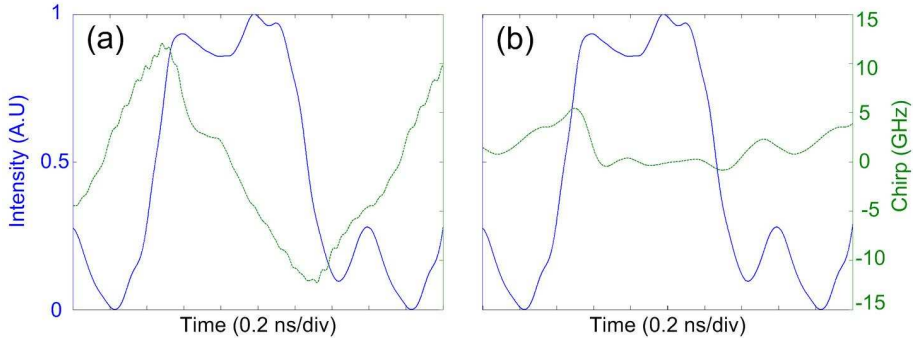

Fig. 5.19. Intensity (solid line) and chirp (dotted line) profile (a) with gain modulation only and (b) with both gain and phase modulation

To understand the transition from the transient to the adiabatic regime a 16-bit pattern (containing four consecutive ‘1-bits’) and a 32-bit pattern (containing ten consecutive ‘1-bits’) were applied to both the laser gain and phase sections at the same clock rate of 2.5 Gb/s. The corresponding spectra were analysed using a conventional OSA (due to the pattern limitation of the complex OSA). Fig. 5.20 (c) and (d) illustrate the spectra corresponding to the 16-bit pattern containing four consecutive 1 symbols. Here again there is a large degree of spectral broadening when only the gain section is modulated.

However, through simultaneous modulation of the phase section there is still a considerable reduction in spectral width. The compensation is not as significant as that achieved using a 4-bit pattern as a longer sequence of 1-bits results in an increased adiabatic chirp.

Conversely, when the 32-bit pattern was applied to the laser almost no compensation was realised when both the gain and phase sections of the SG DBR tuneable laser were simultaneously modulated, as seen in Fig. 5.20 (e) and (f). This poor performance of the frequency chirp compensation scheme is a result of the bit sequence containing a larger succession of 1-bits. Hence, the adiabatic chirp is dominant and the transient components only account for a minor portion of the overall chirp profile. Therefore the modulation of the phase section only results in a minor compensation of the frequency chirp. This problem could be overcome by increasing the data rate to approximately 10 Gb/s [29], thus producing a 100 ps time slot. Such a small duration would result in a transient chirp dominated regime, therefore providing the ideal profile for compensation through modulation of the lasers phase section.

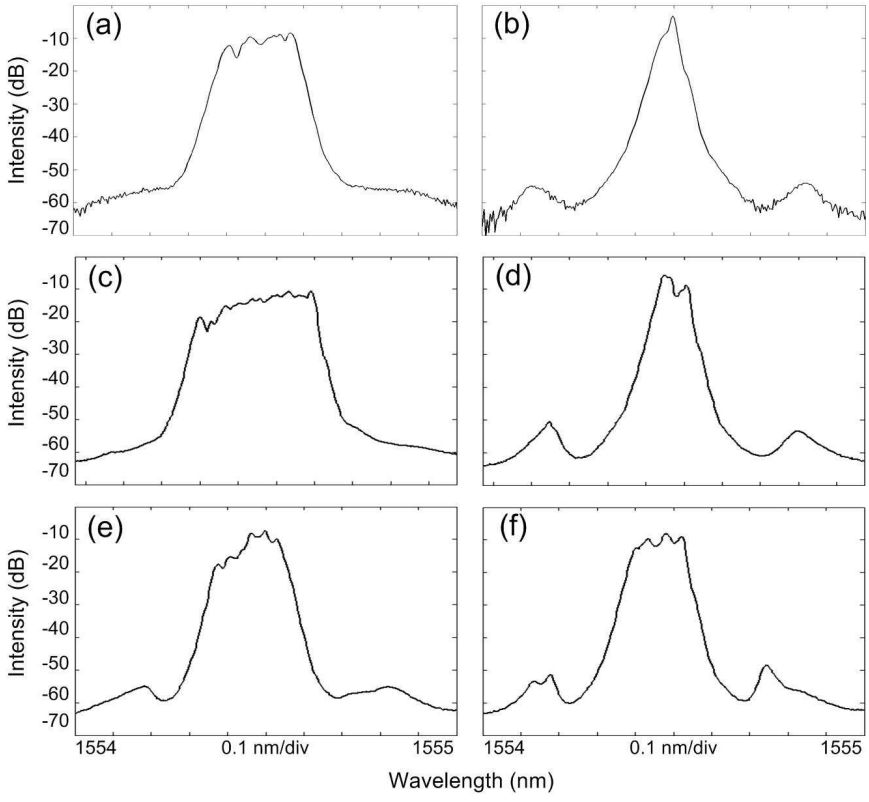

Fig. 5.20. Optical spectra for gain modulation only and for gain and phase modulation for a (a) 4-bit pattern, (b) 16-bit pattern and (c) 32-bit pattern

For efficient direct modulation of a SG DBR laser at data rates as high as 10 Gb/s, new device structures would have to be manufactured. Currently available laser sources are not inherently designed for direct modulation, as their main application involves

providing CW light for external modulation. Therefore to realise a cost efficient directly modulated SG DBR, the device must be designed so that the gain and phase sections exhibit bandwidths capable of high speed NRZ modulation. Each section must also have a high speed RF connector to enable the greatest possible transmission speeds.

5.9 Summary

The direct modulation of a widely tuneable SG DBR laser is an ideal short reach transmitter for future reconfigurable access networks. It has the potential to provide low cost NRZ transmission over a large tuning range with nanosecond switching times. The device structure also enables monolithic integration with other semiconductor devices such as a SOA, thus providing a small form factor module with low power consumption. However, before such a transmitter can be considered for implementation in a high-speed system, the frequency drift caused by the direct modulation of the laser must be analysed. This drift was characterised for a commercially available SG DBR TL module with an incorporated wavelength locker. The frequency offset varied from 13 to 19 GHz when the applied modulation index varied from 0.1 to 0.6 respectively. The effect of this drift on DWDM system performance was analysed by passing the signal through a receiver that incorporated a band pass filter. Results showed that a power penalty of 6.7 dB was incurred when using such a filter in comparison to the unfiltered case. An improvement in performance of 1.64 dB (relative to the filtered case with the filter centred at ITU frequency) was achieved when the filter was centred to match that of the average output frequency of the TL under direct modulation.

To overcome this impairment a novel frequency chirp compensation scheme for directly modulated SG DBR lasers was proposed. A separate tuneable laser which allowed access to all four sections was modulated with a patterned bit sequence of 1100 and analysed with a complex OSA. Frequency chirp of 25 GHz was recorded through modulation of the laser gain section, which subsequently caused a severe broadening of the spectrum. The compensation scheme consisted of the simultaneous modulation of both the laser gain and phase sections. The opposing chirp profiles exhibited after modulation reduced the frequency chirp to approximately zero, resulting in a significant reduction in the width of the laser spectrum. This compensation scheme vastly increases the viability of directly modulated SG DBR lasers for short reach applications such as the access network.

Further improvements to the transmitter could be achieved if the device was designed specifically for direct intensity modulation. Therefore, if both the gain and phase sections of the laser exhibited larger bandwidths, much high data rates of up to 10 Gb/s could be achieved.

REFERENCES

[1] A. Banerjee et al., "Wavelength-division-multiplexed passive optical network (WDM-PON) technologies fro broadband access: a review," OSA J. Opt. Network., vol. 4, no. 11, pp. 737-758, Nov. 2005.

[2] L.A. Coldren et al., "Tunable semiconductor lasers: A tutorial," IEEE/OSA J. Lightwave Technol., vol. 22, no. 1, pp.193-202, Jan. 2004.

[3] E. Bruce, "Tunable lasers," IEEE Spectrum, vol. 39, no. 2, pp. 35-39, Feb. 2002.

[4] G. Fish, "Tunable lasers and their impact on optical networks," [Online], CommsDesign: An EE Times Community, Sep. 2001. Available: http://www.commsdesign.com.

[5] J. Buus et al., "Communications applications and requirements" in Tunable Laser Diodes and Related Optical Sources, Second Edition, Wiley-Interscience, 2005.

[6] J. Buus and E.J. Murphy, "Tunable lasers in optical networks," IEEE/OSA J. Lightwave Technol., vol. 24, no. 1, pp. 5-11, Jan. 2006.

[7] L. Ponnampalam et al., "Dynamically controlled channel-to-channel switching in a full-band DS-DBR laser," IEEE J. Quant. Electron., vol. 42, no. 3, pp. 223-230, Mar. 2006.

[8] J.M. Senior, "Optical sources 1: the laser," in Optical Fiber Communications: Principle and Practice, second edition, Prentice Hall International Series in Optoelectronics, 1992.

[9] G. Sarlet et al., "Tunable laser diodes," in WDM Technologies: Active Optical Components, Academic Press, Elsevier Science, 2002.

[10] K. Kobayashi and I. Mito, "Single frequency and tunable laser diodes," IEEE/OSA J. Lightwave Technol., vol. 6, no. 11, pp. 1623-1633, Nov. 1998.

[11] J. Buus et al., "Basic concepts of tuneable laser diodes" in Tunable Laser Diodes and Related Optical Sources, Second Edition, Wiley-Interscience, 2005.

[12] R.C. Alferness, "Widely tunable semiconductor lasers," in Proc. of Optical Fiber Communications (OFC), paper TuC5, Mar. 1993.

[13] T.J. Reid et al., "3.8 nm continuous tuning range of a low threshold distributed Bragg reflector laser," in Proc. of International Semiconductor Laser Conf., paper M-1, pp. 242-243, 1990.

[14] S. Murata et al., “Tuning ranges for 1.5 µm wavelength tunable DBR lasers,” IEE Electron. Lett., vol. 24, no. 10, pp. 577-579, May 1988.

[15] M. Oberg et al., “A three-electrode distributed Bragg reflector laser with 22 nm wavelength tuning range,” IEEE Photon. Technol. Lett., vol. 3, no. 4, pp. 299-301, Apr. 1991.

[16] S. Murata et al., “Over 720 GHz (5.8 nm) frequency tuning by a 1.5 µm DBR laser with phase and Bragg wavelength control regions,” IEE Electron. Lett., vol. 23, no. 8, pp. 403-405, Apr. 1987.

[17] V. Jayaraman et al., “Theory, design, and performance of extended tuning range semiconductor lasers with sampled gratings,” IEEE J. Quant. Electron., vol. 29, no. 6, pp. 1824-1834, Jun. 1993.

[18] J.O. Wesstrom et al., “State-of-the-art performance of widely tunable modulated Y-branch lasers,” in Proc. of Optical Fiber Communications (OFC), paper TuE2, Mar. 2004.

[19] B. Mason et al., “Design of sampled grating DBR lasers with integrated semiconductor optical amplifiers,” IEEE Photon. Technol. Lett., vol. 12, no. 7, pp. 762-764, Jul. 2000.

[20] H. Han et al., “Development of internal wavelength lockers for tuneable laser applications,” in proc. of Electronics Components and Testing Conference, pp. 805-808, May 2003.

[21] B. Hammond et al., “Integrated wavelength locker for tunable laser applications,” in Proc. of Lasers and Electro-Optics Society (LEOS), paper WO1, Nov. 2002.

[22] H. Ishii et al., “Mode stabilization method for superstructure-grating DBR lasers,” IEEE/OSA J. Lightwave Technol., vol. 16, no. 3, pp. 433-442, Mar. 1998.

[23] G. Sarlet et al., “Control of widely tunable SSG-DBR lasers for dense wavelength division multiplexing,” IEEE/OSA J. Lightwave Technol., vol. 18, no. 8, pp. 1128-1138, Aug. 2000.

[24] E. Buimovich et al., “Measurements of thermal frequency chirp in directly modulated DBF lasers and thermal transient induced frequency drift during fast tuning in GCSR lasers using frequency discrimination technique,” in Proc. of Lasers and Electro-Optics Society (LEOS), paper TuD7, Oct. 2003.

[25] T. Niemi et al., “Device for frequency chirp measurements of optical transmitter in real time,” Rev. Sci. Instrum., vol. 73, no. 3, pp. 1103-1107, Mar. 2002.

[26] J.E. Simsarian and L. Zhang, “Wavelength locking a fast-switching tunable laser,” IEEE Photon. Technol. Lett., vol. 16, no. 7, pp. 1745-1747, Jul. 2004.

[27] B.R. Bennett et al., “Carrier-induced change in refractive index of InP, GaAs and InGaAsP,” IEEE J. Quant. Electron., vol. 26, no. 1, pp. 113-122, Jan. 1990.

[28] I. Tomkos et al., “Extraction of laser rate equation parameters fro representative simulations of metropolitan area transmission systems and networks,” Optics Comms., vol. 194, pp. 109-129, Apr. 2001.

[29] M. Isaksson et al., “10 Gb/s direct modulation of a 40 nm tunable modulated-grating Y-branch laser,” in Proc. of Optical Fiber Communications (OFC), paper OTuE2, Mar. 2005.

Chapter 6 - Conclusion

More flexible optical networks are becoming a necessity to accommodate the fluctuating and unpredictable traffic patterns of today's internet based traffic. This is due to the exploding growth in triple play services, such as video on demand, as it has become increasingly difficult to forecast future bandwidth requirements. Therefore current opaque, pre-determined point-to-point or point-to-multipoint systems are beginning to struggle to supply adequate bandwidth to the geographical areas in most need, in a cost and time efficient manner. Consequently, network reconfiguration is a hot topic for carriers that are beginning to install or upgrade their fibre infrastructure. However, to achieve a truly reconfigurable optical layer, several key components are required. These include the ROADM, AWG, and the wavelength converter, which were discussed in Chapter 1. These components all strive towards all-optical rerouting and wavelength switching, however another key component pivotal to an agile optical network is the wavelength tuneable transmitter.

The requirements of a fast switched optical transmitter, such as data rate, modulation format and obtainable transmission distance are application dependant. Therefore a number of transmitter configurations, capable of meeting specific price points, are needed for each network topology. The RZ modulation format is needed for high-speed transmission in the core or even metro network, while the NRZ format is adequate for short reach access based applications. This thesis focuses on the development and detailed characterisation of wavelength tuneable transmitters for implementation in the core, metro and access based optical networks.

For the core network, a 40 GHz widely tuneable transmitter, consisting of a tuneable laser and a sinusiodally driven EAM was investigated in Chapter 3. One advantage of such a technique is that the characteristics of the generated pulses are tuneable, due to the inherent wavelength dependency of the EAM. The pulse width and frequency chirp sign and magnitude can be easily adjusted through the simple tuning of the EAM reverse bias and modulation voltage. The chirp can therefore be employed to counteract any residual dispersion associated with the dispersion map of a given optical network, providing enhanced transmission performance over a wide wavelength range. Before this performance increase can be achieved, the intensity and phase of the generated pulses must be accurately measured. As standard measurement techniques, such as photodetection, only provides the time dependent intensity information of a pulse, more advanced techniques are required. Chapter 2 outlined a number of standard and more advanced pulse analysis schemes capable of monitoring the characteristics of the

generated pulses. One such method is the linear spectrogram pulse measurement technique.

This pulse characterisation method was employed to perform a detailed analysis of the generated pulses, in terms of pulse width, pedestal suppression and chirp as a function of operating wavelength and EAM drive conditions. This led to the development of EAM performance maps for each operating wavelength that could be employed to optimise the driving conditions of the transmitter (reverse bias and modulation voltage) when a switching event occurs in a reconfigurable optical network. The transmission performance of the wavelength tuneable transmitter in a 1500 km re-circuiting loop system was demonstrated. It was shown that the non-optimisation of the transmitter drive conditions, as the operating wavelength was varied, leads to a severe degradation in transmission reach of up to 33 %. Improvements in transmission performance of 150 and 400 km were obtained at operating wavelengths of 1550 and 1540 nm respectively, relative to the initially optimised wavelength of 1560 nm, through the simple adjustment of the EAM drive conditions.

From the linear spectrogram characterisation, it is possible to create a look-up table, comprising of a DC bias and RF drive for each wavelength channel on the ITU grid. Therefore, if the EAM was integrated within a SG DBR laser module and a wavelength switching request is made, the control module for the laser device would not only alter the current controls to the laser, but would also dynamically adjust the drive conditions of the EAM. This would therefore ensure greater levels of performance uniformity over a large wavelength range, while simultaneously obtaining the maximum transmission distance at each WDM channel.

As the distances spanned by the metro network are much smaller than that required in the core, less stringent performance demands can be placed on the optical transmitter. As a result, directly modulated sources are preferred as they offer a simple and cost efficient solution to externally modulated NRZ or RZ transmitters. Chapter 4 focussed on the development of a simple, robust and cost efficient pulse generation technique capable of operating at data rates up to 10 Gb/s, ideal for metro applications. It involved self-seeding of a gain-switched FP laser diode using a dispersive grating. One of the main limitations of the self-seeding scheme is the timing dependency of the feedback signal, which usually requires that either the external cavity length is tuned or that the repetition rate of the generated pulses is varied. This cavity length dependency poses as a serious drawback of such a pulse source and limits its applicability to commercial systems.

It was demonstrated that, by using a highly chirped FBG, the gain-switched pulses could be dispersed to such an extent that they overlap sufficiently to create a CW like signal.

This continuous light signal was then reflected back into the laser cavity to increase the temporal and spectral purity of the pulses. This novel self-seeding technique negated the need to tune the cavity length or the repetition rate. Optimum pulse generation with suppression ratios exceeding 30 dB and pulse duration of approximately 30 ps were achieved at a range of repetition rates from 2.5 to 10 GHz. Although pulse generation was only demonstrated at a single wavelength (due to the bandpass wavelength of the FBG filter) this technique could be easily adapted to cover a large tuning range by utilising a tuneable grating. By combining a tuneable grating and a FP laser, a number of longitudinal modes may be seeded, providing wavelength tuneable pulse generation over the C-band wavelength range, ideal for reconfigurable metro based optical networks. Finally, by integrating the laser and grating, the cost, footprint and power consumption of the source could be reduced.

Chapter 5 provided an introduction to widely tuneable lasers, with specific attention being placed on the SG DBR laser. Although such lasers are primarily employed to provide CW light for external modulation, we proposed a direct modulation scheme, suited for short reach applications. However, before such wavelength tuneable transmitters can be employed in commercial systems, several detrimental effects must be analysed. One such problem is the frequency fluctuation experienced at the output of the laser upon direct modulation. The magnitude and settling of this frequency drift was characterised for a commercially available SG DBR TL module. The magnitude of the drift increased with an increase in the index of the modulation signal, with a maximum drift of 19 GHz being recorded. As the module incorporated a wavelength locker, settling times of approximately 8 to 15ns were also displayed.

The extent of the frequency drift on DWDM performance was also investigated by carrying out BER measurements on the NRZ data stream, using an optical pre-amplified receiver that incorporated an OBPF. The frequency drift exhibited by the TL manifested into intensity variations upon filtration, thus causing a severe degradation in the received eye diagram leading to a poorer BER. A power penalty of 6.7 dB was realised when the filter was used in the receiver (centred at the specified ITU frequency of the laser), relative to the unfiltered case. By tuning the filter to match the average shifted frequency under modulation, a power penalty improvement of 1.64 dB (relative to the filtered case with the filter centred at ITU frequency) was achieved. Although a finite improvement in system performance was observed by tuning the receiving filter, this solution would be impractical in a real optical system.

Therefore, the second part of the experimental work discussed in Chapter 5 investigated a frequency chirp compensation scheme for directly modulated DBR lasers. The technique

comprised of the simultaneous modulation of both the laser gain and phase sections. As each section produced conflicting signs of chirp for an identical applied bit pattern, optimum bit-by-bit chirp compensation could be achieved. The directly modulated output from a commercially available TL was monitored using a complex OSA for a programmed pattern sequence. Frequency chirp of approximately 25 GHz was experienced with only gain modulation, while this was reduced to almost zero after the simultaneous modulation of the phase section. One important aspect of this technique however, entailed that the chirp profile produced through the individual modulation of the laser gain section remained in the transient dominated regime. It was demonstrated that if a long string of consecutive one symbols were applied to the laser, little or no compensation would be observed. This was due to the presence of a large adiabatic chirp, which cannot be compensated through the modulation of the phase section. Therefore to negate this problem, larger data rates could be employed which would result in considerably shorter bit duration, thus ensuring that the exhibited chirp remains in the transient dominated regime. Future work on this short reach transmitter could include device optimisation, which may lead to modulation rates of up to 10 Gb/s, thus providing the potential for a widely tuneable, extremely fast switched transmitter, capable of operation in a reconfigurable optical access network.

As wide scale deployments of reconfigurable optical networks are currently becoming a reality, the continued development of key optical components and sub-systems required to provide network agility and optical transparency in a cost efficient manner is critical. This thesis has focussed on the development of cost efficient, high performance wavelength tuneable transmitters for implementation in future dynamic optical networks. In particular, it has demonstrated performance issues associated with EAM based transmitters for long haul applications at 40 Gb/s, provided a cost efficient solution to the cavity length dependency of self-seeded gain-switched pulses for medium haul applications and finally proposed an almost chirp free directly modulated SG DBR tuneable laser for short haul applications.

APPENDIX I – LIST OF PUBLICATIONS ARISING FROM THIS WORK

Referred Journals

80 Gb/s OTDM system analysis of a vertical microcavity based saturable absorber for the enhancement of pulse pedestal suppression

A.M. Clarke, P.M. Anandarajah, L. Bramerie, C. Guignard, R. Maher, D. Massoubre, A. Shen, J.L. Oudar, L.P. Barry and J.C. Simon

IEEE Photon. Technol. Lett., vol. 19, no. 5, pp. 321-323, Mar. 2007.

Optimized performance map of an EAM for pulse generation and demultiplexing via FROG characterization

R. Maher, P.M. Anandarajah and L.P. Barry

J. Opt. Comms., vol. 273, no. 2, pp. 500-505, May 2007.

Cavity length independent continuous repetition rate tuning of a self-seeded gain-switched fabry-perot laser

R. Maher, P.M. Anandarajah and L.P. Barry

IEEE Photon. Technol. Lett., vol. 19, no. 20, pp. 1625-1627, Oct. 2007.

Characterization of frequency drift of sampled-grating DBR laser module under direct modulation

P.M. Anandarajah, R. Maher, L.P. Barry, A. Kaszubowska, E. Connolly, T. Farrell and D. McDonald

IEEE Photon. Technol. Lett., vol. 20, no. 2, pp. 72-74, Jan. 2008.

Characterization of a turbo-switch SOA wavelength converter using spectrographic pulse measurement

D.A. Reid, A.M. Clarke, X. Yang, R. Maher, R.P. Webb, R.J. Manning and L.P. Barry

IEEE J. Sel. Topics in Quant. Electron., vol. 14, no. 3, pp. 841-848, May/Jun. 2008.

Lyot filter based multiwavelength fiber ring laser actively mode-locked at 10 GHz using an electroabsorption modulator

C. O' Riordan, M.J. Connelly, P.M. Anandarajah, R. Maher, and L.P. Barry

J. Opt. Comms., vol. 281, no. 13, pp. 3538-3541, Jul. 2008.

Optimization of a 42.7 Gb/s wavelength tunable RZ transmitter using a linear spectrogram technique

R. Maher, P.M. Anandarajah, A.D. Ellis, D. Reid and L.P. Barry

OSA Opt. Express, vol. 16, no. 15, pp. 11281-11288, Jul. 2008.

Novel frequency chirp compensation scheme for directly modulated SG DBR tunable lasers

R. Maher, K. Shi, P.M. Anandarajah, A. Kaszubowska, L.P. Barry and Y. Yu

IEEE Photon. Technol. Lett., vol. 21, no. 5, pp. 340-342, Mar. 2009.

Characterization of wavelength tunable lasers for future optical communications systems

P.M. Anandarajah, A. Kaszubowska, R. Maher, K. Shi and L.P. Barry

Academy Publisher, Journal of Networks, Special Issue: Selected Papers of the 10th Anniversary International Conference on Transparent Optical Networks, ICTON 2008, Invited Paper, Accepted for Publication, 2009.

Conference Papers

Generation and characterisation of 40 GHz picosecond optical pulses generated using an EAM

R. Maher, P.M. Anandarajah and L.P. Barry

International Conf. on Transparent Optical Networks (ICTON), paper TuP32, Jun. 2006.

Performance of pulse source consisting of an externally injected gain-switched laser followed by a nonlinearly/linearly chirped grating in an 80 Gb/s OTDM system

R. Maher, P.M. Anandarajah, A.M. Clarke, C. Guignard, L.P. Barry, L. Bramerie and J. Harvey

Lasers and Electro-Optics Society (LEOS) Annual Meeting, paper ThX3, Nov. 2006.

Actively mode-locked multiwavelength fibre ting laser incorporating a Lyot filter, hybrid gain medium and birefringence compensated LiNbO3 modulator

C. O' Riordan, M.J. Connelly, I. Evans, P.M. Anandarajah, R. Maher and L.P. Barry

International Conf. on Transparent Optical Networks (ICTON), paper WeP10, Jun. 2007.

FROG characterisation of a turbo-switch wavelength convertor

X. Yang, A.M. Clarke, R. Maher, R.P. Webb, R.J. Manning and L.P. Barry

European Conf. Optical Commun. (ECOC), paper PO37, Sep. 2007.

Frequency drift characterisation of a SG-DBR tunable laser

R. Maher, P.M. Anandarajah, E. Connolly, A. Kaszubowska and L.P. Barry

China-Ireland International Conf. on Information and Commun. Technologies (CIICT), vol. 2, pp. 661-666, Aug. 2007.

Multiwavelength fibre ting laser incorporating a Lyot filter and hybrid gain medium actively mode-locked using a birefringence compensated LiNbO3 modulator

C. O' Riordan, M.J. Connelly, I. Evans, P.M. Anandarajah, R. Maher, and L.P. Barry

China-Ireland International Conf. on Information and Commun. Technologies (CIICT), vol. 2, pp. 632-636, Aug. 2007.

Continuous repetition rate tuning with timing window independent self-seeding of a gain-switched Fabry-Perot laser

P.M. Anandarajah, R. Maher and L.P. Barry

Lasers and Electro-Optics Society (LEOS) Annual Meeting, paper ThBB3, Oct. 2007.

Frequency drift characterisation of directly modulated SG DBR tunable lasers

R. Maher, P.M. Anandarajah, E. Connolly, A. Kaszubowska and L.P. Barry

Lasers and Electro-Optics Society (LEOS) Annual Meeting, paper WJ3, Oct. 2007.

Complete performance analysis of a 3.5 ps pulse source consisting of a gain-switched laser diode followed by a non-linearly chirped grating

R. Maher, P.M. Anandarajah and L.P. Barry

Conf. on Lasers and Electro-Optics (CLEO) paper CThR6, May 2008.

Wavelength tunable lasers in future optical communications systems

P.M. Anandarajah, A. Kaszubowska, R. Maher and L.P. Barry

International Conf. on Transparent Optical Networks (ICTON), invited paper TuD22, Jun. 2008.

Optimised performance analysis of a wavelength tunable 42.7 Gb/s EAM based RZ transmitter

R. Maher, P.M. Anandarajah, D. Reid and L.P. Barry

China-Ireland International Conf. on Information and Commun. Technologies (CIICT), pp. 653-656, Sep. 2008.

APPENDIX II – DATA SHEETS

The following pages contain data sheets for the devices listed below:

- CIP EAM
- Dispersive FBG
- Agility TL

40G-PS-EAM-1550 - Optical Sampling Window Generator

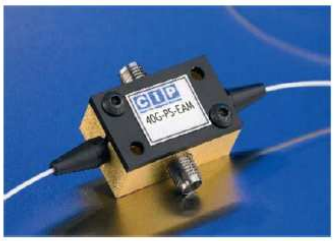

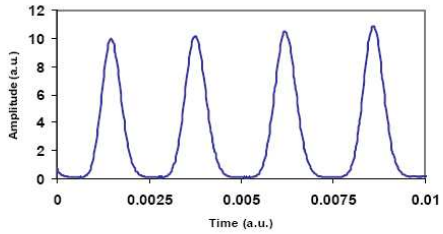

Figure: Autocorrelation trace at 40GHz

Features

- 1.55µm C-band operation
- Up to 40GHz repetition rate
- High modulation depth
- Low drive voltage
- Available as packaged device or chip-on-carrier
- Customer defined specifications available

Applications

- High speed pulse generation
- High speed optical sampling
- 160Gbit/s to 40Gbit/s demultiplexing
- Microwave to optical conversion

Description

The 40G-PS-EAM is a high-speed, semiconductor device capable of generating <5ps (FWHM) temporal optical sampling windows with a repetition rate up to 40GHz. The device is based on a semiconductor Electro Absorption Modulator (EAM) and operates over the 1.55µm wavelength C-Band. Applications include optical pulse generation (up to 40GHz rates), 160Gb/s to 40Gb/s optical demultiplexing, high-speed optical sampling and microwave to optical conversion. The device features high modulation depth and low driving voltage.

The EAM is provided in a RF connectorised package suitable for use in the lab with external RF components and drivers. Customer specified variants of the product may be available upon request

Optical and electrical characteristics

All specifications are at temperature = 20°C and 1550nm unless stated otherwise. P_{in}= Input optical power V_{DC} = Bias voltage V_{PP} = Peak to Peak voltage

Parameter	Test condition	Min.	Typ.	Max.	Unit
Minimum insertion loss	P_{IN} = -1dBm, V_{DC} = 0.6V		8.2	9.6	dB
Modulation depth	P_{IN} = -1dBm, V_{DC} in [0;-3]V	25	30		dB
Polarisation dependent loss (rms)	P_{IN} = -1dBm, V_{DC} in [0;-1]V		0.75	1.75	dB
Small signal 3dBe RF bandwidth	P_{IN} = 0dBm, V_{DC} ~ -1.5V		30		GHz
Sample window duration (FWHM) with 40GHz electrical drive	P_{IN} =+4dBm, V_{DC} ~ -2V, V_{PP}~4V			5	ps

Absolute maximum ratings

Item	Rating	Unit
Maximum DC Reverse Bias to centre pin	4	V
Maximum DC Forward Bias to centre pin	0.6	V
Maximum RF Voltage (peak to peak)	7	V
Maximum Input Optical Power	+10	dBm
Operating Temperature	15 - 50	°C
Storage temperature	10 - 70	°C
Fibre type	SMF-28 900µm tight buffer, >1m - PM fibre option available on request	

Ordering Information— Part Number 40G-PS-EAM-1550

For Chip on carrier, or custom products please contact CIP Sales on +44 1473 663210 or e-mail sales@ciphotonics.com. For details of your local agent, visit www.ciphotonics.com

Wiring Diagram and Dimensions (K connector): V connector version also available

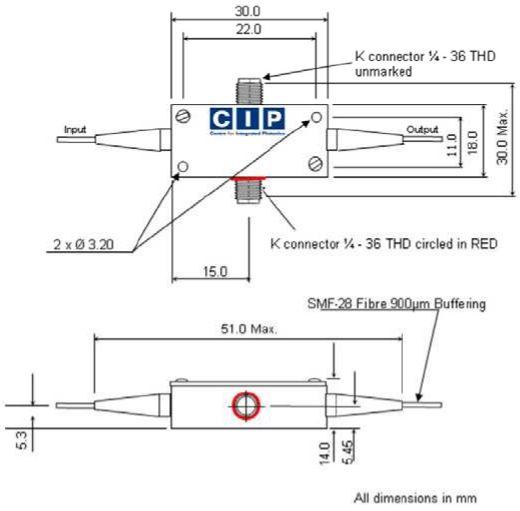

All dimensions in mm

Data Sheet

SERIAL NO: 051028-208

Center Wavelength at 25degC:	1545.13 nm
Peak Reflectivity:	85.1 %
Reflection Bandwidth @ -3 dB:	0.128 nm
Dispersion:	4957.8 ps/nm
Storage Temperature:	-40 to +80 degC

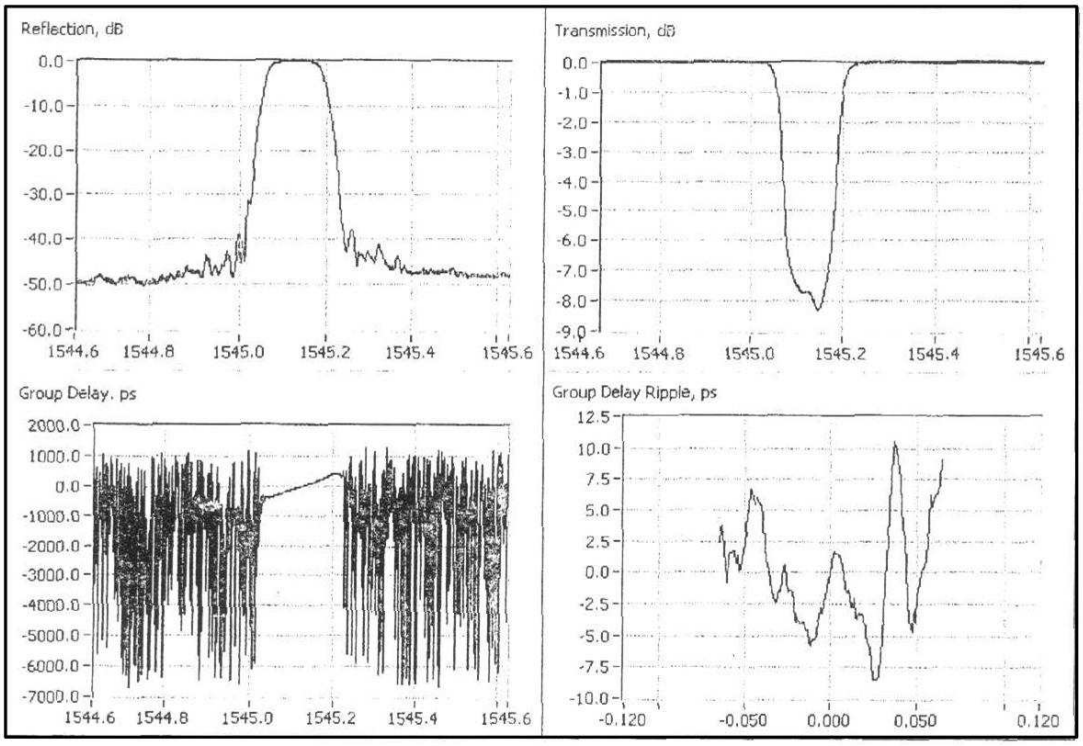

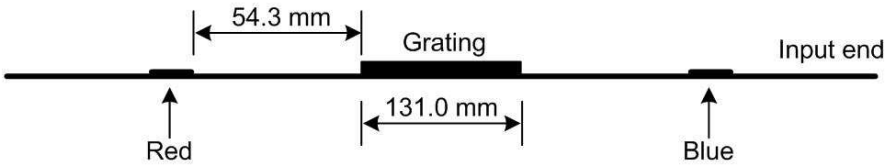

AGILITY

Preliminary Product Data Sheet
August 01, 2001

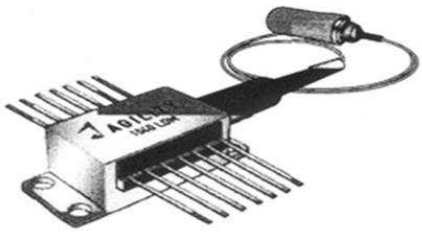

Agility 1040 CW Widely Tunable Laser Diode Module

Pin Descriptions

Pin	Description
1	NC
2	NC
3	NC
4	NC
5	Thermistor (+)
6	Thermistor (–)
7	TEC (–)
8	TEC (+)
9	GND
10	NC
11	Back Mirror
12	Phase
13	Gain
14	Front Mirror

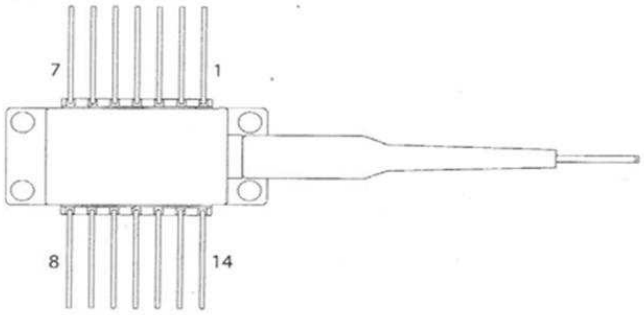

Package Absolute Maximum Ratings

Parameter	Symbol	Min	Typ	Max	Unit
Package Case Operating Temperature	T_P	0		+70	°C
Storage Temperature	T_S	–40		+85	°C
Lead Soldering Time at 260°C				10	sec

Electrical Absolute Maximum Ratings

Parameter	Symbol	Beg. of Life (BOL)	End of Life (EOL)	Absolute Max	Units
Max Gain Section operating current	Ig,max	150	187.5	TBD	mA
Max Phase Section operating current	Ip,max	25	30	TBD	mA
Max Front Mirror operating current	If,max	52	60	TBD	mA
Max Back Mirror operating current	Ib,max	104	120	TBD	mA
Max Gain Section operating voltage	Vg,max		1.85*	2.0*	V
Max Phase Section operating voltage	Vp,max		1.54*	1.6*	V
Max Front Mirror operating voltage	Vf,max		1.54*	1.6*	V
Max Back Mirror operating voltage	Vb,max		1.38*	1.6*	V

Optical Performance

Parameter	Symbol	Min	Typ	Max	Unit	Notes
Optical Power Out at Any Channel	P	2			mW	
Power Variation Between Channels	ΔP				dB	
Wavelength Tuning Range	λ_{Range}	1528.38		1562.645	nm	
		196.15		191.85	THz	
		61.5		18.5	ITU Channel	
Lambda Shift with Case Temperature			0.4		pm/°C	